Synthesis and surface modification of sunflower oil-based non-isocyanate polyurethane coatings containing chitosan: Physicochemical and biological characterization

María del Pilar Maya Serna

Tesis de maestría presentada para optar al título de Magíster en Ingeniería Química

Directora
Carmiña Gartner Vargas, Doctor (PhD) en Ciencias Químicas

Universidad de Antioquia
Facultad de Ingeniería

Maestría en Ingeniería Química

Medellín, Antioquia, Colombia

2022

Cita	(Maya Serna, 2022)
Referencia **Estilo APA 7 (2020)**	Maya Serna, M. (2022). *Synthesis and surface modification of sunflower oil-based non-isocyanate polyurethane coatings containing chitosan: Physicochemical and biological characterization* [Tesis de maestría]. Universidad de Antioquia, Medellín, Colombia.

Maestría en Ingeniería Química, Cohorte XII.

Grupo de Investigación Ciencia de los Materiales.

Centro de Investigación en Ciencias Exactas y Naturales (CIEN).

UNIVERSIDAD DE ANTIOQUIA
Vicerrectoría de Docencia

Sistema de Bibliotecas

Centro de Documentación Ingeniería (CENDOI)

Repositorio Institucional: http://bibliotecadigital.udea.edu.co

Universidad de Antioquia - www.udea.edu.co

Rector: John Jairo Arboleda Céspedes.

Decano/Director: Jesús Francisco Vargas Bonilla.

Jefe departamento: Lina María González Rodríguez

Synthesis and surface modification of sunflower oil-based non-isocyanate polyurethane coatings containing chitosan: Physicochemical and biological characterization.

María del Pilar Maya Serna

A Thesis Submitted in Partial Fulfillment of the Requirements for the Degree of Master
Graduate Program in Chemical Engineering

Advisor(s):

Ph. D. Carmiña Gartner

Ph. D. Betty Lucy López

Ciencia de los Materiales (CIENMATE) research group
University of Antioquia
Faculty of Engineering, Chemical Engineering Graduate Program

Medellín, Colombia
September 2022

Acknowledgments

The development of this project represented a challenge in terms of my study area, and it is satisfying to be able to finish. I want to express my deep gratitude to the *Ciencia de los Materiales* research group (CIENMATE) and the Chemical Engineering Faculty from the University of Antioquia for the financial support of this research work as well as to the Estudiante instructor, scholarship related to Deanship Resolution 0063 from January 23, 2019. Besides, to the the *Comité para el Desarrollo de la innovación* (CODI) for approved the project: "*Síntesis y caracterización de poliuretanos a partir de aceite de girasol y quitosano, libres de isocianatos, con propiedades antibacteriales*", related to the act No.819 in accordance with the terms of reference of the 2019-2020 Programmatic Call: Engineering and Technology area.

This project would not have been possible without the support of many people. Many thanks to my adviser, Carmiña Gartner, who read my high number of revisions and helped make some sense in the middle of the confusion. I would also to express my deep gratitude to my co-advisor, Betty Lucy López, who guided me throughout this project. Thank you, professors, for helping me finalize this research work, and for the constant support, advisory, and accompaniment in the development of this research work, which was only the beginning of the discovery of a whole world related to polymer chemistry.

I would like to thank my colleagues from the CIENMATE group who became my friends and main support when things did not go so well in practice, and other pathways had to be found, thank you for the support, laughter, advice and so many teachings in the practice of this work. Also, I wish to extend my special thanks to the help, support, and advisories provided by professors Felipe Bustamante y Lina Gonzalez, also by the research groups *Catálisis Ambiental* and *Procesos Químicos Industriales* (PQI), and my colleagues belonging to the Chemical Engineering Faculty, who supported me and offered deep insight into the study.

Finally, I want to especially thank my mother, for her inexhaustible love, dedication, and unconditional support all the time, my father who although could not be present during the process was my main inspiration and example to be a chemical engineer in the first place, and my grandmother who from now guides my steps in heaven.

Academic production

Maya Maria D. P., López Betty L., Gartner Carmiña. Synthesis and characterization of sunflower oil-based non-isocyanate polyurethane films obtained through a solvent and catalyst-free route. 34° Congreso Latinoamericano de Química CLAQ 2020, el XVIII COLACRO, el X COCOCRO, el II SPAE y el IV C2B2, Cartagena de Indias, Colombia, October 11-15, 2021.

ABSTRACT

Polyurethanes are a very versatile family of polymers widely used in many applications. Traditionally, they are synthesized from the reaction between di-isocyanates and diols, with the drawback that both monomers are petroleum derivatives, very toxic and polluting. Thus, the aim of this research was the synthesis of environmentally friendly non isocyanate polyurethanes (NIPU), obtaining both monomers from sunflower oil (SFO), which is a renewable source, and using a solvent and catalyst-free route. The surfaces of the NIPU films obtained were modified with chitosan to give them antibacterial properties so that they could be used as biomaterials for medical applications.

For the synthesis of NIPU, the double bonds of unsaturated fatty acids from sunflower oil, were epoxidized with formic acid and excess of hydrogen peroxide. The obtained epoxidized sunflower oil (ESFO) (epoxy content of 4.07 mmol g-1) was used to synthesize both monomers. First, ESFO was catalytic carbonatized with CO_2 under 120 °C and 50 bar to obtain carbonated sunflower oil (CSFO), yielding 90% conversion to cyclic carbonate. Then, polyamine polyol (PAPO) was synthesized by ring-opening polymerization from ESFO and ethylenediamine (EDA), which leads to a non-crosslinked elastomer with a low glass transition temperature (Tg) of −42.97 °C and an amine value of 478.84 mg KOH/g. Crosslinking reaction at 90°C between CSFO and 50% excess of PAPO generated the NIPU films. Urethane group formation occurred between 18 to 24h of curing. The obtained NIPU was a heterogeneous crosslinked network, which was easily shaped like a film. Then, a two step-treatment was employed to perform the surface modification of NIPU films. For this purpose, ultraviolet radiation was used to graft acrylamide (AM), which was then bonded to chitosan (CS) through glutaraldehyde. Chemical, morphological, thermal, mechanical, and biological characterization of the materials was carried out.

Proton Nuclear Magnetic Resonance (^{1}H NRM) and Attenuated Total Reflectance-Fourier Transform Infrared Spectroscopy (ATR-FTIR) were used to identify the structures and to confirm the formation of urethane groups. FTIR-ATR was also used to confirm the graft polymerization as the presence of AM and CS groups on the NIPU, after each step of the surface modification treatment. The changes in glass transition temperatures were studied by differential scanning calorimetry (DSC). NIPUs Tg lied between 5-10°C, associated with the crosslinking degree of 1857.32-14.065 mol/m^3. After the surface modification, Tg decreases to -10.41°C, which may be related to a plasticizing effect, due to the presence of AM and CS related groups.

Unmodified NIPU films showed promising mechanical properties, for future coating purposes, displaying high elongation at break (313.47%). However, CS-modified NIPU films were not suitable for the mechanical test. The thermal stability of NIPU precursors, CSFO, and PAPO as well as of the unmodified and modified NIPU was investigated by thermogravimetric analysis (TGA). After the reaction between CSFO and PAPO, a polymer with enhanced thermal stability was obtained. However, the thermal stability of CS-modified NIPU decreased. Surface modification of NIPU with AM and CS was corroborated throughout each step by measurement of contact angle and scanning electron microscopy (SEM). The contact angle of unmodified NIPU revealed that it had a hydrophobic surface. After the treatment, an improvement of CS modified NIPU hydrophilicity was observed as a decrease in contact angle from 114.2° to 84.2° and the morphological analysis showed topographic changes in the SEM micrographs. CS-modified NIPU films did not show antibacterial performance inhibiting the growth of *S. aureus* and *E. coli*. Additionally, the percentage of cell viability on Detroit ATCC 551 Fibroblasts of the treated and untreated NIPU films was about 75%. Therefore, NIPU films showed potential cytotoxicity.

These results showed a facile and green method to obtain high elastic isocyanate-free polyurethanes, starting from SFO, a renewable resource. However, after the first surface modification treatment, the expected performance of NIPU films as antibacterial biomaterials was not obtained. Therefore, it was presented a promising alternative method to perform the surface modification that involves the use of biomolecules such as heparin, alginate, and chitosan as well as the implementation of a common process as the layer by layer (LbL) self-assembly, which may have a significant role in improving the surface biocompatibility properties of the obtained NIPU films[1]. Besides, NIPU film's flexibility and easy handling might make them useful as coating materials.

Key words:

Non-isocyanate-polyurethane-(NIPU), sunflower-oil-(SFO), chitosan (CH), surface graft modification.

CONTENT

TABLE LIST

FIGURE LIST

Figure 59: Cytotoxic effect of NIUP and CS-NIUP. The bars represent the mean value +/- the standard deviation of the viability percentages of the Detroit cells cultured on NIPU and CS-NIPU vs control cells without treatment.

Figure 60. Conventional optical microscopy of Detroit fibroblasts cultured on the materials and control. a) NIPU 10X, b) NIPU 10X, c) Untreated control 10X.

1. INTRODUCTION

1.1. Significance of the research: Impact and products

Polyurethanes (PU) represent a group of polymers with very high demand in industries, because PU have shown versatile applications in every field of our day-to-day life. They have remarkable mechanical (elasticity, adhesion, hardness, durability etc.) and physical properties. However, the PU production involves the use of highly toxic reagents and requires methods that are environmentally unsustainable and also affects the health of those who handle this type of hazardous substances. Therefore, considering environmental protection and human safety, this work presents a facile and green methodology to synthesize a non-isocyanate polyurethane, starting from renewable sunflower oil-based precursors, taking advantage of the properties of this natural source to obtain polymers with potential coating properties from industrial and economic viewpoints.

On the other hand, for many applications, mainly for biomedical devices, it has been necessary to change or improve the PU surface properties such as adhesion, hydrophilicity and biocompatibility, without modifying the bulk properties of the polymer. Hence, this work presents for first time a two-step methodology to modify the surface of SFO-based NIPU films with acrylamide and chitosan, in order to enhance the surface and biological properties. Other alternative techniques to incorporate different biological characteristics to polymers were proposed considering the advantage of the properties already obtained.

Then, this work focused in evaluate NIPU physicochemical and biological properties before and after being subjected to a surface modification with acrylamide and chitosan, to compare the obtained NIPU performance with the conventional PU.

1.2. Objectives

General objective

- To obtain a non-isocyanate polyurethane based on sunflower oil via green synthesis modified with chitosan as a potential antibacterial biomaterial

Specific objectives

- To synthesize a non-isocyanate polyurethane (NIPU) based on edible sunflower oil through a green method.
- To develop NIPU films modified with chitosan by a surface treatment to provide antibacterial characteristics.

- To evaluate the biological potential of the obtained NIPU as a biomaterial by determining physicochemical, mechanical, antibacterial and cytotoxicity properties**.**

1.3. Polyurethane chemistry:

Polyurethanes (PUs) are the polymers obtained through the reaction between a polyol and a diisocyanate. Because of the diversity of PU precursors and synthetic pathways, these polymers exhibit different macromolecular structures and have versatile applications in many fields of daily use [4]. In fact, the global market volume of PUs was about 24 million tons in 2020 and the volume estimated in the year 2026 may increase to 27.61 million tons [11]. Due to its outstanding physical and mechanical properties, such as toughness, elasticity, adhesion, rigidity, durability, abrasive resistance among many others, it has been used in the manufacture of foams, elastic polymers, sealants, adhesives, paints, coating, and, due to properties such as excellent biocompatibility and biostability, polyurethanes have been applied in the field of biomedical materials [12].

However, despite the wide range of applications and their outstanding properties, the biggest disadvantage of these polymers is that they come from petroleum-derived monomers and their synthesis carries a negative impact on the environment and a health risk. Mainly the monomers derived from isocyanate, are dangerous because they come from phosgene, a toxic and lethal gas that is provided from the reaction between carbon monoxide and chlorine. It is for this reason that the latest advances in PU research focus on the replacement of PU monomers with biological sources that are renewable and friendly to the environment [13].

Polyurethanes were discovered in 1937 by Otto Bayer and his coworkers[14]. Conventional polyurethanes are prepared by polyaddition reaction of diisocyanates with diols[2,15] [16] according to reaction shown in figure 1. The polyaddition reaction of PU synthesis is between the hydroxyl group (−OH) of the polyol and the isocyanate group (−NCO). Therefore, final properties of the PUs such as molecular weight depends on the OH/NCO ratio, the reaction yield as well as the type of diisocyanate and polyol starting materials [16]. PUs can be synthesized either from the polycondensation reaction or also take place by stepwise polyaddition reaction in the presence of either a catalyst or ultraviolet radiation[17].

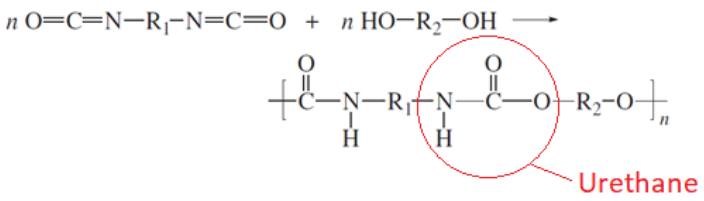

Figure 1. Synthesis of polyurethanes by polyaddition reaction between a polyol and a polyisocyanate[2].

Polyurethanes can have the chemical structure of a thermoplastic or a thermosetting polymer. As chemical composition change according to the specific species of the starting isocyanates and polyols, as well as the synthetic route, physical structure of PU can be that of a rigid solid, a soft elastomer or a rigid or flexible foam[18]. An important fact of these kind of materials is that polyurethanes contain urethane functional groups in the main chain, regardless of the other groups that are present in the rest of the chain [19]. Therefore, this ability to incorporate different functional groups in its structure is the main reason why PUs exhibit a wide variety of properties. It is very common to find different groups such as esters, ethers, amides, urea, among others, in the PU structure[20].

As was mentioned above, the use of conventional PU precursors carries out high environmental and health risks. Therefore, the use of chemical platforms derived from vegetable oils has recently been explored, involving the recovery of polyols that are renewable and derived from natural oils[16]. However, not only polyols should be replaced or obtained PU from other sources. Also, highly toxic isocyanates require new alternatives, as they are derived from phosgene, an insidious odorless poison whose symptoms may appear slowly[21].

For this reason, in consideration of environmental sustainability, alternative methods have been explored to exclude the use of highly toxic substances and employing renewable sources to produce PU [13]. Among these methods is found the synthesis of non-isocyanate polyurethanes, referred as NIPU [22]. Apart from eliminating risks from using isocyanates, this method offers the possibility to replace petroleum-derived chemicals by bio-based compounds.

1.4. Synthesis routes to non-isocyanate polyurethanes (NIPUs)

The first synthesis of NIPU by polycondensation was carried out by Dyer and Scott in 1957[4], who used ethylene carbonates and primary amines to obtain polyurethanes[23]. Moreover, other three synthetic routes to produce NIPU have been reported in the literature, that include step-growth polyaddition, ring opening polymerization (ROP) and rearrangement reactions [13]. Figure 2 shown the synthesis of NIPU by polycondensation and polyaddition. Both pathways prevent the utilization of toxic substances, such as phosgene, aziridines, azides, carboxamides, among others [24].

The NIPU obtained by polycondensation methods have a linear structure, and generally hydroxyl groups are absent in the structure of final polymers. Figure 2 (a) shows this synthetic route. Polycondensation is performed at high temperatures (150°-220°C), because it is necessary to remove the byproduct of the reaction mixture. NIPU obtained by polycondensation method has lower Mn than NIPUs synthesized by solvent-free

polyaddition of cyclic carbonates and diamines[12]. By other hand, the polyaddition is performed generally at medium temperatures (60°-80°C), and the presence of the hydroxyl groups in the polymer chain permits the formation of intra molecular hydrogen bonds, resulting in increased mechanical properties and chemical resistance of the final polymer[3].

According to literature, the formation of byproducts is probably the reason for low molecular masses of NIPU[3]. The NIPU with high molecular masses can be probably obtained by low temperature reactions and the presence of a catalyst, which activates the cyclic carbonate and not the amine during the reaction[25]

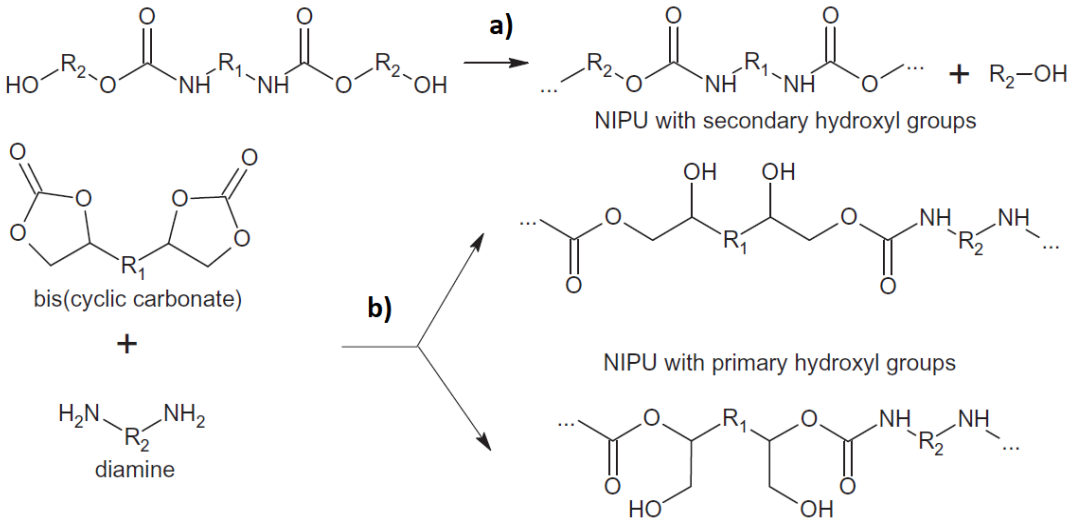

Figure 2: Synthesis of NIPU by a) polycondensation and b) polyaddition, taken from ref [3].

Therefore, even though NIPU can be obtained by different routes, polyaddition of multifunctional cyclic carbonates and primary amines or polyamines to produce NIPU is more economic and can be carried out without solvents or catalysts and does not generate by-products [3]From an industrial point of view, the NIPUs obtained through the polyaddition, turns out to be the most promising alternative to produce these materials. Because the polyaddition reaction can be carried out at ambient temperatures or to a moderately high temperature (60–80 °C) can greatly help in achieving high conversion rate[23], also a wide range of biodegradable, renewable and sustainable resources can be converted into the corresponding bio-based precursors suitable for this reaction[26]. However, the versatility of this route lies in the facts that no require hazardous reagent and don't generates emission of volatile organic compounds, therefore the isolation or avoidance of certain kind of conditions are not necessary in this reaction system and materials produced by this synthetic pathway have showed high potential for coating purposes[27]. In fact, considering excellent benefits offered by this route, the main PU industrial sections such as BASF, Bayer,

Dow and Huntsman had invested in this promising reaction and its potential growth in the global market[28].

The ammonolysis of cyclic carbonates to prepare NIPU that gives rise to polyhydroxyurethanes, is governed by ring opening reaction of cyclic carbonates with amines[18]; this reaction entails the formation of urethane and a β-hydroxyl group. As is shown in Figures 2 and 3, it is clear that the structure of NIPU differs from that of conventional PUs, due to the presence of both primary and secondary hydroxyl groups pendant on the main polymer chain[29]. These secondary hydroxyl groups are responsible for the development of intermolecular hydrogen bonding than can result in greater chemical stability and excellent mechanical properties, besides to offer the possibility for further modification of the hydroxyl groups, grafting the chain with chemical and biological functionalities [4].

Garipov et al[30] in 2003 proposed a three-step mechanism for the ring opening of a cyclic carbonate, as shown in figure 3. In the first step, the nucleophilic attack of the amine on the carbonyl of carbonate, yields a tetrahedral intermediate and is considered as a limiting step of the reaction. In the second step, a secondary amine carries out the deprotonation of the tetrahedral intermediate. In the third step, the negative charge in the oxygen forms a carbonyl, which breaks the neighbor carbon-oxygen bond, and yields the hydroxyurethane. According to the geometry of intermediate molecules, this opening reaction leads to the production of repeating units with primary or secondary alcohols [4].

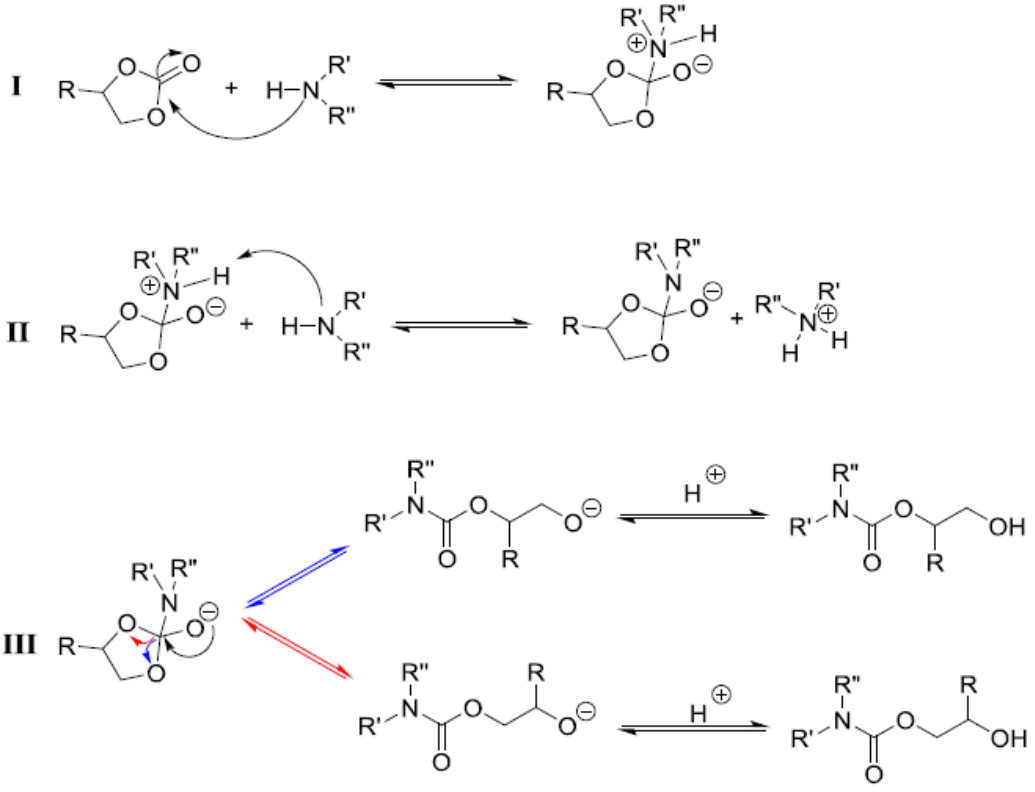

Figure 3: Three steps mechanism of cyclic carbonate/amine reaction taken from ref [4].

Although NIPU synthesis route represents a more sustainable alternative to produce PU, it is important to note that cyclocarbonates and commercial amines are also derived from petroleum-derived sources. Therefore, considering that fossil resources are depleted day by day, the search for biologically based and renewable precursors is imperative for the scientific community[31].

Therefore, one useful, economic, and easy alternative is to replace fossil derivatives with renewable sources such as vegetable oils, which can be used as reliable platforms to produce NIPU with different structural and functional properties and that have been widely used in the synthesis of polymers[31,32].

According to the type of vegetable oil that is used as a starting material, NIPUs with different structures can be synthesized. Many research groups worldwide have intensely investigated the synthesis of NIPU networks from oils obtained from many different plants such as soybean [33] , linseed [34] , sunflower[35], and palm [36], using different catalysts.

1.5. Vegetable oils as green alternative substrates to obtain bio-based non-isocyanate polyurethanes

Vegetable oils have saturated fatty acids such as palmitic and stearic as well as monosaturated fatty acids such as oleic or polyunsaturated fatty acids such as linoleic or linolenic, which differ in the number of unsaturation present in the chain as well as its length, like is shown in Figure 4. Therefore, the physical and chemical properties of vegetable oils are determined by fatty acid composition, chain length and number of double bonds in the chains, which will depend on the source of the oil. [37].

Vegetable oils have been used widely for polymer synthesis because, the triglycerides in their structure presents several highly reactive sites including: 1. carbon-carbon double bond, 2 and 3 allylic position (including mono allylic and bis-allylic positions) and 4. ester group in triglycerides and fatty acids [38].

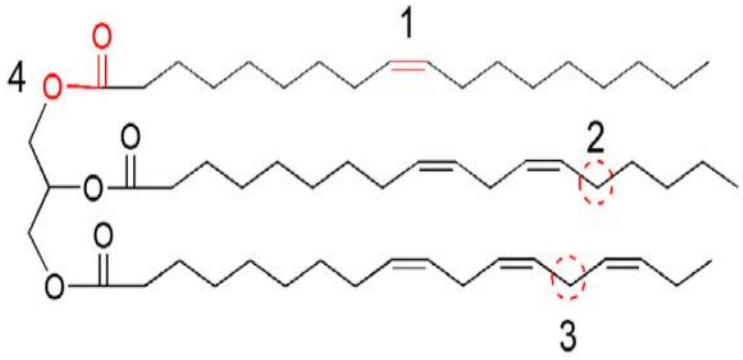

Figure 4: General structure of triglyceride and reactive sites taken from ref [5].

Generally, all vegetable oils contain C=C double bonds and esters that can be functionalized by processes such as ozonolysis, hydroformylation, epoxidation, followed by oxirane ring opening transesterification, among many other chemical modifications that can be made to different unsaturated vegetable oils to obtain functional polymers[39], which demonstrates that these kind of reactions provide many available possibilities to chemically modify the unsaturated vegetable oils triglycerides to synthesize NIPU monomers[35].

Vegetable oils have many combinations of fatty acids profiles. Particularly, sunflower seed oil (SFO) contains a combination of monounsaturated and polyunsaturated fatty acids with low saturated fatty acids. It has several highly reactive sites, including carbon-carbon double bond, allylic position (including mono allylic and bis-allylic positions), and ester groups in triglycerides and fatty acids[38], that can be chemically modified. Due to the higher level of unsaturation compared to some other vegetable oils[40], SFO was chosen as raw material for the present non-isocyanate polyurethane (NIPU) synthesis, its high contents of unsaturated fatty acid can be converted into epoxy fatty acid by conventional epoxidation. The epoxidized vegetable oil can act as a raw material for synthesis of variety of chemicals including polyols, glycol, carbonyl compound, lubricants, plasticizers for polymer etc. because of their respectable oxirane oxygen content and high reactivity of oxirane ring[39]. In the research of vegetable oil-based alternatives, as a substitution for petrochemical reactions, fatty epoxides are very important because they can be used as intermediates to produce a variety of chemicals[41]. Therefore, the epoxidized sunflower oil ESFO was selected as a main precursor for the synthesis of the NIPU monomers, considering that ESFO can react both with CO_2 and with diamines to produce both cyclic carbonate and polyamine, respectively.

1.5.1. *Synthesis of epoxidized vegetable oil*

Double bonds present in vegetable oils can be used as reactive sites to be functionalized by epoxidation, converting the double bonds into oxirane rings[38]. Figure 5 illustrates the epoxidation reaction of a vegetable oil triglyceride. During the reaction, a weak acid, such as acetic acid or formic acid, transfers oxygen atoms to the double bonds of the unsaturated fatty acid chains, forming oxirane rings in the aqueous phase of the reaction system [6].

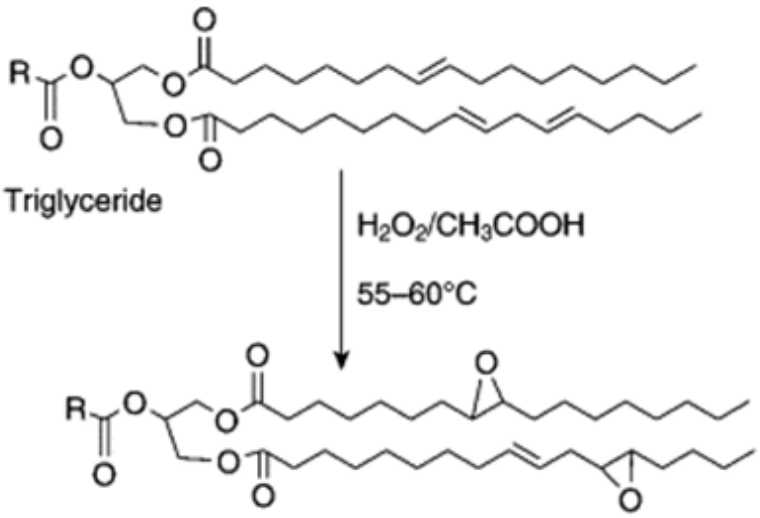

Figure 5. Epoxidation of vegetable oil reaction [6].

The properties of polymers derived from epoxides of edible oils depend closely on several process variables, including the characteristics of the raw material, the type of catalyst, the reaction temperature, the molar ratio of the reagents and the speed of agitation of the product system[39]. Therefore, vegetable oils with a higher content of unsaturation in their fatty acids produce polymeric precursors with greater functionality, which can subsequently be related to the crosslinking density of the polymers as well as variations in the thermal and mechanical performance of the final materials [38].

1.5.2. Cyclic carbonate intermediate for NIPU synthesis

The catalytic fixation of carbon dioxide by carbonation of oxiranes is considered a green chemistry route. It consists of a simple reaction, with high yield and whose reagents are harmless, to obtain di and polyfunctional cyclic carbonates, which have been used as precursors for the synthesis of NIPU [7].

The reaction is carried out in the presence of a catalyst, at specific pressure and temperature conditions. Different catalytic systems have been reported, with alkali metal halide, quaternary ammonium halides and polystyrene bound quaternary ammonium salts being the most effective[42]. Also, different authors have worked with temperatures from 100 to 140°C as well as pressures from atmospheric to supercritical [33–35].

Generally, carbonated vegetable oils are obtained by converting the oxirane rings of epoxidized vegetable oils with carbon dioxide in the presence of alkyl ammonium bromide catalysts. Where the bromide of the catalyst attacks the epoxide promoting ring opening followed by a nucleophilic attack of the alkoxide on carbon dioxide. Subsequently, the ring

closure reaction of the carboxylate that is obtained yields the five-membered carbonate [13]. Figure 6 illustrates the previously described mechanism.

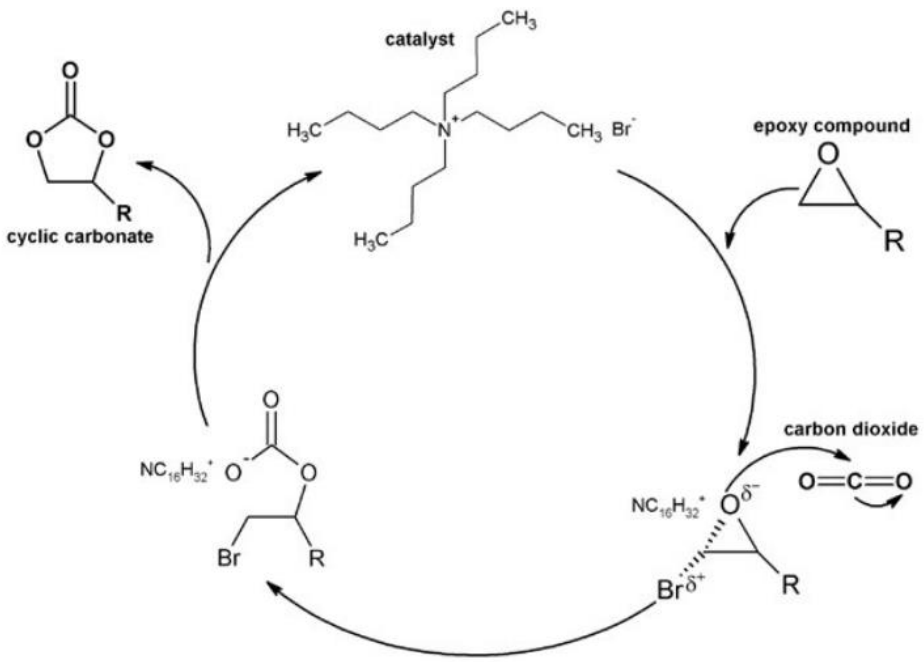

Figure 6: Mechanism for generation cyclocarbonates by the conversion of oxirane rings with carbon dioxide in the presence of TBAB as a catalyst[7].

The synthesis of polycarbonates through the mechanism described above, from different types of vegetable oils and various conditions, is been reported. Tamami et al[42], successfully obtained carbonated soybean oil from its epoxidized equivalent by incorporating CO_2 at atmospheric pressure and a temperature of 110°C in the presence of tetrabutyl ammonium bromide (TBAB) as a catalyst. It was demostrated that the carbonate obtained could easily react with different amines to form NIPU[42]. Using a similar strategy but using supercritical conditions(100 bar, 120°C), Poussard et al [43], developed the reaction between epoxidized soybean oil with CO_2 using TBAB as catalyst. The soybean cyclocarbonate obtained was subsequently used for the reaction with short amines, that were previously derived from biobased fatty acids, obtaining a fully biobased thermoplastic NIPU[33]. On the other hand, Doley and Dolui[44], used sunflower oil, instead of soybean or other vegetable oils, to obtain epoxidized analogus. This compound then reacts with CO_2 at the same supercritical conditions of the other studies in the presence of TBAB to form a sunflower oil cyclocarbonate, which was used to obtain NIPUs. These authors obtained an epoxide conversion of 90% with high selectivity[35], showing that TBAB as a catalyst, and the pressure and temperature conditions studied are optimal for the synthesis of cyclocarbonates from vegetable oils.

Within the catalyst systems, that have been employed to carry out carbonation reactions, such as halogenated salts, halides, metal complexes, ion-exchange resins and ionic liquids

[45], quaternary ammonium salts, such as TBAB, were selected because ensure satisfactory acceleration of the reaction[13]. Therefore, TBAB was selected as catalyst because have been widely used for this synthesis. In this reaction, the halide group (Br-) opens the epoxy ring, leading to an alkoxide ion that attacks CO_2 to give five-membered cyclic carbonate rings[46].

This approach for CSFO synthesis is promising because implies a path to disposal of a high amount of CO_2, considered a greenhouse effect gas. On the other hand, CO_2 is a highly attractive and inexpensive building block, that could be converted into high-value organic molecules such as CSFO [47].

.

1.5.3. Polyamine polyol intermediate for NIPU synthesis

Modified vegetable oils, particularly epoxidized vegetable oils, have been used to obtain various types of compounds and polymers such as polyamine polyols, which can also be used as precursors for NIPU synthesis. They also play a fundamental role in the ammonolysis reaction and the final properties of the obtained polymers [48].

The reaction between an epoxidized vegetable oil and diamines involves the ring-opening reaction and ammonolysis, where the former contributes to chain growth and the latter is expected to favor the breakage of the glycerol center of the epoxidized oil. This synthetic pathway is illustrated in Figure 7.

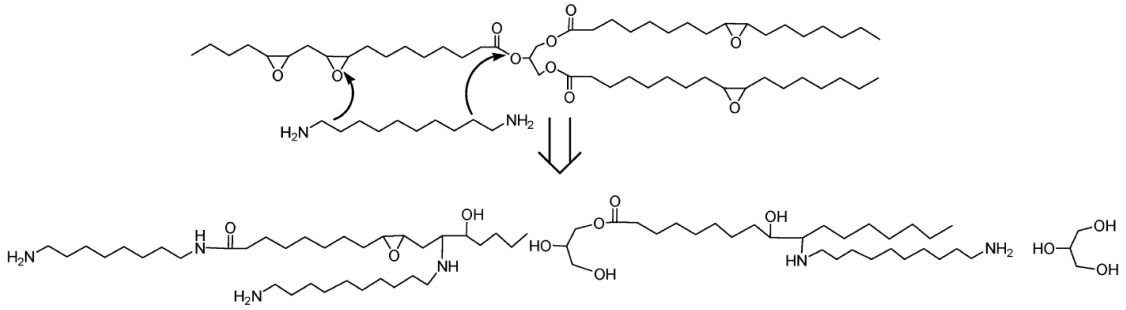

Figure 7. Poly amine polyol formation reaction[8].

Wang et al[8], synthesized poly(epoxidized soybean oil-co-decamethylene diamine) (PESD) from epoxidized soybean oil and decamethylene diamine (DDA) in different ratios. The authors found that when a molar ratio of DDA to ESO is 2:1, polymers with the highest molecular weight were obtained and were more appropriate for further processing. In addition, the optimum temperature reported for this reaction is 130°C, because at lower temperatures long reaction times are taken, and higher temperatures might lead to amine loss. This reaction is carried out until the product begins the crosslinking reaction[8]. The obtained product from this synthesis is a thermosetting polymer, which is not suitable for further processing, but it can be used in a secondary process as a biobased amine source for the NIPU synthesis, providing different properties to the resulting material from those

obtained with commercial amines. Recently, it has been reported that secondary amines can react under certain conditions with carbonates to form NIPU [49].
In a recent study, Farhadian et al[22], focused their investigations on the use of vegetable oils to synthesize non-isocyanate poly (ester amide/urethane) networks. They synthesized three amines from castor oil and oleic acid; then, they synthesized a polyamine polyol from sunflower oil, which was also used to produce carbonated sunflower oil (CSFO). Finally, they obtained NIPU networks from the reaction of CSFO with bio-based amines. This study demonstrates that bio-based amines derived from ester, amide, amines, and polyamine-polyols groups without any rigid and aromatic structures, can improve thermal stability of NIPU networks, besides, NIPU synthesized by this method can form strong hydrogen bonds[50].

In conclusion, this type of approach offers the possibility of synthesizing a NIPU obtained via green synthesis, whose biological response such as, antibacterial properties could be improved by surface modification.

1.6. Surface modification of polyurethanes for antibacterial purposes

PUs have shown suitability for biomedical applications and are used in this area since decades. Besides, the wide spectrum of physical, chemical, mechanical and structural properties of PU as well as the diversity in their structure/property relationship, PUs are highly biocompatible biomaterials[51]. PUs biocompatibility is related to self-properties such as long-term stability, to simple, inert materials that do not produce toxic effects or to surfaces that interact with tissue, allowing a full tissue integration [52]. Therefore, PUs play a very important role in the development of medical devices such as blood bags, vascular catheters, heart valves, grafts, and successfully used in clinical trials .[53]

However, biomaterials made from PU perform moderately well in bacterial adhesion studies compared to other polymers and have been shown to be susceptible to bacterial colonization, entailing a serious risk of infection from the use of PUs based medical devices [54].

Unfavorable biofilm formation due to bacterial adhesion decreases the expected functions of a biomaterial and can cause pathogenic side effects [55]. Therefore, current strategies to obtain antibacterial PU generally focus on designing bactericidal or bacteriostatic surfaces that eliminate, repel, or resist bactericidal attachment through the incorporation, coating or surface modification with antibiotic agents, to generate this effect in the materials[54]. In this work it is proposed a surface modification strategy, since the chemical characteristics of the materials surface play an important role in the performance of biomaterials.

1.6.1. Grafting techniques for surface modification of polymers

The surface modification of biomaterials allows to improve characteristics such as composition, area, energy, wettability, thickness, roughness of the surface, which are critical factors that affect protein adsorption and thereby their antibacterial activity[56].

Modifications are made on the surface of materials because the interaction between the cell and the material is mainly modulated by the superlayer of a material, while general properties, such as mechanical strength, must be preserved [57]. Surface techniques to improve antibacterial activity and other biological properties such as hemocompatibility include chemical treatments such as surface oxidation, introduction of reactive groups, fluorination, surface grafting, glow plasma discharge, photo-oxidation, as well as surface grafting, and UV irradiation polymerization[58].

Photo-induced polymerizations, using ultraviolet light, proceed through a chain reaction mechanism consisting of the propagation of an active center by interaction with a monomer. The active center can usually be a radical, a cation and rarely an anion. These photogenerated species are considered the true initiators of the polymerization of a reactive monomer, which is usually carried out by means of addition to multiple bonds or ring opening processes. The photoinitiation step of the radical polymerization reaction usually requires the presence of a photoinitiator, which absorbs the exciting light and leads to the production of radicals. Benzophenone has been widely used as a photoinitiator in the surface modification of polymers[59]. The UV induced radicals can abstract hydrogens from polymers and, the so formed polymeric radicals may lead to grafting polymerization with other monomers[60].

The methods described above have been used to introduce hydrophilic compounds on PU surfaces. Zhu et al[61]. studied the immobilization of hydrophilic polyacrylamide (PAMm) on porous PU scaffolds by photooxidation and UV irradiation polymerization techniques of PAMm. The results showed, graft polymerization of hydrophilic PAMm on PU, used as a surface modification method, is effective in improving the cytocompatibility of PU[61]. Otherwise, Feng et al[62], graft benzophenone (BP) on polycarbonateurethane surfaces and, by using ultraviolet light, induced the polymerization of poly(ethylene glycol) monomers with different molecular weights to improve hemocompatibility and increase hydrophilicity[62]. In particular, the photografting of AM on NIPU surface is showed in Figure 8. The benzophenone groups in the photo-initiator treated NIPU films would attract hydrogen atoms from the urethane under UV irradiation. The most possible position to lose hydrogen atoms in the NIPU would be the hydrogen bonded to the nitrogen atom of the urethane structure. The formed radical on NIPU could also initiate the polymerization of acrylamide during the polymerization process[60].

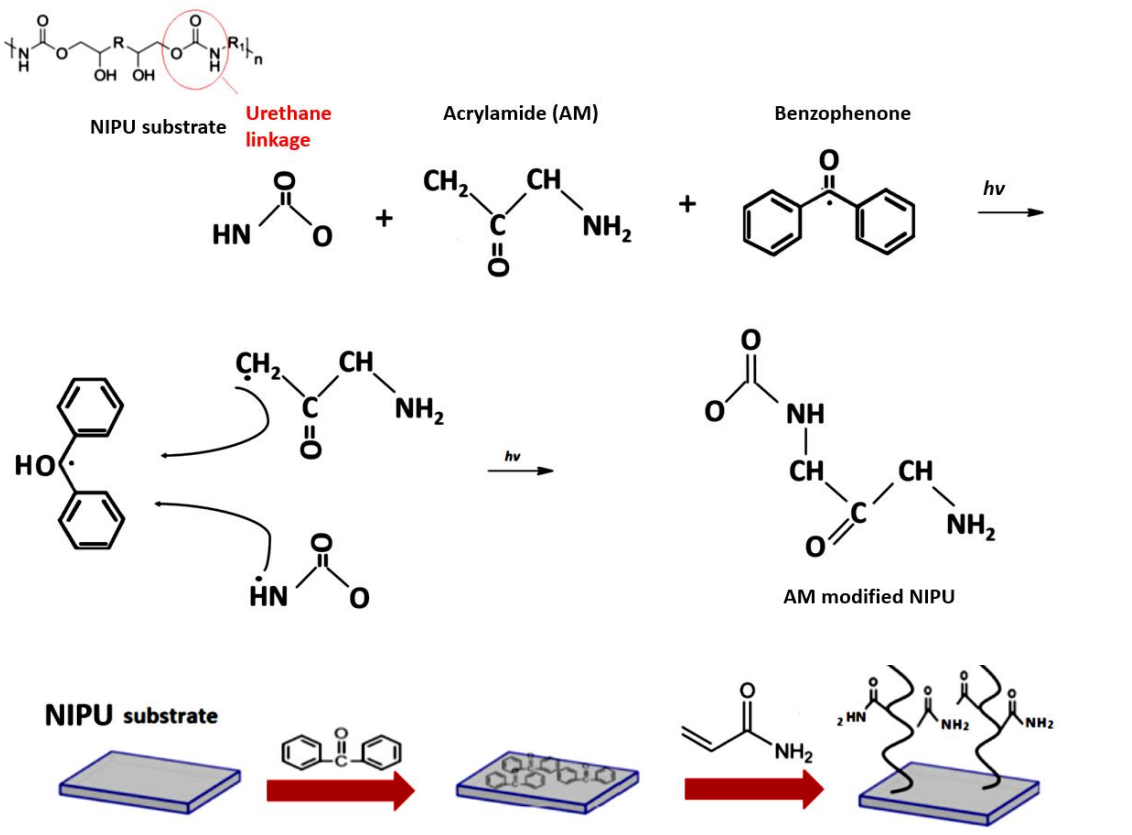

Figure 8: Scheme with reaction of acrylamide grafting on benzophenone group cross-linked NIPU films using UV radiation.

Reaction of polyacrylamide grafting on benzophenone group cross-linked cotton fabric

On the other hand, the incandescent plasma discharge is a constant bombardment of the surface with active molecules such as free electrons, radicals, excited atoms and neutral particles, altering the surface chemistry, breaking bonds of surface molecules and generating new ones. Therefore, a chemical change occurs on the surface while the main structure of the substrate remains unchanged. Depending on the type of gas used, the power applied, the duration of the plasma, it is possible to change the hydrophilicity of the surface or create a layer that is completely different from the bulk structure[58].

Several studies have shown that graft copolymerization of polyurethanes with hydrophilic vinyl monomers, such as acrylic acid or acrylamide is an appropriate method to enhance surface hydrophilicity, and improve its hemocompatibility [63]. Besides, these techniques have been used to modify polymeric surfaces with antibacterial properties, for example, it is reported that chitosan immobilized on acrylic acid grafted on a polypropylene fabric, exhibited antibacterial activity[64].

Many functional groups such as metal (silver) ions, quaternary ammonium or phosphonium salts, triclosan and N-halamine have been used for antibacterial purposes over the years. Natural biopolymers such as polysaccharides are a sustainable and renewable source for the development of bioactive materials, with outstanding properties [65]. Among these, chitosan is found, which has been employed as a functional material in a wide range of applications such as in control drug delivery, wound and tissue healing material [66].

1.6.2. Chitosan chemistry

Chitosan is a copolymer that contain glucosamine and N-acetylglucosamine units. It is a natural, non-toxic and biocompatible biopolymer obtained from deacetylation of chitin, which is extracted from the exoesqueletons of crustaceans. Chemical structure of chitosan is shown in Figure 9 [9]. Chitosan is a cationic polysaccharide when dissolved in acidic solutions and also a weak electrolyte, whose antibacterial activity has been highlighted in recent years [67]. Additionally, chitosan has shown high moisture absorption performance, since its main chain contains amino and hydroxyl groups, which provide chitosan with active properties. The D-glucosamine linkage in its structure consists of a rigid unit that increases the crystallinity and hydrophobicity of chitosan and makes it a valuable compound for surface coating and desirable for biomedical applications[66]. Therefore, chitosan due to its biological significance, can be considered as a sustainable alternative to other antimicrobial agents.

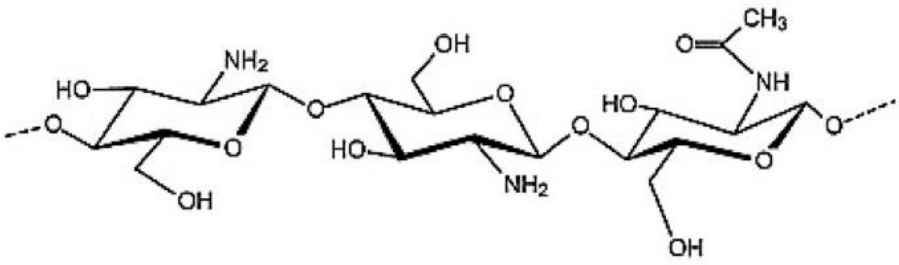

Figure 9: Chemical structure of chitosan [9].

1.6.3. Chitosan antibacterial mechanism

Exact mechanism for the antibacterial action of chitosan is still unknown. However, different approaches have been proposed. Many studies suggested that the antimicrobial activities of chitosan and its derivatives depend on numerous intrinsic and extrinsic factors, such as pH, microorganism species, presence, or absence of metal cations, pKa, molecular weight (Mw) and degree of deacetylation (DD) of chitosan, where the polycationic structure of chitosan is a fundamental requirement for its antibacterial activity[68].

The main mechanism for antimicrobial activity of chitosan should be due to the interaction between the positively charged amino (-NH_3) groups of chitosan and the negatively charged carboxylate (-COO-) groups on the surface of bacterial cell membranes[69] (such as gram-negative lipopolysaccharide bacteria and cell surface proteins)[70]. Therefore, higher positive charge density leads to strong electrostatic interaction and, the positive charge in chitosan or its derivatives is associated with DD, which affect positive charge density[68]. This strong interaction between positively charged chitosan molecules and negatively charged microbial cell membranes causes the leakage of proteinaceous and other intracellular constituents out of the cell membrane [54].

There are studies where chitosan has been applied to polyurethane surface to provide antibacterial activity. For example, Ayati Najafabadi et al[71], made the surface modification of PU films with heparin and chitosan, by two step plasma treatment, showing a great enhancement of PU films biocompatibility[71]. It is noteworthy that the NHCOO group present in PU resembles the peptide linkage (NHCO) present in the protein. Therefore, the incorporation of chitin or chitosan could improve the biocompatibility and reduce the cytotoxicity of the resulting polyurethane[9].

Chitosan also can be blended with other polymers as in the coating applied onto the surfaces. Yang et al[72]. reported on a four-step surface modification method to create a thin lubricious layer of chitosan/poly (vinyl alcohol) hydrogel on the polyurethane catheter surface, which possessed significantly better antibacterial effects against *Staphylococcus aureus, Pseudomonas aeruginosa*, and *Escherichia Coli* [72].

On the other hand, chitosan has been attached onto polyurethane surfaces by covalent immobilization. Kara et al[55]. synthesized and modified polyurethane film surfaces with chitosan. The modified polyurethane surfaces were more hydrophilic and rougher, with strong antibacterial activity against *Staphylococcus aureus* and *Pseudomonas aeruginosa*, [55].

In conclusion, $NHCOCH_3$, NH_2, NHCOO groups present in chitosan and polyurethane can impart bioactive properties beneficial for biomedical applications [72]. Therefore, this work consists in development of sunflower oil based NIPU films, starting from both precursors derived from epoxidized sunflower oil, and modified with acrylamide and chitosan using a two-step methodology that includes the by a covalent attachment to the polymeric surface, with the aim to evaluate the performance of the resulting material as a potential antibacterial biomaterial. Starting from AM-modified NIPU films, glutaraldehyde could be used as a crosslinking agent to bind the chitosan moieties to the polymeric films surface. The reactions involved in this step of the modifications are showed in figure 10.

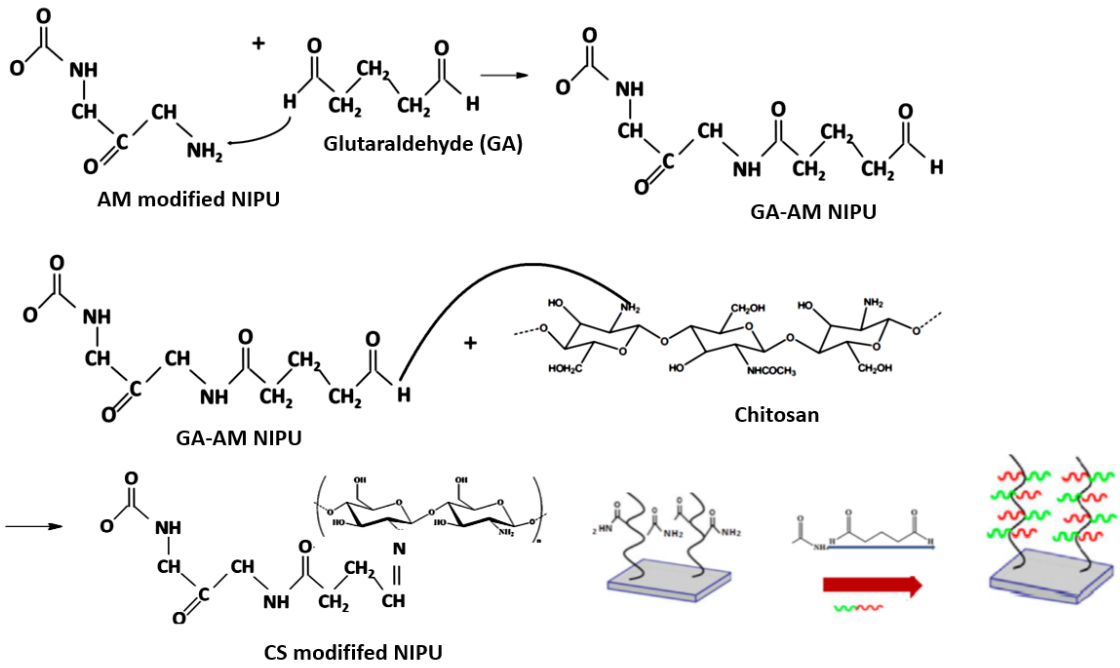

Figure 10: Reactions scheme for the chitosan immobilization onto AM-grafted NIPU films.

MATERIALS AND METHODS

2.1. Materials

Edible sunflower oil (SFO) was purchased from a local market. Chitosan, medium molecular weight was purchased from Sigma-Aldrich, batch # STBJ3281. Hydrogen peroxide (H_2O_2, 30%, w/v), formic acid (98%), tetra-n-butyl ammonium bromide (TBAB) and ethylenediamine (EDA), were purchased from Merck Chemical Co. Glutaraldehyde solution (GA, 25% aqueous solution), acrylamide (AM), benzophenone (BP), glacial acetic acid, and methanol were supplied by Sigma Aldrich. CO_2 gas with a purity of 99.99% was supplied by Cryogas. All the materials were used as received without any further purification.

The culture medium and supplements used for *in vitro* evaluation of the antibacterial activity of the materials were BHI Broth (Becton Dickinson), agar Luria Bertani (Becton Dickinson), saline solution (Corpaul), and salt phosphate Buffer (Chem Cruz).

For the *in vitro* evaluation of the cytotoxicity of the materials the cell line was Detroit ATCC 551 (ATCC®CCL 110), purchased from ATCC (American Type Cell Collection) cell bank. The culture medium and supplements used were DMEM culture medium (Sigma), fetal bovine serum (Invitrogen), trypsin 1X (Invitrogen), and (3-(4,5-dimethylthiazol-2-yl)-2,5-diphenyltetrazolium bromide (MTT) purchased from Sigma.

2.2. Raw material characterization

2.2.1. Sunflower oil characterization

The main starting material for NIPU synthesis, was edible sunflower oil (SFO). Reactive sites in oils are mainly related to the fatty acid composition and double bonds present in the dominating fatty acids of the oil. Unsaturation content measured by iodine value, and fatty acid composition, strongly influence the application of SFO as a precursor for the polymeric synthesis. There are many titration methods as well as spectroscopic techniques available to characterize both, fatty acid composition and iodine value of vegetable oils[73,74]. The methods used in the present work are described below:

2.2.1.1. Determination of SFO Fatty Acid Composition

The fatty acid composition (FAC) allows to estimate the molecular weight of the starting oil. Generally, it can be determined by gas chromatography (GC). However, this method uses procedures that are laborious, time- and chemical-consuming [10]. Therefore, the common unsaturated fatty acids (oleic, linoleic and linolenic acids) present in SFO were quantified by protonic nuclear magnetic Resonance (^{1}H-NMR), a non-destructive and fast technique to get information based on distinct peak shift, intensity and peak area[75]. Therefore, this

technique was a very useful tool for simultaneous determination of both the unsaturation degree and the proportions of the different acyl groups of the SFO[76].

Considering that the signals of the terminal methyl group of linolenic acid are shifted downfield from the corresponding signals in the other fatty acids, permitting their separate integration and quantification of linolenic acid fatty acid allowing to determine the relative FAC of many unsaturated vegetable oils[77].

There are many different approaches and mathematical approximations that have been used to determine the FAC developed in literature[78–80] , because the area of the signals in the ^{1}H NMR spectrum is proportional to the number of hydrogens of each type in the sample of oil[10]. Therefore, the relative proportions of unsaturated and average saturated fatty acids of starting SFO used in this work were determined by the ratios of the integrated areas of some representative ^{1}H NMR signals spectrum that will be presented in the results and discussion section with their respective assignment.

For the present work, the approximation propesed by Castejón D. et al[78], which consider that each acyl chain contains two methylenic protons in α-position to the carboxyl group was used. This approximation contemplate exclusively the fatty acid chain to obtain the proportional intensity between proton signals[78]. An outline of the calculation method is as follows:

$$\omega - 3\ (linolenic) = \frac{\mathrm{B}}{\mathrm{A+B}} \quad (1)$$

$$\omega - 6\ (linoleic) = \frac{3*\mathrm{G}-4*\mathrm{B}}{3*\mathrm{F}} \quad (2)$$

$$\omega - 9\ (oleic) = \frac{\mathrm{E}}{2*\mathrm{F}} - \omega - 3\ (linolenic)\ \omega - 6\ (linoleic) \quad (3)$$

Equations (1)-(3) consider the total fatty acid content as sum of the methyl signals A and B using the integral value of some other ^{1}H NMR signals.

2.2.1.2. *Iodine value:*

The iodine value (IV) is a chemical parameter of the relative degree of unsaturation present in the components of oil. It is determined from the reactivity of the double bonds of the triglyceride. The most widely used procedure is the Wijs method, where the iodine value is obtained by quantifying the iodine monohalide incorporated in samples [73] and is expressed in terms of centigrams of iodine absorbed per gram of sample[81]. Using Wijs method, the traditional IV of SFO was measured according to ASTM D 5554-95 standard method[81].

However, this procedure is relatively expensive, slow, and it consumes a significant amount of reagents, producing wastes that require specific treatment and it is time-consuming because involves several steps [82]. Instead, ^{1}H-NMR as was mentioned above is a non-destructive technique that have been widely used to estimate iodine value and also was

used to determine relative iodine values of the starting SFO employing different approximations used in the literature[0,78,80,81,100].

The proton signals that were used for quantifying the unsaturated fatty acids, were those of olefinic protons (5.3–5.4 ppm), protons attached to the bis-allylic carbons (2.7–2.8 ppm), protons attached to the allylic carbons (2.0–2.1 ppm) and the terminal methyl group protons (0.8–0.9 ppm). Furthermore, the amounts of saturated fatty acids can be determined through the signal of the methylene (CH_2) protons at 1.2–1.4 ppm[77]. The procedure satisfactorily reflects the overall amount of saturated fatty acids in a sample, compared to similar studies, reported on literature, that use analytical and chromatographic techniques[10,77,78,83,84].

Iodine value obtained by the standard chemical (Wijs) method was compared with those determined by ^{1}H-NMR[73] technique using different approximations developed in literature [85–87] that will be discussed in the results and discussion section.

2.2.2. Chitosan characterization

The antibacterial agent chosen for the surface modification was chitosan. Then, to determine molecular conformation as well as the reactivity of the starting chitosan and, considering that chitosan is a partially deacetylated derivative of chitin, the molecular weight and degree of deacetylation (DD) are the most important properties of chitosan to determine.

2.2.2.1. *Degree of deacetylation (%DD)*:

The degree of deacetylation (DD) influences chemical, physical and biological properties of chitosan. The potentiometric titration proposed by Broussignac in 1968 is one of the simplest methods[88], and was used in this work. Chitosan was dissolved in a known excess of hydrochloric acid, then the solution was titrated potentiometrically with sodium hydroxide, which give place a titration curve that have two inflection points which represent the equivalent points of the titration of excess hydrochloric acid and the titration of protonated chitosan, respectively[89]. Ingman and Still[90] derived a the simplified form of the linear function that was used for linearizing the titration curves, as is showed in equation 4.

$$V = V_e - \left(\frac{V_0+V}{C_B}\right)([H^+] - [OH^-]) \quad (4)$$

where V_0 was the initial volume of chitosan solution, V was the volume of strong base added, and C_B was the concentration of titrant solution. If the function was plotted against V; a straight line was obtained that intersects the V-axis at V_e; the equivalence volume. DD is calculated from the equation 5 [91].

$$DD(\%) = \frac{d}{\left(\frac{W-161d}{204}+d\right)} * 100 \quad (5)$$

$$d = \frac{(C_1V_1 - C_BV_e)}{1000} \text{ (6)}$$

2.2.2.2. Measurement of viscosity average molar mass from intrinsic viscosity, [η]:

Considering that the application of chitosan is limited by its molecular weight, many times resulting in its low solubility in acidic aqueous media, it is important to determine this property of the starting chitosan [92].The determination of molecular weight by intrinsic viscosity measurement was used because is a rapid and easy method that have been widely used for chitosan.

The viscosity average molar mass for chitosan was measured using a 0.1 M acetic acid / 0.2 M sodium acetate solution. An Ostwald type viscosimeter (diameter = 0.50 mm) was used at a controlled temperature of 25°± 0.1 C. Relative viscosity was measured to a series of solutions with concentrations in the range between 0.005 and 0.03 g/dL.

Intrinsic viscosity, $[\eta]$ was determined using the reduced viscosity (to fit the Huggins equation) and inherent viscosity (to fit the Kraemer equation). Huggins equation is derived from a virial expansion of the specific viscosity in powers of the intrinsic viscosity, while Kraemer equation results from an expansion of the inherent viscosity.

The value of intrinsic viscosity was used to calculate the viscosity average molecular mass, M_V, through the Mark-Howink-Kuhn-Sakurada equation:

$$[\eta] = KM_V^a. \text{ (7)}$$

For this experimental set, the found reported values for the parameters were: a = 0.93 and K = 1.81 X 10^{-5} dL g^{-1}, given by Rinaudo and Kasaai[92,93].

2.3. Chemical characterization using spectroscopic techniques

Spectroscopic methods, have been used for analytical determination of different parameters of vegetable oils such as iodine value and fatty acid composition, besides yield information about all the components in a mixture in only one spectrum, usually without the need to derivatize or destroy the sample[77].

2.3.1. Proton nuclear magnetic resonance (^{1}H-NMR)

SFO and its derivatives were characterized by ^{1}H NMR spectroscopy. ^{1}H NMR analysis were performed on a Brucker AMX-400, 300 MHz spectrometer. Approximately 30 mg of sample

was dissolved in 0.6 mL of deuterated chloroform ($CDCl_3$) as solvent. The resulting solution was placed in a 5-mm diameter NMR tube. ^1H NMR spectra were taken with 7.5-degree pulse angle, 2.5 s recovery delay, and 16 scan and resolution 4 cm^{-1}.

2.3.2. Attenuated total reflectance-Fourier transform infrared spectroscopy (ATR-FTIR)

Each step of the methodology was characterized by ATR-FTIR using a Perkin-Elmer Spectrum Two FTIR Spectrophotometer, with a Smart Orbit diamond attenuated total reflection (ATR) accessory. Absorption spectra were acquired between 4000-500 cm^{-1} and the signal averaged 16 scans, with resolution 4 cm^{-1}.

2.4. Synthesis of sunflower oil-based non isocyanate polyurethanes (NIPU)

Once the required properties of the starting materials were determined. The first step of the synthetic pathway is the epoxidation of SFO to obtain the precursors for NIPU synthesis as will be explained below. After to characterize the structure and unsaturation degree of the starting SFO

2.4.1. Preparation of epoxidized sunflower oil (ESFO)

For edible SFO some authors have reported similar conditions for the epoxidation reaction [35,94–96]. Epoxidation of sunflower oil was carried out in the presence of a mixture of formic acid and hydrogen peroxide. The molar ratio of double bond: formic acid: hydrogen peroxide was 1:0.5:3. The formic acid was added to SFO in a three-neck round-bottom flask and the reaction temperature was raised to 60 °C under continuous stirring conditions of 1400 rpm. Then, H_2O_2 was added dropwise to the reaction mixture[94]. The organic acid is converted to peroxoacid and then regenerated; as hydrogen peroxide is consumed in the process, an excess relative to double bonds was used for ESFO synthesis [94,35]. The reaction time fixed at six hours[96]. The organic phase of the reaction mixture was decanted, cooled to room temperature, and washed with distilled water followed by 5wt% of sodium bicarbonate solution repeatedly until neutral pH was attained. Epoxidized sunflower oil (ESFO) was obtained after drying with $MgSO_4$ and filtered [97]. The experimental arrangement used for ESFO synthesis is shown in figure 11.

Figure 11: Experimental arrangement of the epoxidation reaction.

Oxirane content was determined according to NTC 2366 standard method[98]. In this method the oxygen is titrated directly with the hydrogen bromide solution in acetic acid. From the oxirane content, the percentage of relative conversion to oxirane was determined using the following formula.

$$\text{Relative conversion of oxirane} = \frac{\text{OOC}_{\text{ex}}}{\text{OOC}_{\text{th}}} * 100 \quad (8)$$

Where, OOC_{ex} is the experimentally determined content of oxirane oxygen, OOC_{th} is the theoretical maximum oxirane oxygen content in 100 g of oil, determined as:

$$\text{OOC}_{\text{th}} = \left\{\frac{\text{IV°}/2\text{A}_{\text{i}}}{100} + (\text{IV°}/2\text{A}_{\text{i}}) * \text{A°}\right\} * \text{A°} * 100 \quad (9)$$

With A_i=126.9 and A°=16.0 were the atomic weights of iodine and oxygen respectively and IV° is the initial iodine value of the oil sample[99].

The relative conversion of double bonds was also studied using Attenuated total ATR-FTIR and ^{1}H-NMR which will be presented in the results section. ^{1}H NMR has been widely applied to the study of epoxides in both oxidized and epoxidized oils [84]. This technique has been used to analyze both mono- and diepoxides, considering that the presence of peaks between 3.13 and 3.08 ppm as well as between 2.98 and 2.9 ppm indicate the presence of mono and di-epoxides groups of the epoxidized oil[83].

Using ^{1}H NMR, yields of epoxidation reaction as well as conversion of double bonds. By using the procedures described by Aerts[41], the conversion of epoxidation reaction and the selectivities were determined for both mono and diepoxides. The equation 7 was used to

calculate the relative conversion of double bond in the epoxidation reaction; the procedure is applied for oleic- and linoleic-based species:

$$X(\%) = 100 * \left[\frac{\frac{N_{s,0}.A_{2,0}}{N_{2.01}A_{s,0}} - \frac{N_{s,t}.A_{2,t}}{N_{2.01}A_{s,t}}}{\frac{N_{s,0}.A_{2,0}}{N_{2.01}A_{s,0}}} \right] (10)$$

Where, the relative reaction conversion of double bonds is denoted as X and can be determined by using the normalized peak intensity of ESFO and SFO signals at 2.01 ppm ($A_{2,t}$ and $A_{2,0}$), respectively and using the peak area at 0.88 ppm ($A_{s,0}$ and $A_{S,t}$). Where N_S represents the number of protons of the internal standard (N_S=1) and $N_{2,01}$ stands for the number of protons of the signal at 2.01 ppm ($N_{2.01}$ = 4).

On the other hand, to determine the selectivity, it is important to consider that only one epoxide product can be formed from oleic species, whereas for linoleic species mono and diepoxides are formed. Reaction selectivities for linoleic species are calculated from signals at 2.9 and 3.1 ppm. Because the signal intensity at 2.9 ppm ($A_{2.9,t}$) is due to the protons of the mono- and diepoxide and the intensity of the peak at 3.1 ppm ($A_{3.1,t}$) only to those of the diepoxide. Then, selectivities to these species can be calculated using equations 11 and 12:

$$S_{MO}(\%) = 100 * \left[\frac{\frac{1.A_{2.9,t}}{N_{2.9}A_{s,t}} - \frac{1.A_{3.1,t}}{N_{3.1}A_{s,t}}}{\frac{1.A_{2.9,t}}{N_{2.9}A_{s,t}}} \right] (11)$$

$$S_{DO}(\%) = 100 - S_{MO}(\%) (12)$$

where $A_{2.9,t}$, $A_{3.1,t}$ and $A_{S,t}$ are the intensities of the peaks at 2.9, 3.1 and 0.88 ppm (internal standard) and $A_{z,t}$ are the intensities of the byproducts peaks. N is the number of protons of the functional group ($N_{2.9}$ = 2; $N_{3.1}$ = 2). It is assumed that there is not by-products after reaction[41] .

2.4.2. Preparation of carbonated sunflower oil (CSFO)

Sunflower oil-based five membered cyclic carbonate was synthesized following the procedure proposed by Doley and Dolui[35]. The reaction of CO_2 with ESFO was carried out under 50 bar CO_2 at 120 °C for 12 h in a high-pressure reactor by using 3.5 w/w% of the catalyst TBAB, with respect to the added weight of ESFO to the reactor. After completion of the reaction, CO_2 pressure was released by venting. Finally, a viscous honey like oil was collected. In order to determine the carbonate equivalent weight (in mol/g of carbonated

oil), measurement of oxirane oxygen content of CSFO was carried out according to NTC 2366 standard method[98], to determine the residual oxirane groups that were present on the product and estimate the conversion of the reaction consider the oxirane value of the starting ESFO and assuming almost complete selectivity. Relative conversion of epoxy groups was also studied by ^{1}H NMR and will be presented in the results section. The viscosity measurements of SFO, ESFO and CSFO were done in a rotational disk viscometer Lamy technologies model B-one plus. Reaction conditions for the three batches realized for the synthesis of CSFO, the products were named $CSFO_1$-$CSFO_3$ are shown in table 1 and the experimental arrangement used for CSFO synthesis is shown in figure 12.

Table 1: Reaction conditions for the synthesis of CSFO.

CSFO sample	**$CSFO_1$**	**$CSFO_2$**	**$CSFO_3$**
T (°C)	120		
Stirring Rate (rpm)	500	1200	1200
Reaction Time (h)	12	14	16
P_{CO2} (bar)	50	50	60
% mol catalyst TBAB	3.5		

Figure 12: Experimental arrangement for the carbonation reaction.

2.4.3. Preparation of polyamine polyol PAPO

PAPO was synthesized according to the method reported by Z. Wang [8]. By using ethylenediamine (EDA), the ring-opening reaction of ESFO was carried out in a 100 mL three- mouth flask equipped with a thermometer and a spherical condenser. EDA and ESFO, in molar ratio 1:2, were added into the flask, which was sealed. The system was then purged with high purity nitrogen, stirred at 250 rpm, and heated to 130 °C. The reaction was

terminated after 6 h, when the crosslinking was observed in the reaction mixture. Reaction conditions used for different PAPOs synthesis are shown in Table 2.

Table 2: Reaction conditions for the synthesis of PAPO samples.

PAPO sample	**$PAPO_1$**	**$PAPO_2$**	**$PAPO_3$**	**$PAPO_4$**
T (°C)	130			
Stirring Rate (rpm)	250			
$R_{ESFO: EDA}$	1:2			
Reaction Time (h)	5	6	6	7

The experimental arrangement implemented for the PAPO synthesis is shown in Figure 13.

Figure 13: Experimental arrangement for the polyamine polyol reaction.

Total amine value of PAPO was determined using Standard Test Methods for Total, Primary, Secondary, and Tertiary Amine Values of Fatty Amines ASTM D2074 – 07 [100].

These methods describe the procedure for determining the total, primary, secondary, and tertiary amine values of fatty amines. For this case. The total amine value was measured as the number of milligrams of potassium hydroxide (KOH) equivalent to the basicity in 1 g of sample. The sample was melting in a water bath. Then, it was accurately weighted 1 to 4 g to 0.1 mg into a 250 mL flask. Then, it was added 50 mL of alcohol and boiled for 1 min to drive off any free ammonia that may be present. Finally, it was added 5 drops of bromophenol blue indicator and titrated, while swirling, with 0.2 N HCl to the yellow end point.

Total amine value was calculated as follows:

$$\text{Total amine value} = \frac{(V*N*56.1)}{S} \quad (13)$$

Where:

V: HCl required for titration of the specimen in mL
N: Normality of the HCl solution
S: Specimen weight used in g.

2.4.4. NIPU synthesis

NIPU networks were produced by the reaction of CSFO and PAPO at molar ratios of 1:1 and 1:1.5, based on the functionality of monomers, that is, the carbonate equivalent weight of CSFO, expressed as mol of carbonate per 100 g of carbonated oil and the total amine value of PAPO, expressed as mg KOH per g of polyamine polyol, considering that the molecular weight of KOH is 56.1 g/mol.

After homogenization by mechanical stirring both monomers at 90°C for 1-3 min, the viscous solution was poured over silicon molds and maintained at 90 °C for 24 h to promote crosslinking. Curing time was studied as a parameter associated with crosslinking degree by taking account the increase on glass transition temperature of the obtained films at different curing times, because temperature and time of curing clearly influence the final properties of the obtained material.

The reaction progress was monitored by Differential Scanning Calorimeter (DSC) through the changes in glass transition and Infrared Spectroscopy (IR) through the changes on the band at 1800 cm^{-1}, which is associated to the decrease on the absorption of carbonyl stretching related to the carbonate group of CSFO.

2.5. Surface modification of NIPU films with chitosan

Polyurethane biomaterials perform moderately well in antibacterial studies in comparison to other polymers and it is estimated that infections associated with the use of indwelling medical devices such as polyurethane biomaterials, affect 5% of hospitalized patients every year [54]. Therefore, NIPU films were surface modified by grafting through ultraviolet radiation (UV) using a CURE UV/LED 48W curing lamp. Acrylamide (AM) was used as a grafting co-monomer, where the active functional groups ($–NH_2$) present on the surface were used for binding chitosan molecules on the surface to impart antibacterial activity to the NIPU films.

The first step included the photo-induced graft polymerization initiated by UV radiation, in which benzophenone (BP), was used as the photo initiator, which absorbs the exciting light

and leads to radical production, and acrylamide (AM) as a grafting co-monomer. Methanol was used as the solvent, in which AM and BP are soluble. NIPU films were placed in glass Petri dishes, exposed to UV light at 365-415 nm and irradiated for 30 minutes for both sides[101]. Different acrylamide concentrations (0.5, 1.0, 1.5, 2.0, and 4.0 M) were used and the modified samples were named AM-$NIPU_1$-AM-$NIPU_5$ respectively. Then, the films were immersed in a glutaraldehyde solution (1 %, v/v) for 3 h, rinsed with deionized water and immersed in chitosan solutions (6, 12 and 20 mg/mL chitosan in 1 %, v/v acetic acid) at 4°C for 24 h. The chitosan (CH) modified films were rinsed with 1 %, v/v acetic acid, neutralized with NaOH 0.1M and washed with deionized water [55].

2.6. Morphological characterization

2.6.1. Contact angle measurement

Surface hydrophilicity of NIPU films was determined by measuring the water droplet contact angle via the sessile drop method using a Dataphysis OCA contact angle measurement system. Contact angles of modified and unmodified NIPU films were determined by placing a small drop of water (0.8-10 μL) at room conditions on the NIPU surface, which previously was placed in a solid plate suspended horizontally. The measure records the angle between the horizontal plane and the tangent to a drop of distilled water at the point of contact[102].

2.6.2. Scanning electron microscopy (SEM)

The surface morphology of modified and unmodified NIPU films was observed by SEM. A scanning electron microscope (Cambridge S250) was employed. The accelerated voltage was 15kV using a magnification of 3000x and 500x. The sample bars in the form of thin squares were fixed on graphite and then sputtered with gold. NIPU Samples were evaluated without further covering.

2.7. Thermal characterization

2.7.1. Differential scanning calorimetry (DSC)

The glass transition temperatures of modified and unmodified NIPU films were determined by DSC, using a TA Instruments model Q100. The samples in the form of small rectangles about 0.2 mm thick were accurately weighed and sealed in aluminum crucibles. The temperature was first raised to 100 °C at 10 °C per minute, keeping an isotherm for 5 minutes to eliminate any thermal history and moisture from the sample, and then lowered

to −100 °C at 10 °C per minute. Thermograms data were recorded in the temperature range −100 to +100 °C at a heating rate of 10 °C per minute.

2.7.2. Thermogravimetric analysis (TGA)

NIPU films thermal stability behavior and thermal degradation were characterized by thermogravimetric analysis (TGA). The measurements of sample weight loss were carried out on a TA Instrument, model Q500. Samples of approximately similar weight of 10± 1 mg were measured under nitrogen atmosphere and heated to 600 °C at a heating rate of 10 °C/ min.

2.8. Mechanical properties

Tensile test were measured in a universal test machine Shimadzu model GSX 50KN with a crosshead speed 50 mm/min^{-1} at room temperature to record stress–strain curves of modified and unmodified NIPU films. Samples were cut into the bar model with 50 mm length and 5 mm width. Using these curves, tensile strength, elongation-at break, and modulus were calculated. The values reported were the average of five measurements.

The degree of crosslinking of the obtained NIPU materials was calculated considering the obtained tensile properties. In a thermoset this value represents a critical parameter that has a major influence on the mechanical strength and viscoelasticity of the material[103]. The crosslink density (υ) of a polymer is the number of crosslinks in a unit volume and can be predicted from the rubber elasticity theory, which is expressed by the following relation: [104]

$$G = \upsilon RT \quad (14)$$

where G is the shear modulus of the polymer, R is the gas constant and T is temperature (K). The above relationship shows that the G increases with an increase in υ. The shear modulus may be related with Young's modulus (E) (assuming isotropic and homogeneous materials) by the following expression:

$$G = \frac{E}{2(1+V)} \quad (15)$$

Assuming that NIPU materials can have rubber behavior, Poisson's ratio, V; for rubber is approximately 0.5 (incompressibility assumption)[105,104]. Mechanical test of elastic unmodified $NIPU_3$ before to break to break and CS $NIPU_{3\text{-}3}$ failed test are showed in figure 12 a and b, respectively. Tensile tests were not able to be measured to modified samples

because their mechanical properties were affected after the modification treatment. Therefore, the samples could not be extended under tension, as is shown in the figure 14 b.

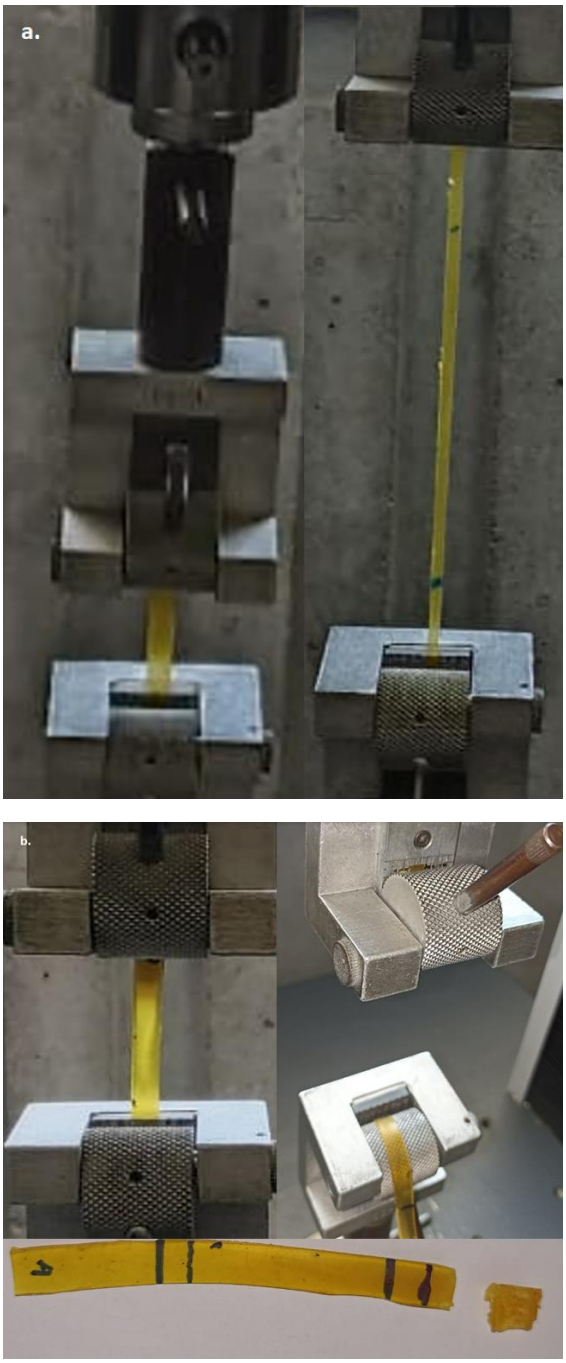

Figure 14: Images of mechanical test for a) NIPU and b) CS NIPU under tension.

2.9. Biological characterization

2.9.1. Antibacterial activity:

Antibacterial activities of the prepared films were tested by using *Staphylococcus aureus* (ATCC®29213TM) and *Escherichia coli* (ATCC®25922TM), bacteria which are common microbial pathogens encountered in infections.

Antibacterial activity of the materials was determined by the inhibition of bacterial growth. Colony counting method was used to estimate the number of viable bacteria remained in the suspension. For this purpose, established concentrations of the bacterial inoculum were added in LB agar at 37 °C, homogenized, and served in Petri dishes. Then, the material was kept in a flow cabinet until the gelation was achieved. The samples were incubated for 18 hours at 37 °C. The assay was performed in triplicate. After incubation, each plate was examined, and the presence of colonies grown on the surface of the material, or the formation of inhibition halos was observed. The absence of colony-forming units (CFU) or a low count of these growths on the material indicates its antibacterial action; the presence of multiple CFUs on the material indicates that it does not inhibit its growth[55].

2.9.2. Evaluation of biocompatibility: Cytotoxicity

The *in vitro* cell viability of Detroit cells were evaluated upon direct contact with NIPU samples using the MTT colorimetric method defined in the ISO/CD 10993-5 that describes test methods to assess the in vitro cytotoxicity of medical devices [106].

The cells were seeded on the materials in culture dishes using DMEM with 10% fetal bovine serum as culture medium. Then, the cells culture was established, and 2 mL of both cultures were poured, separately, on the sterilized sample films that were placed in wells in the culture plate, as well as in the blank well, and incubated for 48 h at 37 °C in a humid CO_2 incubator at 5% (v/v) CO_2.

Then, the MTT was added and after 4 hours of incubation at 37 ˚C, DMSO was added. Finally, the absorbance at 570 nm was determined in a spectrophotometer. The viability percentages were calculated and are presented in the results. Assays were performed in two independent experiments and with two replicates per assay. The control used was untreated Detroit cells. The statistical average of the measurements on at least five test specimens was taken to obtain the mean value for all tests conducted.

Figure 15 shows a scheme of the overall methodology employed in this research work.

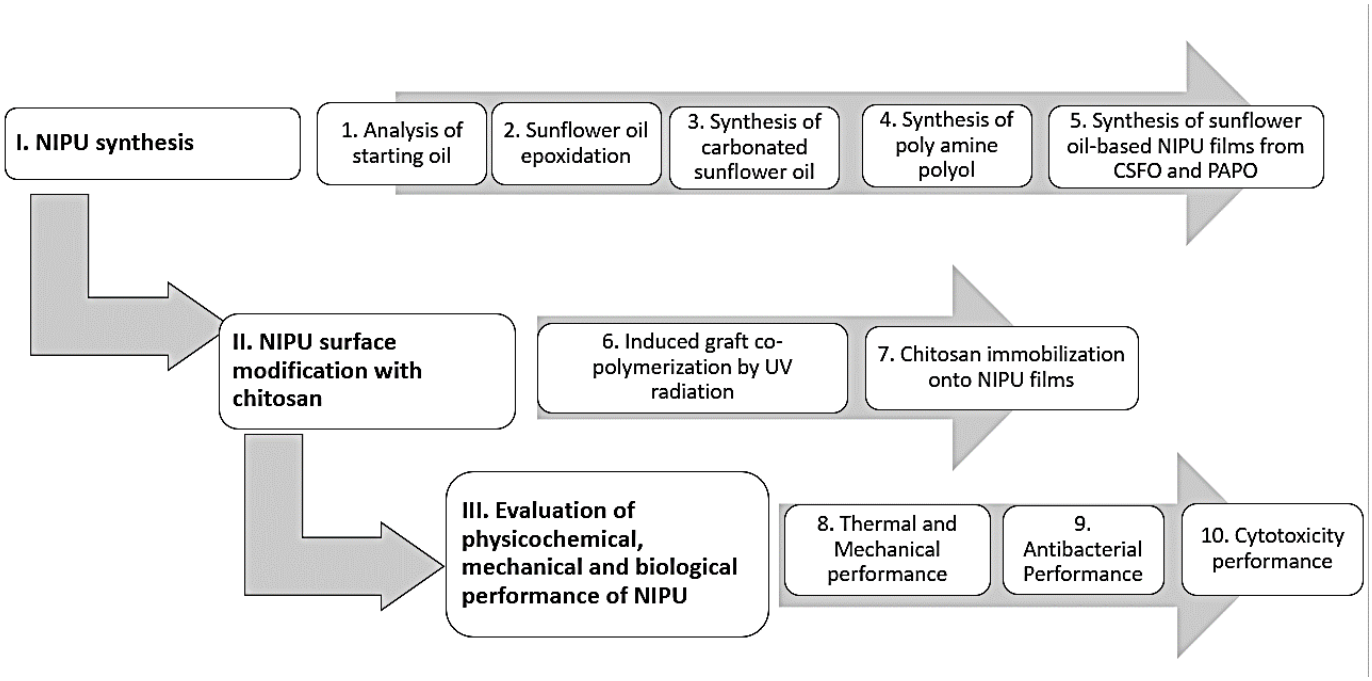

Figure 15: Outline of the research methodology.

3. RESULTS AND DISCUSSIÓN

Since this research work has three main objectives, the discussion was divided in three sections: one related to the NIPU synthesis from sunflower oil, followed by the surface modification with chitosan and finally the NIPU characterization. An initial section includes the characterization of SFO, as the main material for NIPU synthesis, and chitosan for NIPU surface modification.

3.1. Sunflower oil characterization

For the present study, it was chosen commercial SFO as raw material for non-isocyanate polyurethane (NIPU) synthesis because its higher level of unsaturation compared to some other vegetable oils. The starting SFO was characterized as follow:

3.1.1. Qualitative identification of starting SFO functional groups by using FTIR

Figure 16 shows the FTIR spectrum of sunflower oil. Among the peaks, the high-intensity frequency band at 1746 cm^{-1} corresponds to the stretching band of ester carbonyl of SFO triglycerides. For C=O there is a stronger absorption, whereas the stretching vibration of the C=C bond usually gives rise to a moderate band in 1653 $cm^{-1,}$ therefore there is no interference with C=O stretching frequency[75]. Unsaturated long-chain cis olefinic =C-H stretching frequency appeared at ~3008 cm^{-1} while saturated carbon-carbon symmetrical and asymmetrical stretching are observed at 2925 and 2854 cm^{-1}. Methylene (CH_2) symmetrical bending is observed in 1465 cm^{-1}. The CO stretching of the ester bond is appeared in 1158 cm^{-1}. The appearance of a band at 722 cm^{-1} is attributed to cis disubstituted alkenes. Bands at ~3008 and 1653 cm^{-1} indicated a high level of unsaturation in SFO as it was expected. Double bonds are necessary since they are the reactive sites in the synthesis of epoxidized sunflower oil (ESFO), one of the precursors for the synthesis of NIPU.

The spectrum also shows an overtone of a weak band at 3474 cm^{-1} associated with the glyceride ester carbonyl absorption[75]. Table 3 represents major band assignments for FTIR spectrum of SFO.

Table 3: Major band assignments for the FTIR spectra of SFO.

Attribution	Wave number (cm^{-1})
Symmetric and asymmetric absorption of unsaturated long-chain cis olefinic C-H stretching frequency	3008

Elongation vibration of from ester carbonyl groups (O-C=O)	1746
Double bond C=C weak absorption	1653
bands of methylene and methyl of alkyl chains (-CH_2-, CH_3)	1463
Ether C-O symmetric stretching	1158
Cis- double bond angular deformation	1096
Bending of cis disubstituted double bond C=C	722

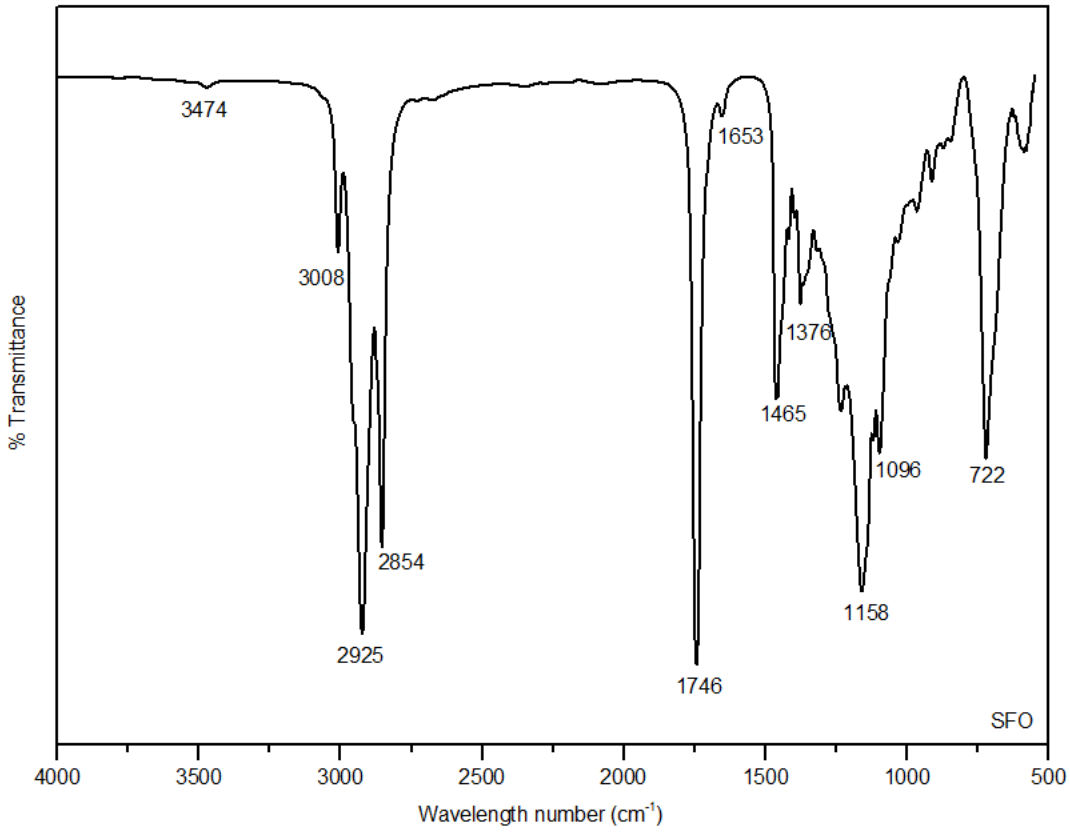

Figure 16: FTIR spectrum of sunflower oil.

3.1.2. Identification of SFO structure and related Iodine Value as well as Fatty acid composition by studying ^1H NMR technique

In the triglycerides of vegetable oils, such as sunflower, soybean, palm and linseed, the oleic, linoleic, and linolenic acids predominate. Therefore, they contain more than 80% unsaturated acids, and can easily be chemically modified[31].

Proton nuclear magnetic resonance (^{1}H NMR) has been widely reported for edible oil analysis and composition[15,83,84]. Therefore, this technique was useful to determine the most approximated structure, iodine value and fatty acid composition of the SFO used for the NIPU synthesis developed in this work.

Figure 17 represents the ^{1}H NMR spectrum of SFO recorded in chloroform-(D) at room temperature. The spectrum of the starting sunflower oil shows nine well-known signals, with chemical shifts in the region between 0 and 5.5 ppm that were assigned to the different types of hydrogen atoms in the oil, which have been broadly described, the obtained spectrum was in agreement and very similar with the reported for other authors for sunflower oil[83] [79]. The spectrum signals of SFO were annotated from A to J and are listed with its respective assignment in table 4 according to previous studies for sunflower oil [107]. The integral limits that were taken for each signal, to determine the relative fatty acid composition of SFO was calculated and presented also in the table 4.

The proton signals that were used for quantifying the unsaturated fatty acids, were: olefinic (5.3–5.4 ppm), bis-allylic carbons (2.7–2.8 ppm), allylic carbons (2.0–2.1 ppm) and terminal methyl group 0.8–0.9 ppm). Furthermore, the amounts of saturated fatty acids can be determined through the signal of the methylene (CH_2) protons at 1.2–1.4 ppm[108].

Table 4: Chemical shift assignment of 1H-NMR signals (A–J) for the main components in vegetable oils with the peak notation shown in Fig. 14

Peak Notation	δ (ppm)	Assignment	Proton	Integral Limit*
A	0.91	Fatty acids	CH_3	0.98 - 0.79
B	1.02	Fatty acids + omega-3	$CH{=}CH{-}CH_2{-}CH_3$	1.03 - 0.98
C	1.32	Fatty acids	$(CH_2)_n$	1.47 - 1.23
D	1.64	Fatty acids	CH_2CH_2COOH	1.77 - 1.55
E	2.07	All unsaturated fatty acids	$(CH_2)_n{-}CH_2{-}CH{=}CH{-}CH_2{-}(CH_2)_n$	2.17 - 1.99
F	2.33	Fatty acids	$CH_2{-}CH_2{-}COOR$	2.41 - 2.29
G	2.79	Linoleyl and linolenyl	$CH{=}CH{-}CH_2{-}CH{=}CH{-}CH_2{-}CH{=}CH$	2.87 - 2.72
H	4.17	Glycerol (triacylglycerols)	CH_2OCOR (CH_2– a (letter H on Fig.2)	4.37 - 4.13
H	4.32	Glycerol (triacylglycerols)	CH2OCOR (CH_2– a(letter Hon Fig.2)	
I	5.28	Glycerol (triacylglycerols)	CHOCOR-b	5.48 - 5.26
J	5.37	All unsaturated fatty acids	CH:CH	

*The table also includes the values of the integral regions selected for the fatty acid composition calculation[78]

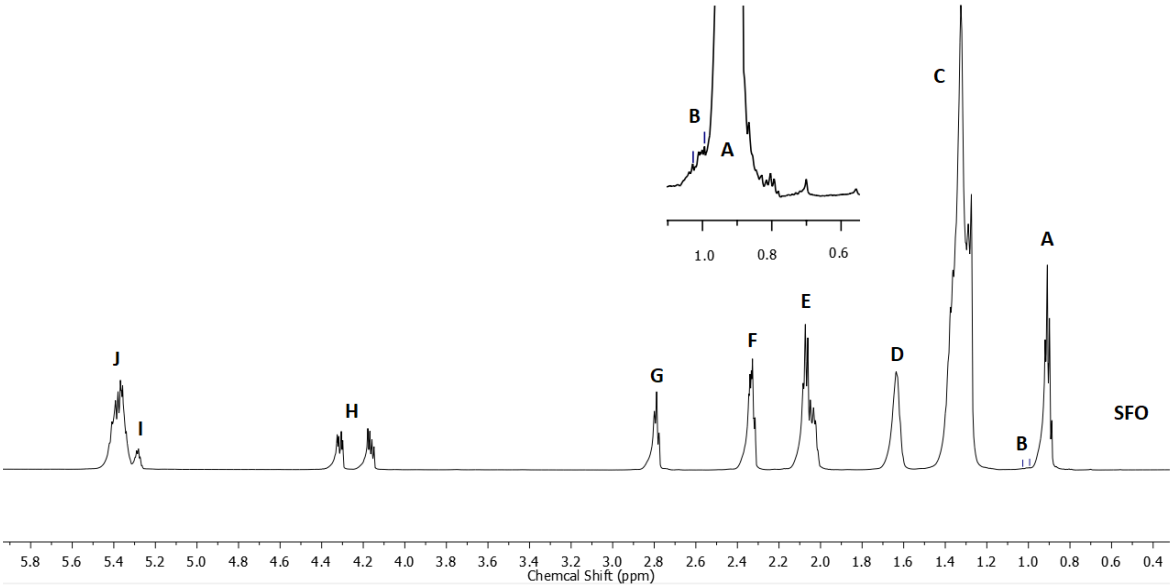

Figure 17: ^{1}H NMR spectrum of SFO recorded in chloroform-(D) at room temperature. The magnification corresponds to the region between 1.03 to 0.81 ppm. It is shown the peak notation for the glycerol and fatty acid protons, marked from A to J.

The chemical shifts showed for SFO in figure 17 were attributed to the respective chemical group present in the oil. A scheme of the glycerol unit and the different types of fatty acids, as R- groups, attributed to the signals of the glycerol unit, and the fatty acid chains of SFO, is showed in figure 18, as one approximated structure of the starting oil, considering and in agreement with previous reports[10].

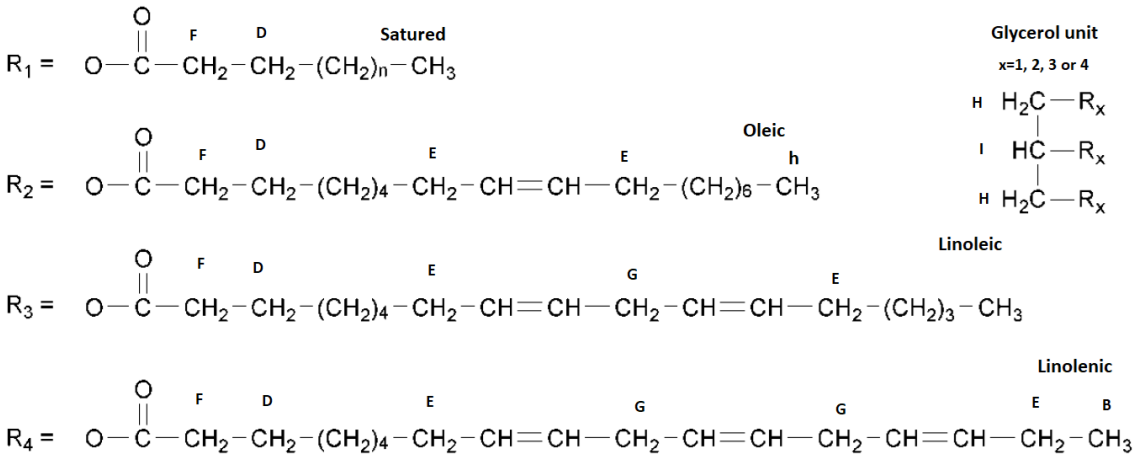

Figure 18: SFO structure related to ^{1}H NMR signal peak assignment[10]

The relative FAC of SFO was estimate by ^{1}H NMR taking account the approaches developed in previous studies [73,78], and mentioned in the methodology section. The FAC of the samples using two different approaches were close each other and are showed in table 5.

Table 5 Fatty Acid Composition of edible sunflower oil determined by ^{1}H NMR following two different approaches.

Reference	Linolenic	Linoleic	Oleic	SFA
[78]	0.643%	55.634%	31.796%	11.284%
[73]	0.643%	55.485%	33.528%	10.344%

The results for the FAC of SFO suggested that the starting oil contains more than 80% unsaturated fatty acids, where more than 50% are polyunsaturated acids (linoleic) and 30% are monounsaturated acids (oleic). This high level of unsaturated groups favors the synthesis of the precursors, since a higher content of reactive sites in SFO implies a higher functionality of its products.

The results showed and listed in figure 17 and table 4 corresponding to the analysis of the ^{1}H NMR spectrum of SFO sample, satisfactorily reflect the relative amount of unsaturated and saturated fatty acids present in the SFO sample and match with the values reported in literature, that use analytical and chromatographic techniques[10,77,78,83,84]. The previous analysis also demonstrates that a complete structural assignment of individual linking segments of the SFO ^{1}H NMR spectrum, provides useful data for analyzing fatty acid compositions of edible vegetable oils [107].

3.1.3. Iodine Value

To determine the amount reactive sites as the degree of unsaturation of SFO that could be chemically modified by epoxidation, the main parameter that was necessary to characterize SFO was the iodine value[37] .The percentage of unsaturated fatty acids largely varies among different types of vegetable oils [83]. For the starting SFO an iodine value of 127.635 g I_2/100 g was measured according to ASTM D 5554-95 standard method[81], in agreement with the values reported by other authors for sunflower oil[35,97,109].

^{1}H NMR technique also was an effective tool for the direct, and rapid determination of the iodine value of SFO[107]. Three different approaches from literature were used to estimate the iodine value and average molecular weight of SFO through the ^{1}H NMR signals which are summarized on table 6. Relative error of these values compared with the iodine value determined by the Wijs standard method was calculated. Although similar values for SFO were found in the literature, the iodine value estimated by spectroscopy (123.03-124.08 g

I_2/100 g) differs to the obtained from the Wijs standard method (127.627 g I_2/100 g). Therefore, estimations of iodine value and molecular weight of SFO were made using two different models[73,86]. It can be concluded that the most accurate results correspond to those obtained using the model proposed by Guillen et al[73].

Table 6: Results of iodine value SFO using the Wijs method and three different approaches by ^{1}H-NMR.

Starting SFO sample				
Molecular Weight (g/mol)	Iodine value ^{1}H NMR (g I_2/100 g)	Iodine value Wijs (g I_2/100 g)	Relative Error (%)	Reference
890.88	136.23	127.67	6.73%	[83]
872.08	123.03		3.61%	[82]
866.36	124.08		2.79%	[69]

Iodine values determined by ^{1}H NMR agreed with those obtained by the classical Wijs method for SFO, with a lower relative error of 2.79%. This technique have been useful to characterize a significant number of samples of different vegetable oils[107]. Therefore, from ^{1}H NMR spectra it was possible to elucidate the SFO chemical structure shown in figure 18, and besides, it allowed the measurement of the unsaturation degree, and the estimation of the relative fatty acid composition.

3.2. Chitosan characterization

3.2.1. Degree of deacetylation (%DD)

The value of degree of deacetylation (DD) for the chitosan was 78.4%, which was determined following the procedure described previously in the methodology. This DD might be considered as suitable for surface modification, as there will be more reactive sites with a higher amount of glucose amine units

3.2.2. Measurement of viscosity average molar mass from intrinsic viscosity, [η]:

The molecular weight of chitosan was 340391.01 g/mol estimated by equation 4, , using the methodology described in the previous chapter. This measurement indicates a high molecular weight chitosan, which might have further effects due to the very high viscosity of the solutions.

3.3. Analysis of epoxidized sunflower oil (ESFO)

The first step to obtaining entirely sunflower oil-based non-isocyanate polyurethane (NIPU) films, includes the epoxidation of the double bonds of monounsaturated and polyunsaturated fatty acids of SFO, in presence of a mixture of formic acid with an excess of hydrogen peroxide. Thanks to the high degree of unsaturation of the used SFO, this raw material could easily undergo an epoxidation reaction. The epoxidized product was decanted, thoroughly washed with sodium carbonate and distilled water, and dried to further be used to prepare both monomers needed for the synthesis of NIPU.

The obtained epoxidized sunflower oil was a viscous clear liquid oil, as is shown in figure 19, with an increased viscosity of 840 cP, at room conditions, compared with 124 cP of SFO starting oil.

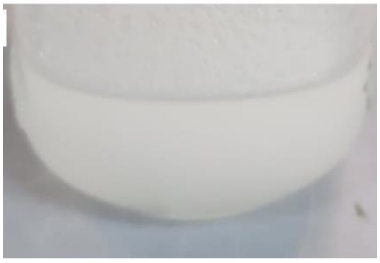

Figure 19: Viscous clear liquid oil obtained to the epoxidation of SFO reaction.

Measurement of the oxirane oxygen content of ESFO was carried out according to a standard method. The calculated value of oxirane content OO_{exp} was 6.5%, and the epoxy content was 4.07 $mmol.g^{-1}$. Oxirane oxygen content of epoxidized SFO determines the conversion of double bonds in the vegetable oil into epoxy rings[110] and the following reactivity of these groups to be used as the precursor of the NIPU synthesis monomers. A theoretical maximum oxirane oxygen content was estimated by using equation 6 as 7.447%. Therefore, the relative conversion of double bonds, estimated by using equation 11, was 88.36%. A good conversion was achieved for ESFO synthesis confirming that most of SFO double bonds were converted into oxirane rings, that could give place to adequate functionality of ESFO-based products, CSFO and PAPO.

FTIR was used to confirm the conversion of double bonds and the formation of the epoxy group. The FTIR spectra of SFO and ESFO are shown in figure 20. Epoxidation was confirmed due to the presence of the transmittance peaks at 1241 cm^{-1} and 825 cm^{-1} that correspond to C−O−C stretching from the oxirane vibration of epoxide group[111]. The formation of epoxy group was also confirmed, because, epoxidation resulted in a drastic reduction of the C=C-H absorption band in 3008 cm^{-1}, related to double bonds of SFO (figure 17), along with the appearance of the epoxide bands around 825 cm^{-1} [112]. The decrease in the intensity of the signal at 1653 cm^{-1}, related to the absorption of the C=C double bond, provided another

way to confirm the conversion of SFO unsaturated groups. A weak O−H stretching peak at 3492 cm^{-1} indicates that the sample is not completely free from moisture or contaminants.

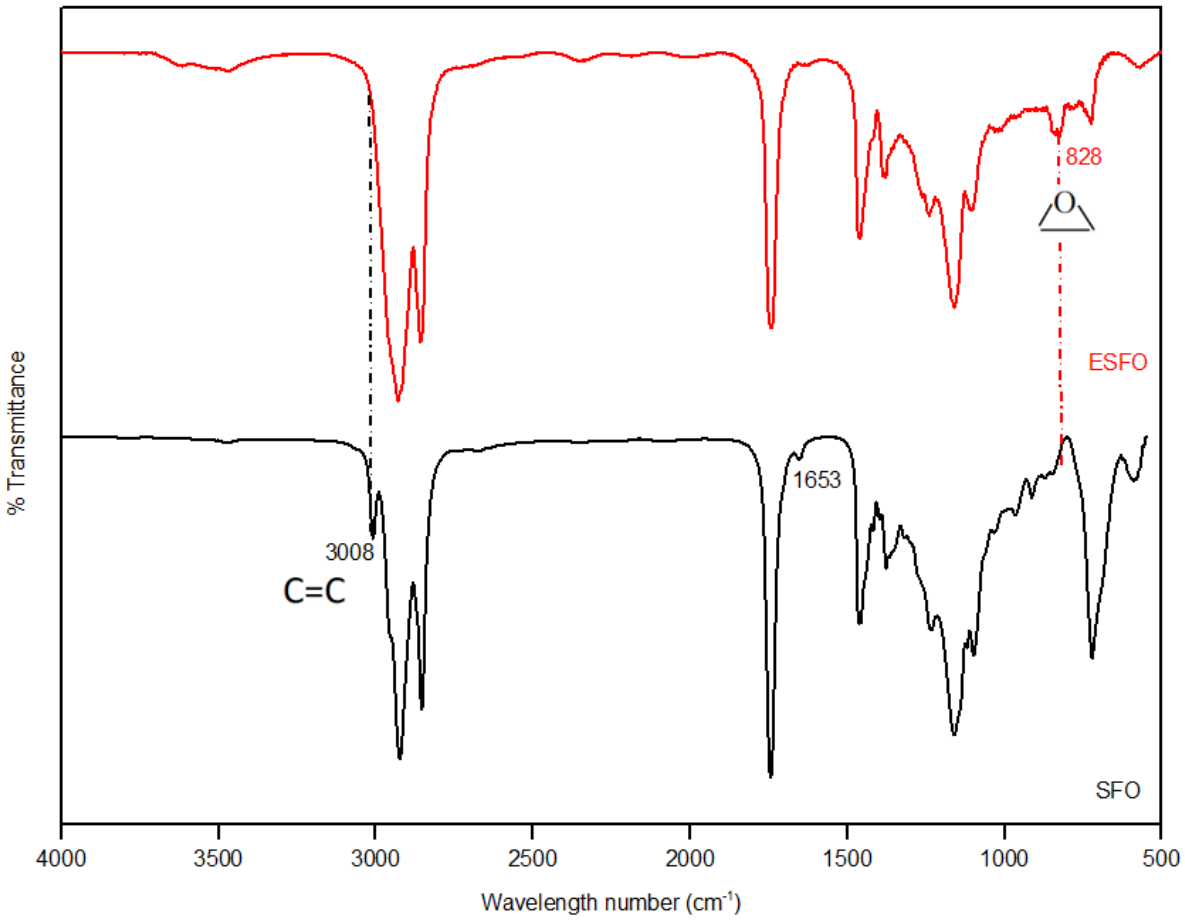

Figure 20: FTIR spectra of SFO and ESFO with the related functional groups scheme and characteristic bands.

The synthesis of ESFO was also corroborated by ^{1}H NMR. In Figure 21, is presented the comparison between SFO and ESFO. After epoxidation, the disappearance of the signals due to double bonds (~5.50 ppm) and methylene groups adjacent to the double bonds (~2.10 ppm), and the appearance of the signals due to epoxy groups (~3.00 ppm) and methylene groups adjacent to these epoxy groups (~1.50 ppm), confirms that the C=C double bonds of SFO were successfully converted into epoxy groups[97]. Finally, in both SFO and ESFO spectra, the signals associated with the glycerol backbone (5.2 and 4.5 ppm) remained constant[41]. The peaks at 2.98–3.1 ppm represent the CH protons attached to the oxygen atoms of the epoxy groups[112], and confirm the formation of mono epoxides and di epoxides from mono and polyunsaturated fatty acids [83].

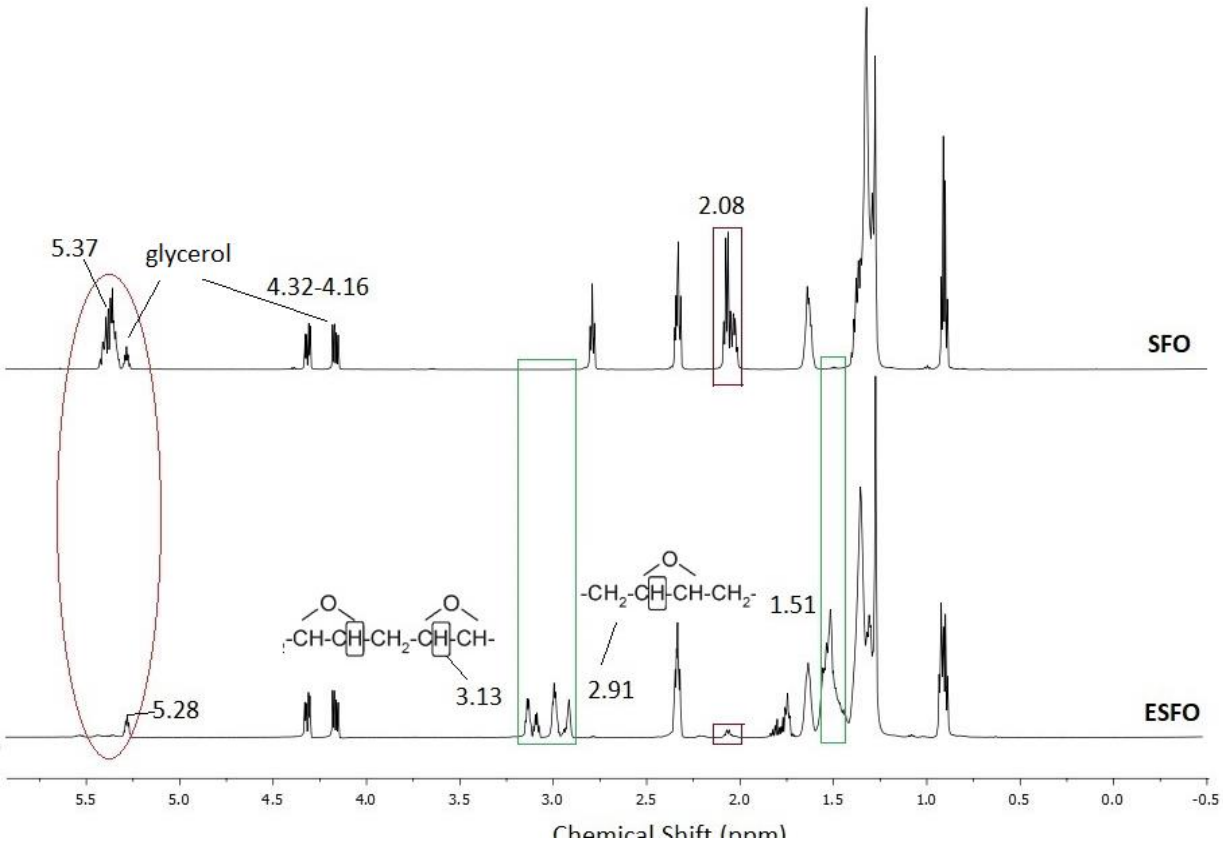

Figure 21: Comparison of ^{1}H NMR chemical shift signals on ESFO and SFO spectra, with the related chemical group scheme.

Tables 7 and 8 show the most representative chemical shifts and the absolute and normalized intensities of the of SFO and ESFO ^{1}H NMR spectrum. These values were used to determine the relative conversion of double bonds of SFO into epoxides groups of ESFO, as well as the relative selectivity for mono and di epoxides.

Table 7: Absolute and normalized intensities of SFO ^{1}H NMR chemical shifts to determine conversion of double bonds and selectivity for mono and di-epoxides.

Chemical shift range	Normalized chemical shift intensity (%)	Absolut intensity value
5.45 - 5.25	8.68%	316122.88
4.37 - 4.13	3.41%	124136.19
2.85 - 2.75	3.03%	110360.36
2.40 - 2.28	5.33%	194164.28
2.15 - 1.99 ($A_{2,0}$)	9.39%	341806.62
1.71 - 1.57	6.31%	229676.57
1.46 - 1.22	47.87%	1743220.22

1.00 - 0.86	8.03%	292614.36
0.97 - 0.87 ($A_{s,0}$)	7.96%	289730.91

Table 8: Absolute and normalized intensities of ESFO ^{1}H NMR chemical shifts to determine conversion of double bonds and selectivity for mono and di-epoxides.

Chemical shift range	Normalized chemical shift intensity (%)	Absolut intensity value
5.51 - 5.20	1.38%	55304.94
4.33 - 4.09	3.85%	154196.71
3.12 - 2.99 ($A_{3.1,t}$)	2.91%	116493.96
2.99 - 2.84 ($A_{2.9,t}$)	4.72%	188889.02
2.34 - 2.24	5.96%	238340.25
2.10 - 1.96 ($A_{2.1,t}$)	0.41%	16378.67
1.80 - 1.66	2.97%	118917.87
1.66 - 1.56	6.24%	249859.17
1.56 - 1.38	19.55%	782052.68
1.38 - 0.98	42.86%	1715122.56
0.98 - 0.76 ($A_{s,t}$)	9.14%	365694.25

The conversion and selectivity of mono-epoxides (S_{MO}) and di-epoxides (S_{DO}) were calculated using the equations 7, 8 and 9 and are shown in table 9:

Table 9: Results for conversion and selectivities for both mono and di epoxides of ESFO product.

Property	Estimated value
C=C Conversion	96.20%
S_{MO}	38.33
S_{DO}	61.67

The results for relative conversion estimated by ^{1}H NMR agreed with the quantitative results obtained by titration oxirane method, as well as to the FTIR spectrum, which showed an almost complete conversion to double bonds to epoxides. On the other hand, NMR proved to be a useful tool to determine the selectivity of the epoxidation reaction to mono-epoxides, relating the number of monounsaturated oleic fatty acid groups to the di-epoxide

groups of the polyunsaturated fatty acids, which allows a deeper elucidation of the structure of the starting materials.

3.4. Analysis of carbonated sunflower oil (CSFO) synthesis

From ESFO both monomers for NIPU synthesis were obtained, the first one was the cyclic carbonate which was synthesized by the reaction of ESFO with CO_2 in a high-pressure reactor using TBAB as a catalyst. The obtained carbonated product was a highly viscous material like brown honey, as is shown in figure 22. This product had a viscosity and color completely different to the initial ESFO aspect and similar to the carbonated products reported by other authors[50, 35]. These features suggested high yield of the carbonation reaction. The viscosity of $CSFO_1$ at 25°C was 23034 cP, compared to the much lower values of 840 cP and 124 cP for ESFO and SFO, respectively. The high value of viscosity may be related to the presence of the polar cyclic carbonate groups causing enhanced intermolecular interactions[113]. CSFO product was used without further purification to produce NIPU, owing the high viscosity of the samples which difficult the handling. Otherwise the product was used without any washes of extraction treatments, considering the high purity of the obtained carbonate as well as high conversion if epoxide groups that throw the spectroscopic and analytical characterization that show These features will be discussed below.

Figure 22: Carbonated sunflower oil obtained from the synthesis between ESFO and CO_2.

The epoxy conversion was determined by the measurement of the residual oxirane oxygen content follow the standard method previously described[98], and it was corroborated with ^{1}H NMR study of the normalized integral shift value of the CH protons attached to the

oxygen atoms of the epoxy groups between 3.13-2.84 ppm[112]. Conversion results by the two methods are summarized in table 10.

Table 10: Epoxy conversion determined by a standard method and by ^{1}H-NMR and the estimated carbonated equivalent weight.

CSFO $_{sample}$	**$CSFO_1$**	**$CSFO_2$**	**$CSFO_3$**
O.Ox $_{std\ ESFO}$ (%)	6.576	6.394	6.568
O.Ox $_{std\ CSFO}$ (%)	2.337	1.271	0.673
O.Ox $_{NMR\ ESFO}$ (%)	7.957	7.865	7.812
O.Ox $_{NMR\ CSFO}$ (%)	2.674	1.569	0.593
Conversion $_{std}$	64.45%	80.13%	89.75%
Conversion $_{NMR}$	66.40%	80.05%	92.41%
Relative error (%)	3.022%	0.100%	2.966%
CEW (mmol/g)	2.649	3.202	3.684

Where O.Ox $_{std}$ represent oxirane value for both starting ESFO and CSFO, determined by the standard methods, while O.Ox $_{NMR}$, represent the values obtained by the normalized integral of the chemical shift in the range of 3.13-2.84 ppm. The carbonate equivalent weight (CEW) was estimated assuming almost complete conversion of epoxide groups into cyclic carbonates. $CSFO_3$ was the carbonated product with the highest conversion, while $CSFO_2$ presented the lowest conversion.

The use of CO_2 in organic synthesis is a challenge owing to its high thermodynamic and kinetic stability, low reactivity and the difficulty to activate bond formation reactions of CO_2 with energy-rich substrates such as epoxides[13]. Therefore, a high CO_2 pressure may guarantee high solubility and hence high conversion of the reaction. As was demonstrated by Doll and Erhan[114], who implemented an improved synthesis pathway of a cyclic carbonate of soybean oil (CSO) utilizing supercritical CO_2 as the solvent, increasing the mutual solubility of supercritical CO_2.

The obtained results for the overall conversion of the different CSFO samples is highly influenced by the pressure of the system and high CO_2 pressure conditions, which allowed higher degree of conversion without the presence of subproducts. The results were compared with those obtained for other authors which required high pressure to achieve high yields[114]. The present results suggest that the stirring rate has to be considered as an

important variable to promote the reaction. It is noteworthy, that the oxirane value of the starting ESFO must affect the conversion. Therefore, $CSFO_3$ with a higher conversion was selected as the first monomer for NIPU synthesis.

The successful conversion of epoxide groups into cyclic carbonate determined by ^1H NMR was compared to the results obtained with analytical methods and was qualitatively corroborated by FTIR.

FTIR spectra of CSFO compared with ESFO are shown in figure 23. The disappearance of the peaks at 842–822 cm^{-1} and the appearance of a peak at 1803 cm^{-1} confirm the conversion to the carbonated product. The peak at 1744-1740 cm^{-1} is due to the ester group of the oil. The formation of cyclic carbonated oil is confirmed by appearance of a new intense band at 1796 cm^{-1} due to C=O carbonyl stretching due to the formation of a carbonate function [35]. The band at 1273 cm^{-1} showed in CSFO FTIR spectrum was attributed to C–O stretching vibration of carbonates[115].

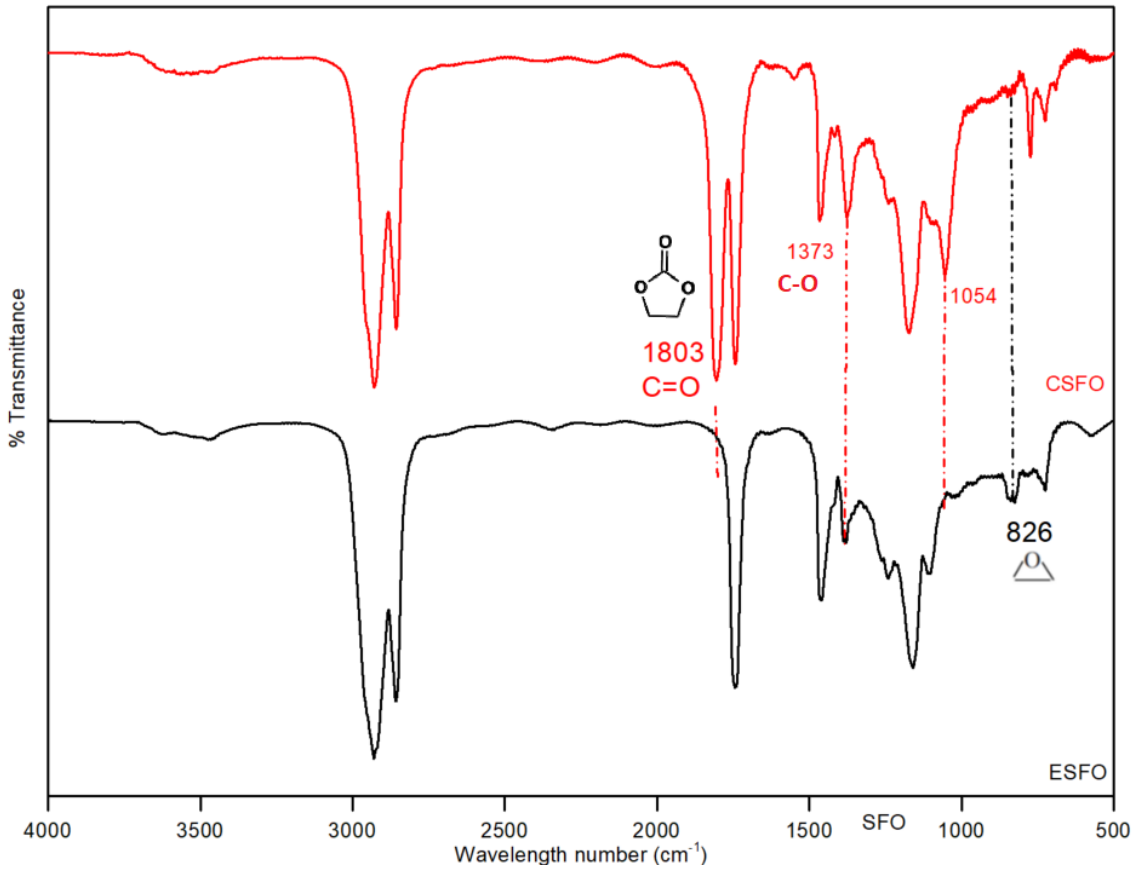

Figure 23: FTIR spectra of epoxidized sunflower oil (ESFO, upper spectrum) and carbonated sunflower oil ($CSFO_3$, lower spectrum).

The ^{1}H NMR spectra of CSFO compared with ESFO are shown in figure 2. The disappearance of peaks at 2.95–3.13 ppm corresponding to C-H in the α-position of epoxy function of ESFO and the appearance of a new peak at 4.64 ppm attributed to C-H in the α-position of cyclic carbonate group of CSFO confirm the conversion[46]. The signal at the region of 4.2–4.5 ppm corresponds to the protons of the carbonate group. The disappearance of the signals at 3.1-2.9 ppm shows the reaction progress. New signals at 4.2-4.5 ppm shows the conversion to the carbonated product. The change in the signals in the range of 1.74 to 1.04 ppm could be attributed to some impurities as rests of the catalyst TBAB, or secondary components of the analyzed samples.

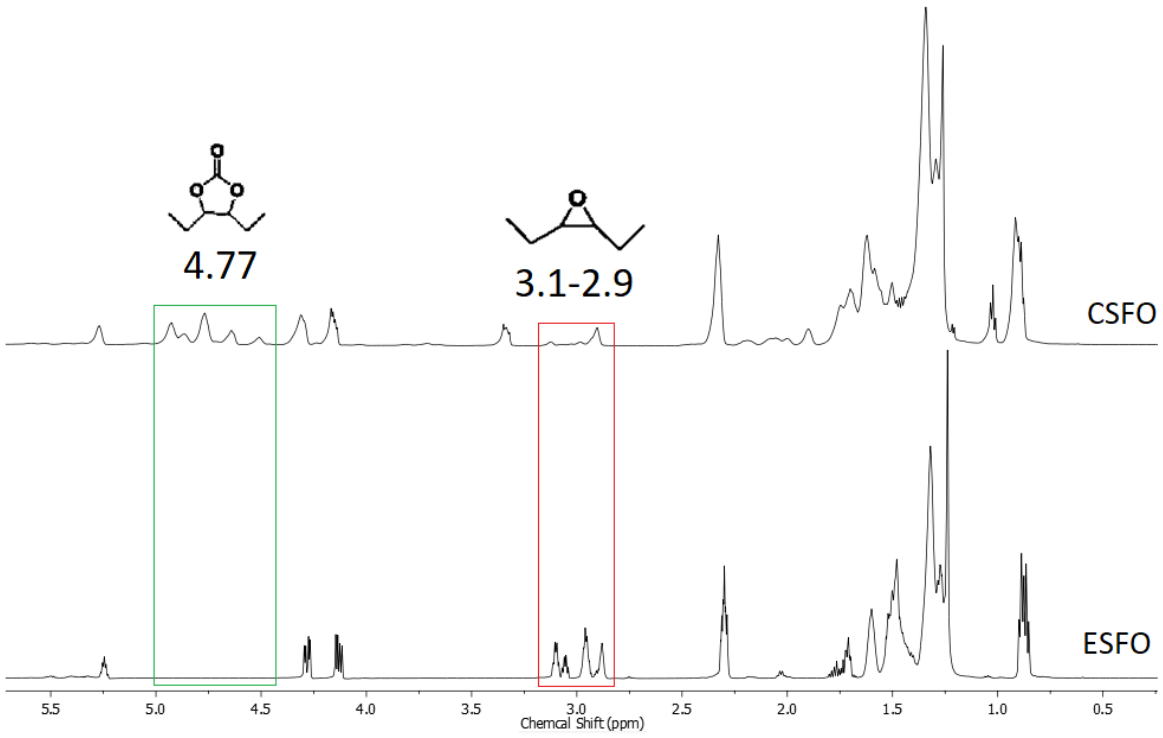

Figure 24 ^{1}H NMR spectra of epoxidized sunflower oil (ESFO, lower spectrum) and carbonated sunflower oil ($CSFO_3$, upper spectrum).

A comparison of ^{1}H NMR spectra of the synthesized carbonated products are shown in figure 23. It can be seen in $CSFO_1$ spectrum that the signals in the region of 3.1-2.9 ppm do not completely disappear at the end of the reaction which indicate the incomplete conversion of epoxy groups, while for $CSFO_3$, the complete changing in these peaks indicate a conversion thoroughly. These results agree with the values of oxirane of the CSFO products reported in table 9. Other changes in the chemical shift signals of the different CSFO samples were attributed to the different batches of ESFO from which they came from.

The differences in the conversion to carbonate for the samples are shown in figure 25, where it can be clearly seen that $CSFO_3$ produced the highest conversion.

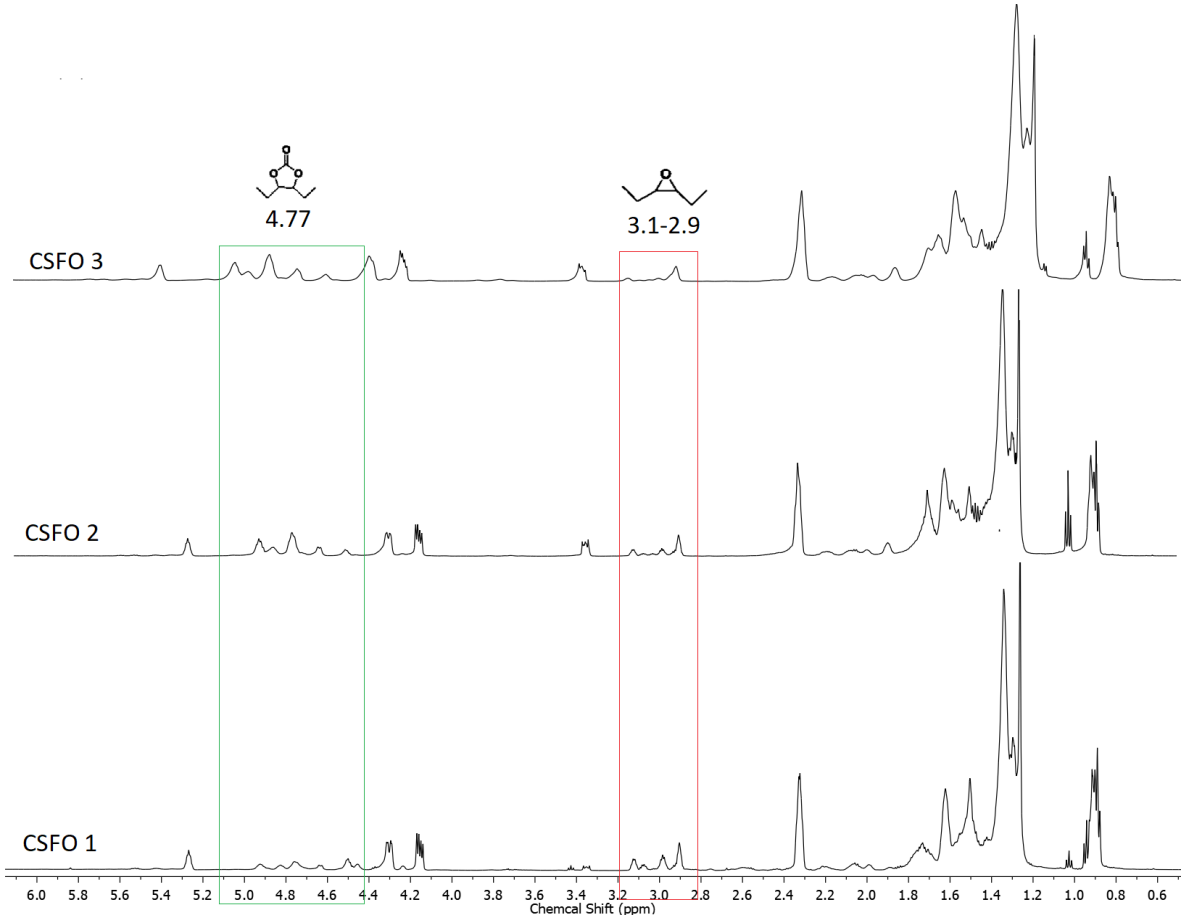

Figure 25: ^{1}HNMR spectra of the carbonated products. Chemical shift corresponding to the epoxide and cyclic carbonate protons, are highlighted.

3.5. Analysis of polyamine polyol PAPO

The second monomer for NIPU synthesis is the polyamine. In this work it was used the approach developed by Wang et al[8] to prepare a polyamine polyol (PAPO). Starting from ESFO, ethylenediamine (EDA), was used to react with epoxy groups to contribute to chain growth and with ester groups to break the glycerol center during the polymerization[8]. The thermosetting sunflower oil-based PAPO product was rubbery, yellow in color, and soluble in either ethanol or tetrahydrofuran, as shown in Figure 26. The reaction involved in PAPO synthesis was presented in the first chapter in Figure 7.

Figure 26: Polyamine polyol product obtained from the synthesis between ESFO and EDA.

The polyamine polyol (PAPO) obtained was not purified due to its stickiness and softness which made it difficult to handle Also, the high amine content of this compound is advantageous for the synthesis. No epoxide residues were observed by using spectroscopic techniques as will be discussed below.

The total amine value that is related with a relative measure of the overall content of primary and secondary amines, present in PAPO, was used as a parameter to formulate NIPU from PAPO. This relative value allowing to know the possible amines amount that could be react with carbonate, without assumed that the total amount of calculated amines will going to react with carbonate to form urethane because as will be show later the value does not directly show the number of available amines that are going to react.

To have a better control over the reaction products, different reaction times were used for the PAPO synthesis. Considering that it was necessary to prepare several batches to prepare ESFO, oxirane oxygen content in some cases varied, which is directly related to the obtained polymer properties. Total amine values for each PAPO samples were determined based on ASTM D2074-92[100] and summarized in table 11.

Table 11: Amine value of PAPO samples.

PAPO $_{sample}$	$PAPO_1$	$PAPO_2$	$PAPO_3$	$PAPO_4$
Reaction Time (h)	5	6	6	7
O.Ox $_{starting\ ESFO}$ (%)	5.94	5.91	6.43	6.44
Total amine value (mg KOH/g)	290.08	346.72	478.84	253.25

For PAPO synthesis, an excess of EDA to ESFO was used because with a high molar ratio of diamine to epoxidized oil, more ester groups of the glycerol center take part in ammonolysis as one ester group is cleaved from each glycerol center, which favors a lower degree of crosslinking, for further processing. The reaction was carried out at 130 °C because lower temperatures would result in very long reaction times and higher temperatures would lead to the loss of diamine[8]. As is shown in Table 10, $PAPO_3$ with the higher oxirane oxygen content of the starting ESFO at 6 h of reaction, had the higher total amine value. Increasing the reaction times to 7 hours, yielded a polymer with a lower functionality and a higher crosslinking degree. This may be associated with a larger steric hindrance, which prevents the other epoxy groups to react. Consequently, the other functional groups of PAPO are less prone to react. Therefore, $PAPO_3$ obtained was preferred as a precursor for the NIPU synthesis, because more degree of ammonolysis is achieved in a lower time.

To analyze the $PAPO_3$ structure and to confirm the ammonolysis reaction, FTIR and ^{1}H NMR spectroscopic techniques were used. Figure 27 shows the FTIR spectra of PAPO and ESFO. The peak at 3290 cm^{-1} increases, due to O-H and N-H stretching, while the absorption band at 828 cm-1 from epoxy groups almost disappeared indicating that the reaction between the epoxy groups and amine groups occurred. The absence of a strong peak at 1739 cm^{-1} due to C=O stretching of ester present in glycerol units[116] indicates no formation of this subproduct.

The ammonolysis was confirmed by the changes in the peaks for the C-O stretching vibrations of the ester and amide groups. The replacement of the band at 1742 cm^{-1} associated with the carbonyl group of ester, by the C-O stretching vibration of amide at 1638 cm^{-1} (amide I) and the N−H stretching vibration at 1555 cm^{-1} (amide II) demonstrates the formation of primary and secondary amines and the glycerol center was broken, because of the disappearing of ester stretching band[117]. The reduction of the bands at the region of 1158 cm^{-1} that is assigned to C-O symmetric stretching of SFO related to the breakage of the glycerol center.

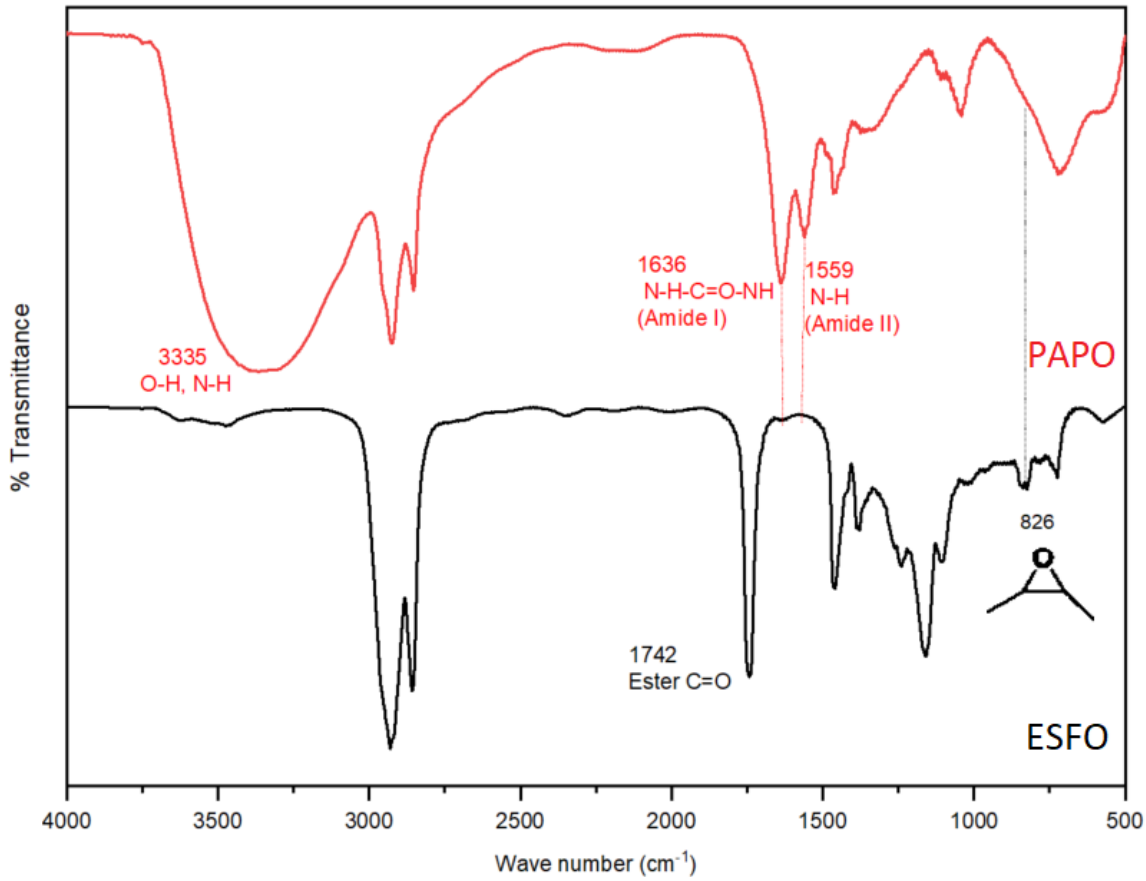

Figure 27: FT-IR spectra of ESFO and PAPO with the related functional groups.

Figure 28 shows the PAPO and ESFO ^{1}H NMR spectra, which were used to identify the structure of PAPO and to confirm the ammonolysis reaction. The disappearance of the signals in the 2.90−3.10 ppm region shows an almost complete conversion of the epoxide groups. The signal at 3.29 ppm is attributed to the resulting hydroxyl proton −OH, indicating that the amine and epoxy group reaction occurred. The signal at 2.16 ppm corresponds to the protons of CH_2−CO−NH−, indicating that the ammonolysis indeed occurred. The disappearance of the signals coming from the methine proton of −CH_2−CH−CH_2− at 5.24 ppm, the methylene protons of −CH_2−CH−CH_2− at 4.14−4.29 and −CH_2−COO− at 2.29 ppm along with the appearance of the signal of the protons of CH_2−CO−NH− at 2.2 ppm appears and increase, indicating a high degree of ammonolysis. Finally, the signal at 2.72-2.8 corresponds to the protons related to the CH_2-NH_2 group[7], which suggests the presence of primary amines in the PAPO structure. However, a detailed analysis by ^{1}H-NMR spectroscopy was not possible, owing to the nearly identical chemical shifts of methylene groups adjacent to primary and secondary amine functions in the zone of 1.7-0.8 ppm[8].

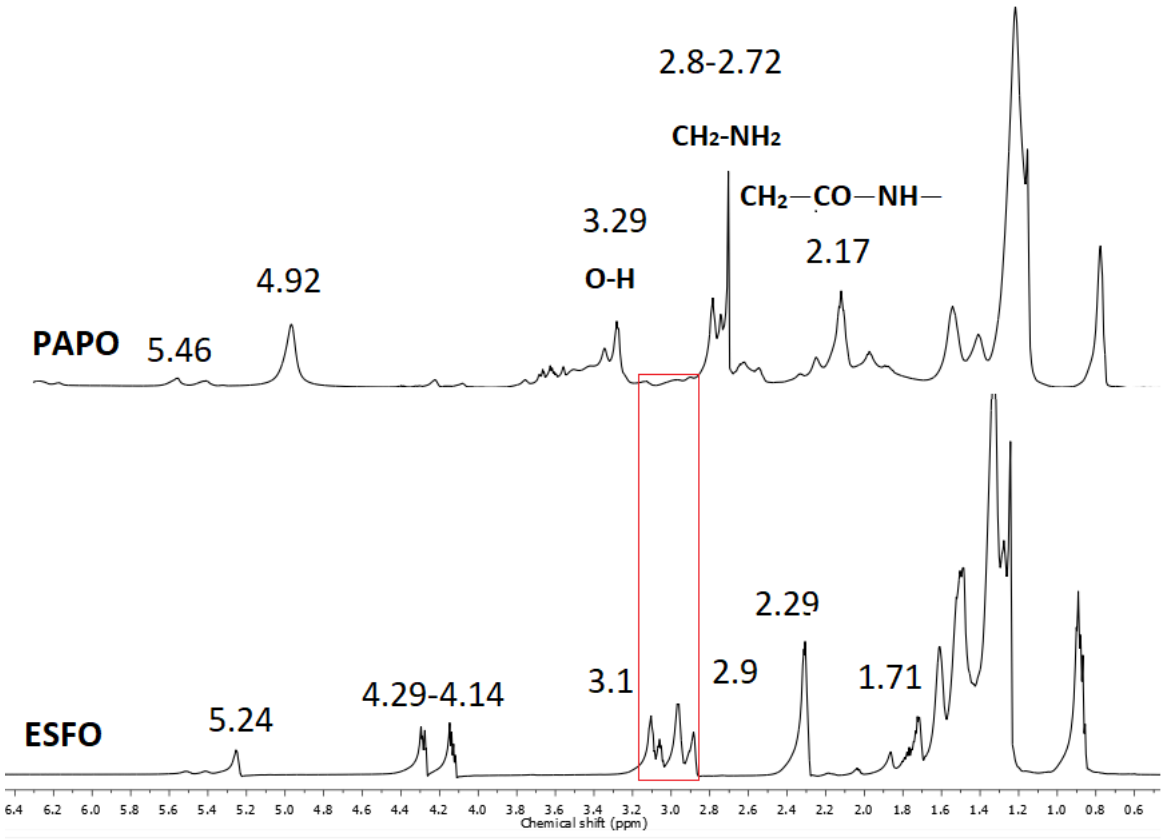

Figure 28: Comparison of ^{1}H NMR chemical shift signals on PAPO and ESFO spectra.

According to the results of FTIR and ^{1}H NMR, the glycerol center of ESFO was broken by ammonolysis as expected in the process of polymerization of PAPO. It is important to note that while the signals of the methine proton of $-CH_2-CH-CH_2-$ and the methylene protons of $-CH_2-CH-CH_2-$ disappeared almost complete, indicating that all ester groups of each glycerol center might have been broken, the signal from the epoxy group is weak but still appears. Therefore, it may be possible that the amine rather reacts with an ester group than with an epoxy group.

3.6. Analysis of entirely sunflower oil-based NIPU films from CSFO and PAPO

NIPU films were synthesized through a isocyanate and solvent-free synthesis route, where sunflower oil was used as a starting material to prepare both precursors. This vegetable oil

was utilized as a building block for the synthesis of cyclic carbonate, and at the same time, it was used as a building block for the synthesis of polyamines[118].

The NIPU films were obtained by mixing CSFO and PAPO products, under mechanical stirring of 250 rpm, at different molar ratios, based on the carbonate equivalent weight of CSFO and the total amine content of PAPO. As was stated in the discussion of PAPO synthesis, $PAPO_3$ was the product with a higher total amine value, therefore, it was selected for the NIPU synthesis. However, $PAPO_2$ was a product with the second-highest amine value. Therefore, to produce NIPU, in some cases, $PAPO_2$, due to also had a high amine value, was used to react with $CSFO_3$, the selected cyclic carbonate product for the NIPU synthesis. The reaction involved in NIPU synthesis was presented in the first chapter in figure 2.

After the mixing and mechanical stirring of precursors, the samples changed their appearance from viscous and sticky solutions to flexible films and defined shapes, obtained after 24 hours of curing. Significant changes in the amount of carbonate present as well as in the formation of urethane bonds, were showed by IR study of NIPU samples at different curing times, which was directly related to the degree of crosslinking of the samples and used as a reaction stop criterion. NIPUs with 24 hours of curing were chosen because they were well-formed elastic films and because after this time, at 36 and 48 hours, there was no further conversion of CSFO to urethane, but instead the films changed the color to a darker brown associated with degradation of polymer network.

Considering that only mechanical stirring and furnace curing were needed to obtain NIPU products with an excellent conversion of CSFO and urethane formation, this synthetic pathway does not use either solvent or catalyst to achieve the most suitable and entirely SFO-based route. Besides, as the synthetic pathway and product are still unknown, NIPU was used without further solvent purification or additional treatments. to avoid damages or possible changes in the polymeric product.

However, owing to the high viscosity of the precursors, the reaction mixture was difficult to handle at room temperature, but at 90°C the viscosity decreases and only between one to three minutes of stirring were required before the curing process. An alternative method to enhance this feature included to prepare NIPU included the addition of 50% of EDA. Because, as a primary amine, EDA may accelerate the crosslinking reaction[119], besides several authors have demonstrated that small diamines cause the formation of more urethane bonds, and the incorporation of different amine structures into polymer backbones and side chains, may enable facile tailoring of a great variety of urethane-functional polymers[22,120–122]. The molar ratios used to produce different NIPU films are listed in table 12. The temperature of the mixing and the curing process was 90°C, which was establish by Camara et al[49] as the optimum temperature to produce polyhydroxy(urethanes), starting from secondary amines and cyclic carbonates, as is the case of PAPO precursor[119]. Light brown NIPU films were obtained, as shown in figure 29. All

samples were sticky before the curing process. However, after this process, elastic films were obtained.

Table 12: Different systems studied for NIPU synthesis from CSFO and PAPO.

NIPU sample	Molar Ratio			
	$CSFO_3$	$PAPO_3$	$PAPO_2$	EDA
$NIPU_1$	1	-	1	-
$NIPU_2$	1	-	1.5	-
$NIPU_3$	1	1.5	-	-
$NIPU_4$	1	1	-	0.5
$NIPU_5$	1	1.5	-	0.5

Figure 29: Polymeric NIPU3 films obtained through the reaction between CSFO and PAPO after 24 hours of oven-curing at 90 °C**.**

3.6.1. Structure and curing study by ATR-FTIR analysis

To confirm the formation of NIPU and examine the effect of various CSFO/PAPO and CSFO/PAPO/EDA molar ratios in the NIPU samples, ATR-FTIR spectroscopy was used. Figures 30-34, show the ATR-FTIR spectra of the prepared NIPU samples at different curing times. All spectra showed representative bands attributed to the different groups of the expected product as well as the unreacted monomers, which are listed in Table 2. Overall, in all the ATR-FTIR spectra, absorption bands appearing at 3300–3440 cm^{-1} are assigned to O-H and N-H stretching from hydroxyl and urethane groups respectively[35]. The occurrence of a signal at around 1700 cm^{-1}, corresponding to vibration of C–O in –NH–COO–, indicates

the formation of urethane and amide groups resulting from ester ammonolysis reaction[123]. The bands at 1536, 1252 and 1162 cm^{-1}, correspond to the N-H, C-N/C-O (in ester fragment) and C-O-C groups, respectively. However, the presence of a shoulder at the peak of a carbonyl from ester at 1808 cm^{-1} indicates that there is residual cyclic carbonate[43]. Besides, the absorption peak of amide at about 1653 cm^{-1} indicates an amide group resulting from ester group from ammonolysis and the C-O stretching vibration from unreacted free secondary NH groups of PAPO, which can be related to the partial reaction of secondary NH groups with cyclic carbonate functions[124]. In all cases except for $NIPU_1$, as the curing time increases, the band associated with the carbonate cycle at 1800 cm^{-1} decreases, indicating that the formation of the urethane group occurs during 24 hours of curing.

$NIPU_1$ was prepared using stoichiometric molar ratio of $PAPO_2$ to $CSFO_3$, ATR-FTIR spectrum of $NIPU_1$ (Figure 30) shows incomplete reaction of carbonate due to the presence of an intense signal at 1804 cm^{-1}, even after 24 hours, which suggested that the number of amines available of $PAPO_2$ to react with $CSFO_3$ were insufficient, besides the peak at 1700 cm^{-1} from urethane group is unclear and is overlapped with the ester carbonyl stretching band at 1741 cm^{-1}. These results indicate that the total content of amine of PAPO does not react completely with CSFO. Maybe the secondary amines present in the PAPO react only partially with the carbonate, while the rest of the NH molecules are impeded to react, due to the starting structure of the PAPO precursor. Therefore, the molar ratio between $PAPO_2$ and $CSFO_3$ was increased to 1:1.5, to achieve a higher degree of conversion of the carbonate groups. Increasing the molar ratio until 1:1.5, an almost complete reaction with carbonate groups was clearly observed as a small shoulder at 1800 cm^{-1} and the appearance of a well defined vibration band at 1705 cm^{-1} corresponding to urethane groups. For all the other prepared NIPU, these bands appeared with variable intensities.

For $NIPU_2$ prepared with $PAPO_2$, ATR-FTIR spectrum (Figure 31), shows a band at 1650 cm^{-1}, that corresponds to unreacted NH, which was more intense than the same band at $NIPU_3$ spectrum (Figure 32), which was prepared by using 50% of excess of $PAPO_3$, with a higher total amine value. Therefore, the functionality of this amine precursor directly affects the degree of reaction, which has the highest number of available free amines to react with the carbonate groups. However, in both cases urethane groups were formed during the reaction, but predominantly for $NIPU_3$.

Finally, to enhance the reactivity of the system, considering the challenge that represents the use of secondary amines of PAPO, 50% EDA relative to $PAPO_3$ was added. For $NIPU_4$, a stoichiometric ratio between $CSFO_3$ and $PAPO_3$ was used, while for $NIPU_5$, an excess of 50% of PAPO was used. ATR-FTIR spectrum of $NIPU_4$ (Figure 33), is similar to the spectrum of $NIPU_3$, however, at 0 hours, higher conversion of carbonate group is appreciated, because

of the presence of a smaller shoulder in the band at 1800 cm^{-1}, indicating that the incorporation of EDA accelerates the reaction between amines and carbonates. On the other hand, the ATR-FTIR spectrum of $NIPU_5$ (Figure 34), shows that the band at 1653 cm^{-1} corresponding to unreacted NH groups of $PAPO_3$ is higher when increasing the molar ratio of $PAPO_3$ and $CSFO_3$. Therefore, a higher amount of PAPO does not represent a higher degree of reaction but a higher amount of unreacted secondary amines, yielding a lower crosslinked network. Due to the ATR-FTIR study of the NIPU samples at different curing times, the direct relationship between the curing time and the crosslinking of the reaction between the carbonate groups of the CSFO and the reactive amines present in the PAPO samples was established and associated to the elastic behavior of the obtained NIPU polymers.

Table 13: Assignment of representative bands of ATR FTIR spectra of NIPU samples.

Wave number (cm^{-1})	**Assignment**
3300	Urethane N-H/hydroxyl OH stretching vibrations
1800	Unreacted cyclic carbonate groups
1740	Steric carbonyl group related to ester double bonds
1699	Stretching of urethane carbonyl
1646	C=O stretching vibration of amide at 1646 cm−1 (amide I) related to free secondary NH groups originate from the PAPO structure
1534	Combination of C-N stretching/N-H out of plane bending
1249	Steric carbonyl group related to single bonds
1148	C-O-C stretching vibration.

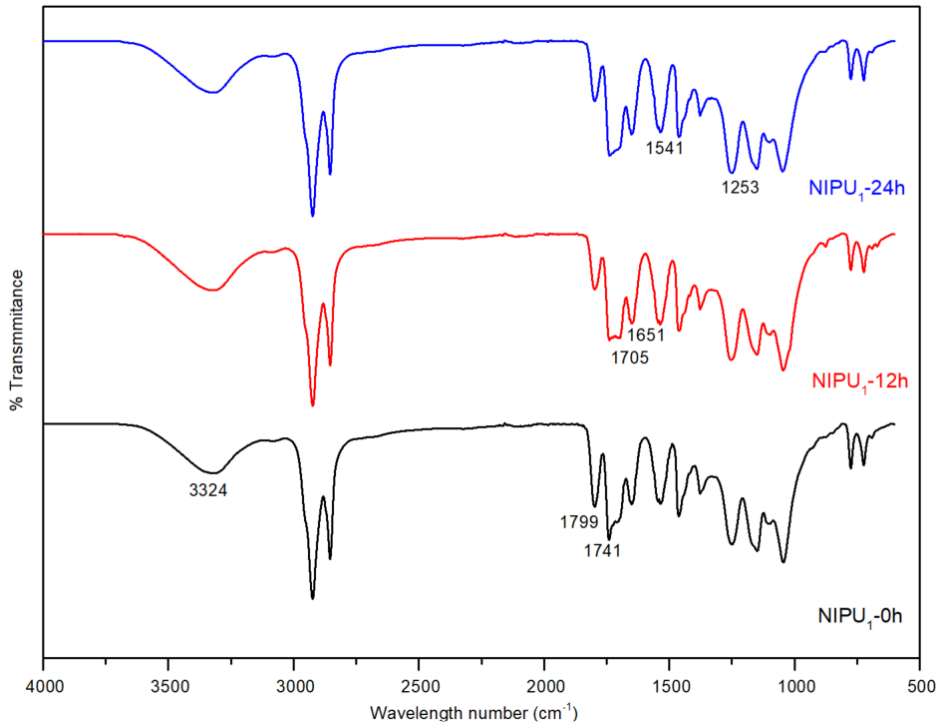

Figure 30 ATR-FTIR spectra of $NIPU_1$ at different curing times.

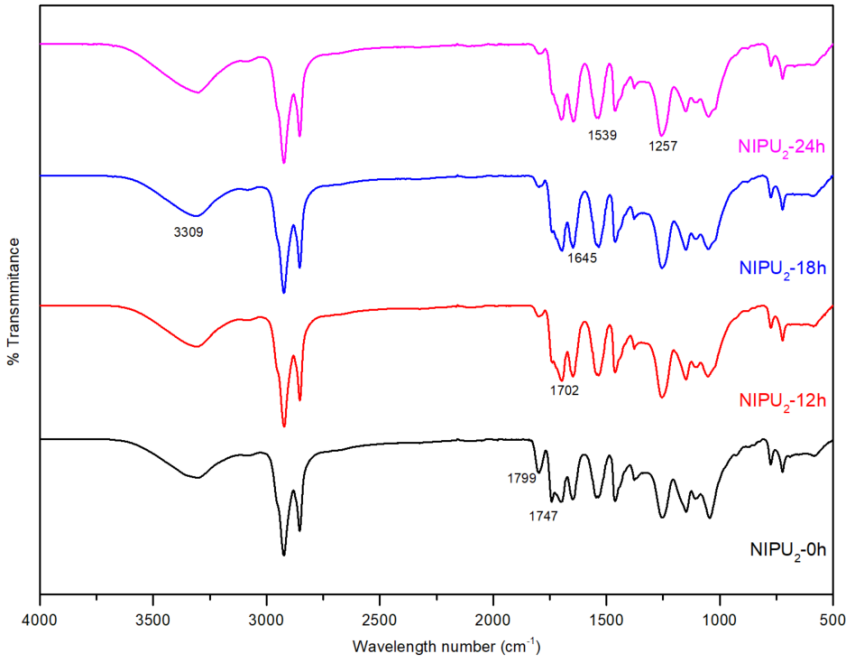

Figure 21: ATR-FTIR spectra of $NIPU_2$ at different curing times.

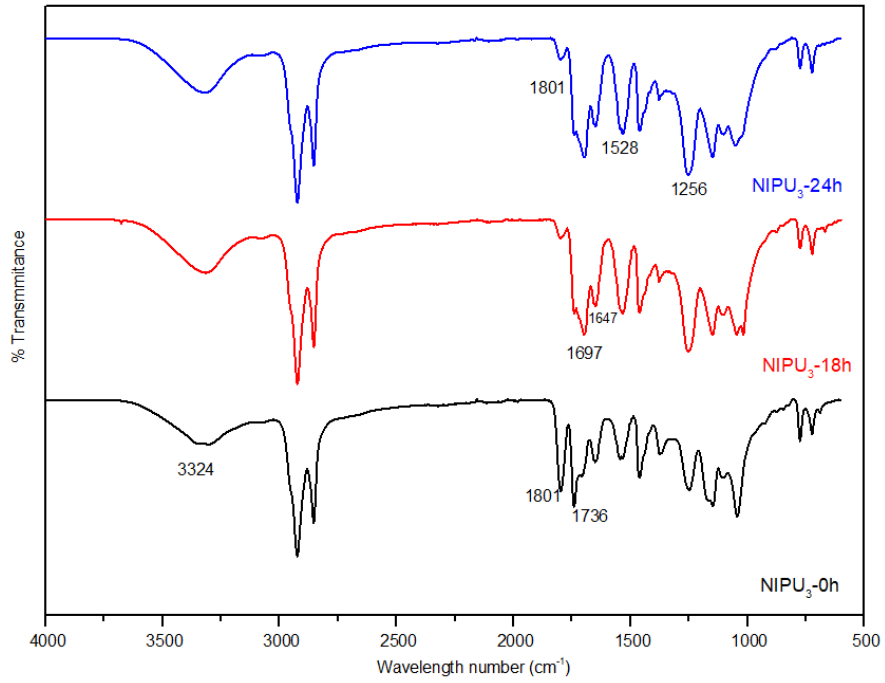

Figure 32: ATR-FTIR spectra of $NIPU_3$ at different curing times.

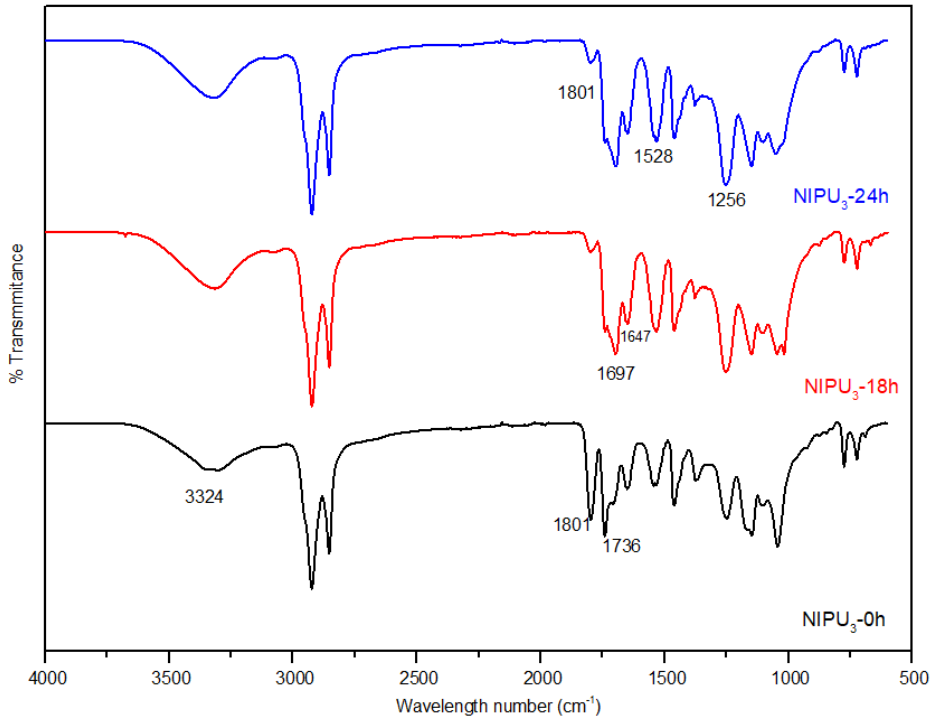

Figure 33: ATR-FTIR spectra of $NIPU_4$ at different curing times.

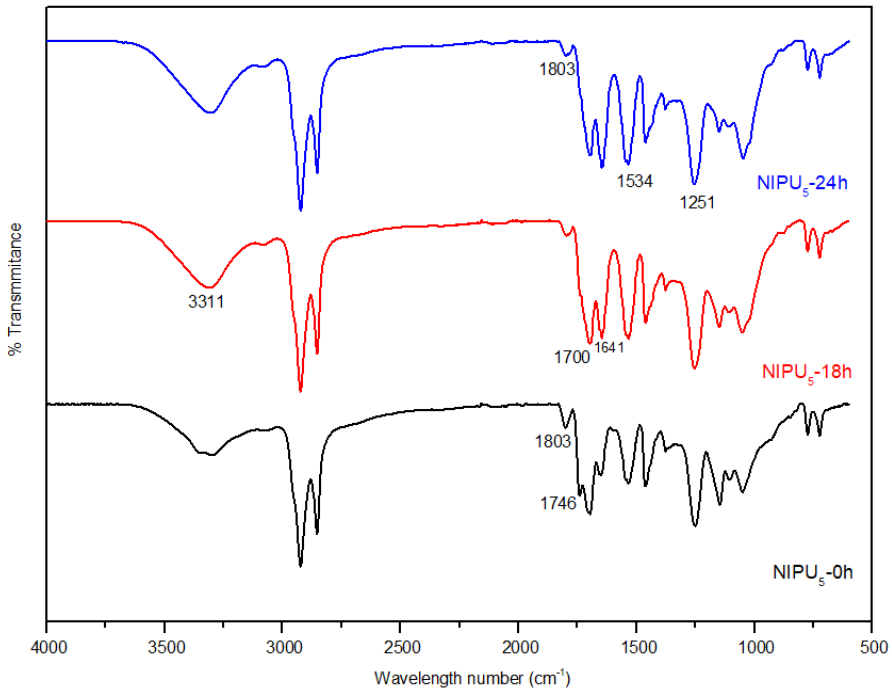

Figure 34: ATR-FTIR spectra of $NIPU_5$ at different curing times.

33.

3.6.2. Glass transition temperature and curing behavior by DSC analysis

To study the thermal behavior of the reaction between CSFO and PAPO at different curing times and using different molar ratios between the precursors, differential scanning calorimetry (DSC) was used to determine the glass transition temperature (Tg) of the NIPU samples and compare it with the thermal behavior of the precursors. Tg of the obtained NIPU films may be affected for different parameters such as molar mass, cross-linking density, type of lateral groups, among others[8]. Therefore, to correlate this parameter with some properties of the resulting material and establish the influence of different variables of the synthesis, such as curing time and reactants molar ratio was possible.

DSC thermograms of the precursors of NIPUs synthesis, $CSFO_3$, $PAPO_2$ and $PAPO_3$ and DSC thermograms of the various NIPU samples at 24 hours are shown in figures 35 and 36, respectively. Glass transitions temperatures of different NIPU samples at different curing times determined by DSC are listed in table 13. DSC thermograms of precursors, $CSFO_3$ show two melting points, while for $PAPO_2$ and $PAPO_3$ glass transition temperatures are observed, but both also showed well defined melting peaks in the range of -39.53 to -42.83 °C. PAPO precursors showed the thermal behavior of elastomers that have very low Tg, which indicates the elevated mobility of their chains (due to conformational changes), leading to

materials with a great elasticity at room temperature[8]. Although, both amine precursors are rubbery at room temperature, Tg of $PAPO_3$ results lower than Tg of $PAPO_2$, possibly because of the presence of higher number of free amines in $PAPO_3$ structure, which suggests a larger mobility of the polymer chains. The obtained Tg values were in accordance with the results reported by Wang et al[8] for the synthesis of elastomers, although they used epoxidized soybean oil.

For NIPU samples, the formation of a crosslinked structure after different curing times can be studied by the DSC thermograms. While a melting behavior was observed for the precursors, for NIPU, the two melting peaks of $CSFO_3$ disappear and abrupt changes in the position of the baseline in DSC plot were observed for each NIPU sample. These events were related to Tg, in which there is a step change in specific heat capacity, which causes an abrupt change in the steady-state value of differential energy input (ΔE), which moves to a higher value of ΔE above Tg[2]. The Tg for each sample was determined and for all NIPUs Tg increases with the longer the curing times, clearly related to the degree of crosslinking as is shown in table 13. However, $NIPU_2$ reached a maximum temperature of 10.54 °C at 18 hours, which can be associated to a higher degree of conversion during the mixing process, leading to a lower reaction time, because within 24 hours of curing, a decrease in Tg until -4.36°C was observed. Because of the accelerated reaction, this behavior may be correlated with a rearrangement of the polymeric network due to degradation of the formed urethane groups. The other polymers needed 24 hours to achieve their higher Tg temperature, as is shown in table 14.

Considering the molar ratio between the precursors, it was observed that $NIPU_4$ at 24 hours, synthesized with a lower amount of PAPO and adding 50% EDA, presented the highest Tg at 23.13°C, while $NIPU_3$ and $NIPU_1$ prepared with different PAPO precursors and with different molar ratios between them, only reached a Tg near 8°C at 24 hours. On the other hand, $NIPU_5$ only reach 8.69 °C after 24 hours, indicating a higher amount of unreacted free secondary amines from PAPO. These results suggested that the addition of EDA clearly accelerates the reaction, obtaining a higher degree of crosslinking at the same time that the systems that use a higher amount of PAPO. It might be possible that the curing reaction slows down due to the steric hindrance caused by secondary amines within the PAPO structure. Therefore, the presence of unreacted free secondary amine in the structure of the resulted NIPU can provide other properties to the material when compared to the commercial petroleum-based amines, or when are blended with a lower amount of the same kind of commercial amines. Because lower values of Tg may give greater elasticity to the resulting polymers.

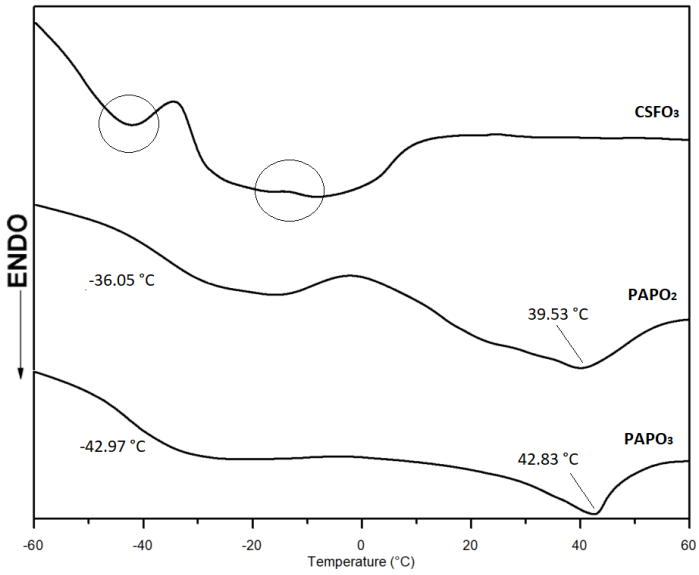

Figure 35: DSC thermograms of CSFO and PAPO precursors used for NIPU synthesis.

Table 14: Glass transitions temperatures of NIPU samples at different curing times determined by DSC.

NIPU sample	Tg (°C)			
	0h	**12h**	**18h**	**24h**
$NIPU_1$	1.7	5.76	-	7.99
$NIPU_2$	-7.86	4.97	10.54	-4.36
$NIPU_3$	0.13	-	8.53	7.98
$NIPU_4$	2.46	-	21.04	23.13
$NIPU_5$	-4.39	2.64	-	8.69

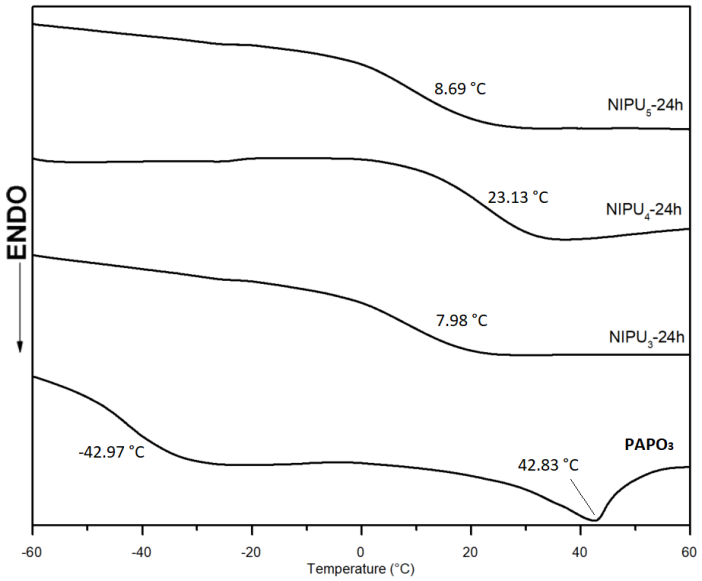

Figure 36: DSC thermograms of NIPU samples prepared with $PAPO_3$ at 24 hours of curing.

$NIPU_3$ at 24h of curing was selected as the polymeric system for this work, because high carbonate conversion was observed by FTIR and corroborated with its DSC thermogram, which showed the higher Tg at this curing time, associated with the degree of conversion. While for $NIPU_1$, although the DSC results shows an increase on Tg, the IR analysis shows low degree of carbonate conversion and for $NIPU_4$ and $NIPU_5$, which contain 50% of EDA, did not result in an easy-to-handle mixture, while a high conversion is also obtained without using EDA. Besides, the use of PAPO as amine source for NIPU synthesis instead of petroleum-based commercial amines, was selected because combination of primary and secondary amines in the precursors has been reported to give polymers with enhanced properties[120,121,125].

A relationship between the relative degree of crosslinking of the $NIPU_3$ polymer and a mechanical property such as the Young's modulus, will be discussed in the characterization section.

In conclusion, to produce NIPU thermosets it is important to study the reaction of cyclic carbonates with amines involved in the curing process, in which simultaneous nucleophilic attack of amine over cyclocarbonate takes places and is followed by a deprotonation reaction. Therefore, a kinetic analysis will be necessary for the reaction, in order to establish the better conditions to enhance the reactivity and selectivity, as well as understand the behavior of the crosslinking process[23]. A scheme related to the crosslinking reaction between CSFO and PAPO is shown in Figure 37. Different cyclic carbonate/amine formulations as well as the difference in the glass transition temperatures directly affect physical, thermal, and mechanical properties of the obtained polymer. Besides, NIPUs

properties can be highly dependent on time and temperature conditions used during the synthesis. Therefore, there are several variables that must be consider on the preparation of this kind of materials.

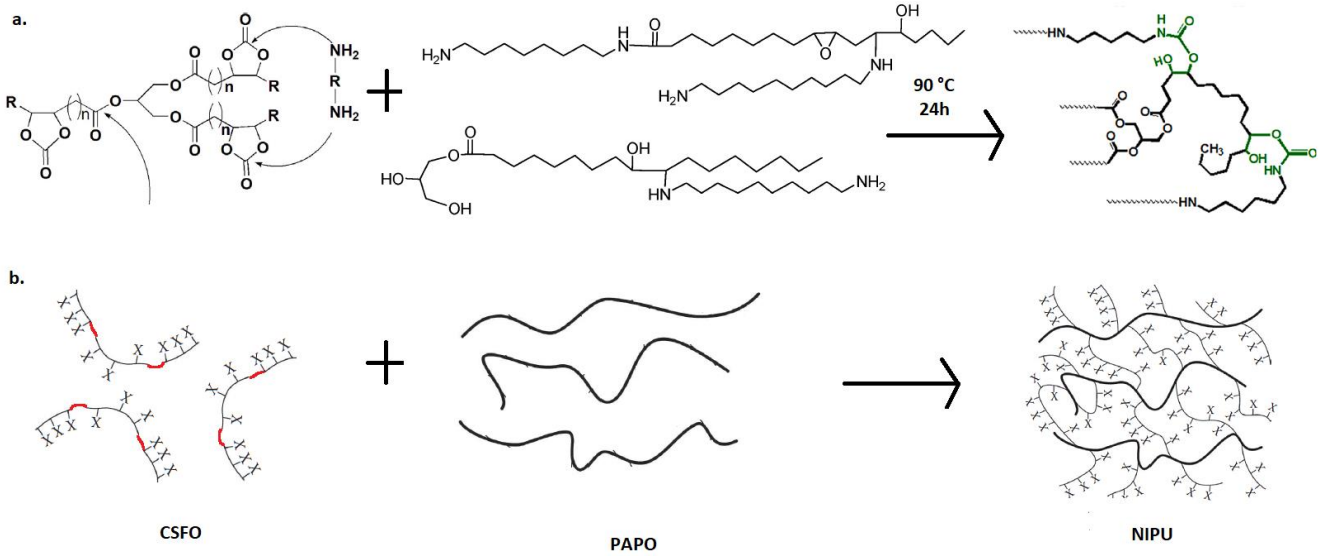

Figure 37: Scheme of crosslinking reaction for NIPU production. a) Reaction between cyclic carbonate and amine and the NIPU product with free secondary amines. b) Sketch of crosslinking reaction between CSFO and PAPO.

3.7. Surface modification of NIPU films with chitosan by using a photo grafting technique

Once $NIPU_3$ films were obtained, to promote biological characteristics of the material, a two-step methodology was executed using acrylamide and chitosan, as antibacterial agent to modify the NIPU surface. The photo grafting reaction to graft AM is shown in figure 38. NIPU films were immersed in a solution containing 0.2 M of the initiator BP, 1.5M of the monomer AM in methanol as solvent, and immediately enclosed into the curing lamp and irradiated with UV light for 15 min in both sides. After the photo grafting process, AM modified films were washed with NaOH 0.1M to neutralize, and several times with water to remove excess of acrylamide. These conditions were selected to perform the photo grafting reaction, as the most appropriate, to avoid deteriorate or change the bulk properties of $NIPU_3$, as will be discussed below.

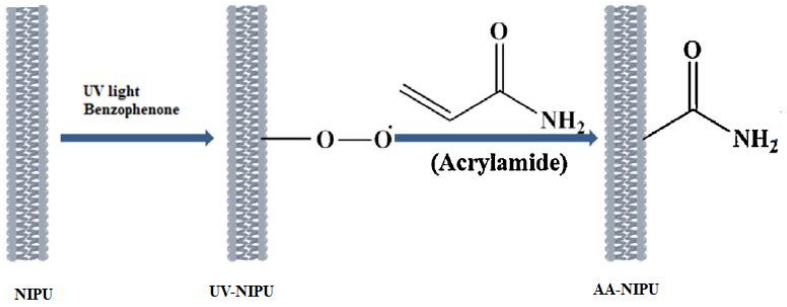

Figure 38: Scheme of acrylamide photo-induced graft polymerization onto NIPU films surface.

The presence of grafted AM on the surface of NIPU was confirmed by ATR-FTIR analysis. Figures 39 and 40 show the NIPU ATR-FTIR spectra before and after UV treatment with AM at a concentration of 1.5 M and the spectra of modified NIPU films using different concentrations of AM, respectively. Significant differences can be observed among the modified and unmodified films. A weak shoulder due to the vibration of H in C=H at 983 cm^{-1}, assigned to the monomer of acrylamide, almost disappears in the modified film. The peak of C-C vibration at 1023 cm^{-1} becomes evident in the modified film, which indicates that the graft polymerization of AM into $NIPU_3$ surface has occurred[126]. All spectra of AM-NIPU films showed that the CO (NCOO) band of urethane at 1700 cm^{-1} decreased, while amide CO (CO NH_2) band at 1676 cm^{-1} increased. Also, the stretching vibration of CN at 1415 cm^{-1} and rocking of NH_2 at 1271 cm^{-1} were present. NH band of NIPU at 3300 cm^{-1}, shifted to 3331 and 3198 cm^{-1} due to amide NH_2 stretching[55], confirming that active functional amide groups ($–NH_2$) of AM were grafted onto NIPU surface.

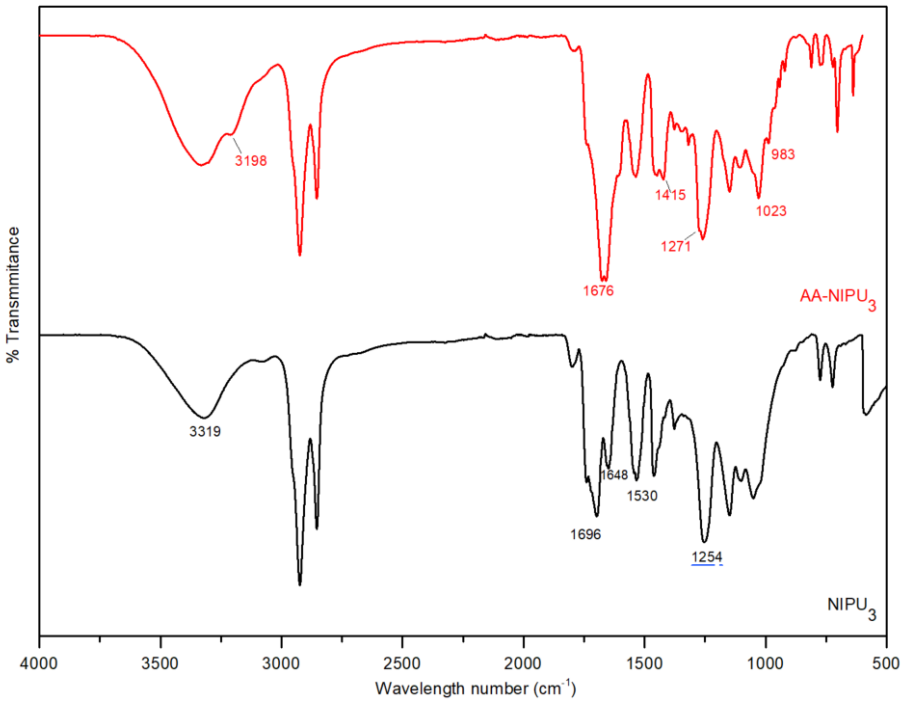

Figure 39: ATR-FTIR spectra of polymeric NIPU films**,** $NIPU_3$ and AM-$NIPU_3$, before and after the UV treatment to the photografting polymerization of acrylamide.

AM-$NIPPU_1$ has the lowest concentration of AM, showing a small decrease in the CO band of urethane at 1700 cm^{-1}, which was associated with a lower degree of grafting. While for AM-$NIPU_3$ modified with 1.5 M of AM, the spectrum showed a well-defined band at 1676 cm^{-1} related to amide CO (CO NH_2) and the presence of a band of C-N stretching and CH_2 deformation at around 1420 cm^{-1}, confirming the presence of AM grafted groups on NIPU surface. These features have been previously used as a proof of AM polymerization under the influence of γ-irradiation[127].

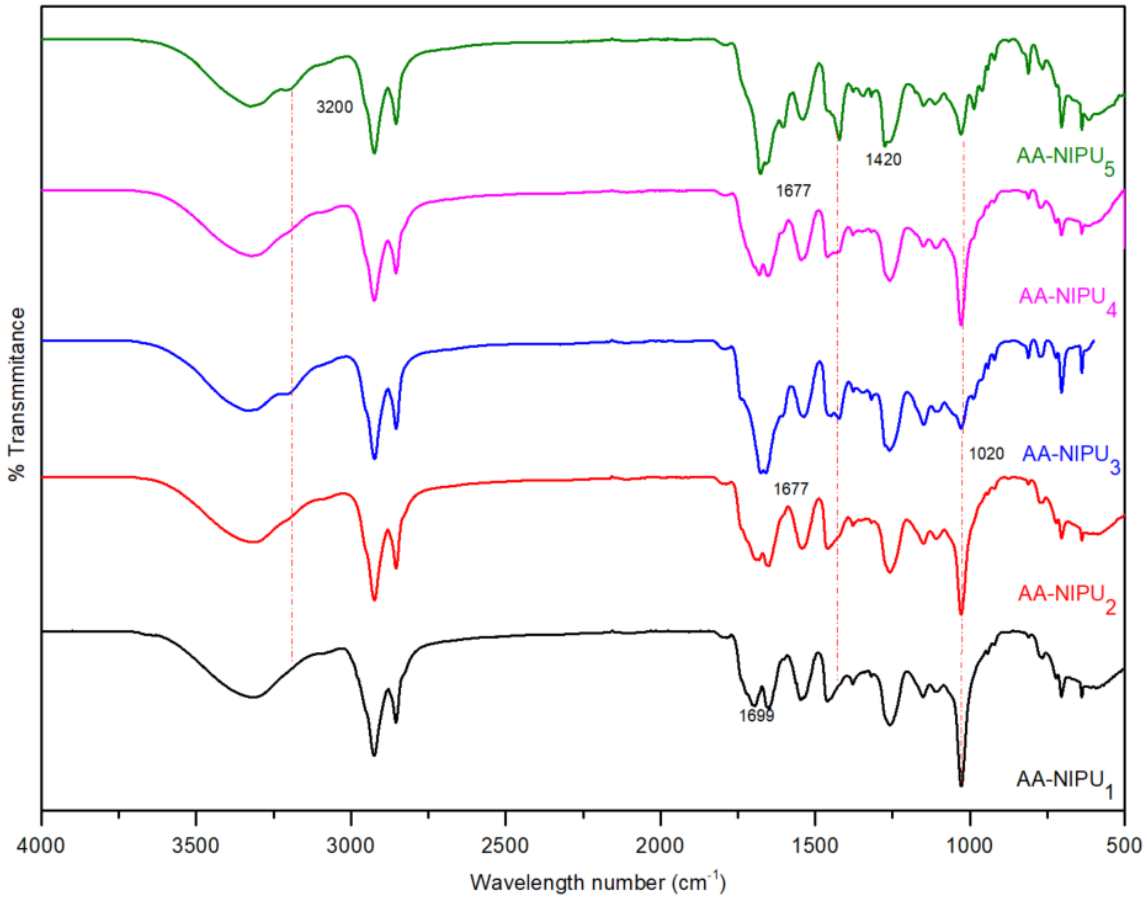

Figure 40: ATR-FTIR spectra of modified NIPU films using different concentrations of AM, indicating changes in the intensity of the bands around 1677 and 1420 cm^{-1}, associated with amide CO (CO NH_2) and C-N stretching, respectively.

Using different AM solutions, it was observed that with concentrations of 2M or higher, a permanent damage of the sample occurred after the photografting procedure. When AM concentration was increased to 4 M, it was observed that a white solid residue is formed and covered almost all the surface of the film. This solid residue was associated to a product from the acrylamide homopolymerization, due to an excess of acrylamide groups, and by the presence of the photoinitiator which may remove hydrogens from the polymer surface, inducing the self-polymerization of AM. Figure 41, shows the spectrum of the white solid residue in which the bands at 3454 and 3184 cm^{-1} were assigned as NH_2 stretching antisymmetric and symmetric modes, respectively, and are associated with acrylamide and polyacrylamide[127]. Only with a concentration of 1.5 M were obtained stickier NIPU films but with defined shape. Therefore, this concentration was used to perform the first step of the

surface modification. The polymeric products described above, before, and after of the photo grafting procedure are shown in Figure 42.

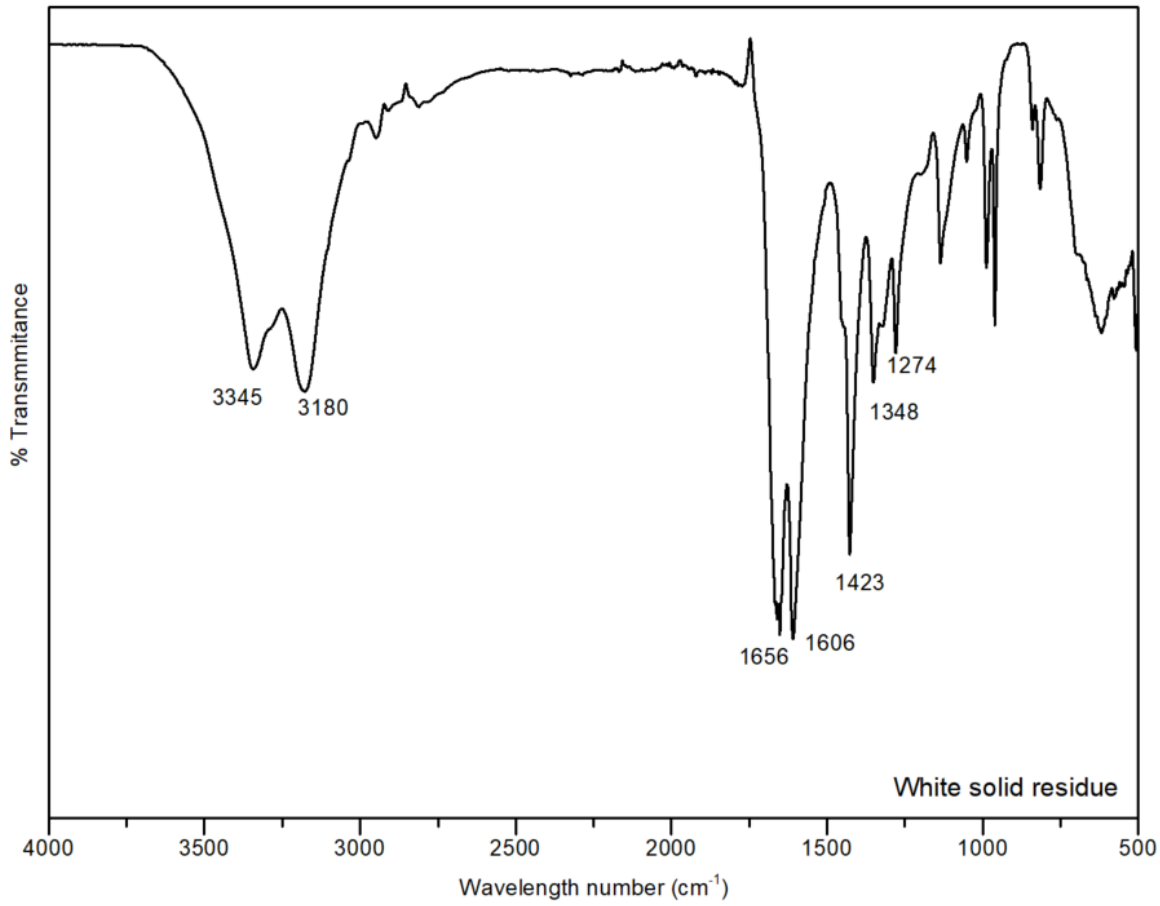

Figure 41: ATR-FTIR spectrum of the white solid residue formed after photografting procedure with acrylamide solution of 4M.

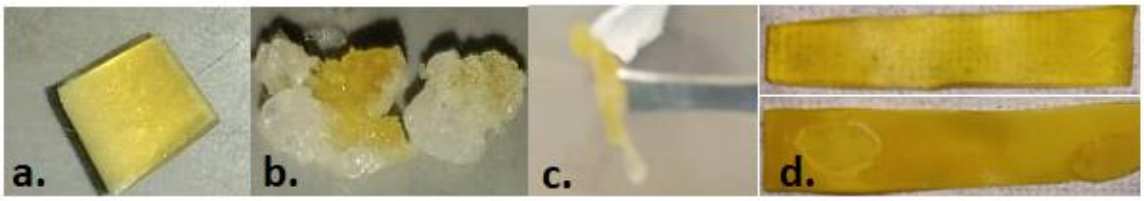

Figure 42: NIPU films before and after the procedure of acrylamide photo grafting. a) Unmodified $NIPU_3$ film of 24h of curing. b) AM-$NIPU_5$ modified with AM solution of 4M and the white solid residue c) AM-$NIPU_4$ modified with AM solution of 2M. d) AM-$NIPU_3$ modified with AM solution of 1.5M.

The second step of the surface modification consisted in using the grafted $–NH_2$ groups on the NIPU surface for binding chitosan molecules. For this purpose, it was adopted an approach previously developed by Kara et al. [55], who immobilized CS into conventional PUR. Briefly, AM-$NIPU_3$ films were dipped in a solution of glutaraldehyde (GA). Then, AM-$NIPU_3$ films were dipped in a solution of chitosan (CS) at different concentrations of 6, 12, and 20 mg/ml. The resulted samples were named CS-$NIPU_1$, CS-$NIPU_2$ and CS-$NIPU_3$, respectively. CS-NIPU samples were washed with acetic acid, to remove non-bonded CS, neutralized with NaOH and washed repeatedly with distilled water.

Figure 43, shows a scheme of the covalent attachment of chitosan into AM grafted NIPU films, by using glutaraldehyde to promote the crosslinking of amide groups[128]. The resulted chitosan modified NIPU films are shown in Figure 44. A whitish layer can be observed on the surface of the polymeric films after the treatment with chitosan.

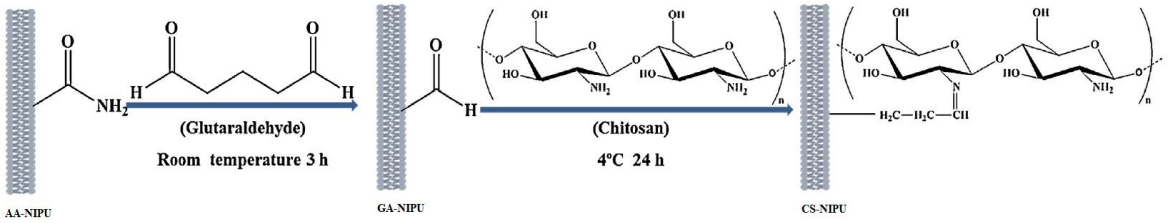

Figure 43: Scheme of covalent incorporation of chitosan into AM grafted NIPU films.

Figure 44: Chitosan modified NIPU film.

ATR-FTIR analysis was also used to evaluate chitosan treatment. Figures 45 and 46 show the ATR-FTIR spectra of the AM-$NIPU_3$ films before and after the treatment with chitosan at a concentration of 12 mg/ml and the spectra of polymeric films modified using different

concentrations of CS, respectively. All CS-NIPU samples had a broad peak between 3200 and 3500 cm^{-1} corresponding to OH and NH stretching groups[55]. The band of amide at 1672 cm^{-1} shifted to 1653 cm^{-1}, confirmed the presence of residual N-acetyl groups of chitin from C=O stretching of amide I [129], directly related to the N-deacetylation of chitosan[130], and the band at 1548 cm^{-1} that corresponds to bending vibrations of primary amines. Finally, the peaks observed at 1000–1200 cm^{-1} region are typical for polysaccharides structure. These absorptions may be related to the covalent attachment of chitosan molecules to the acrylamide grafted molecules[55]. For all cases, changes related to binding of chitosan could be observed in the spectroscopic analysis, indicating that a surface modification with chitosan was performed over NIPU films.

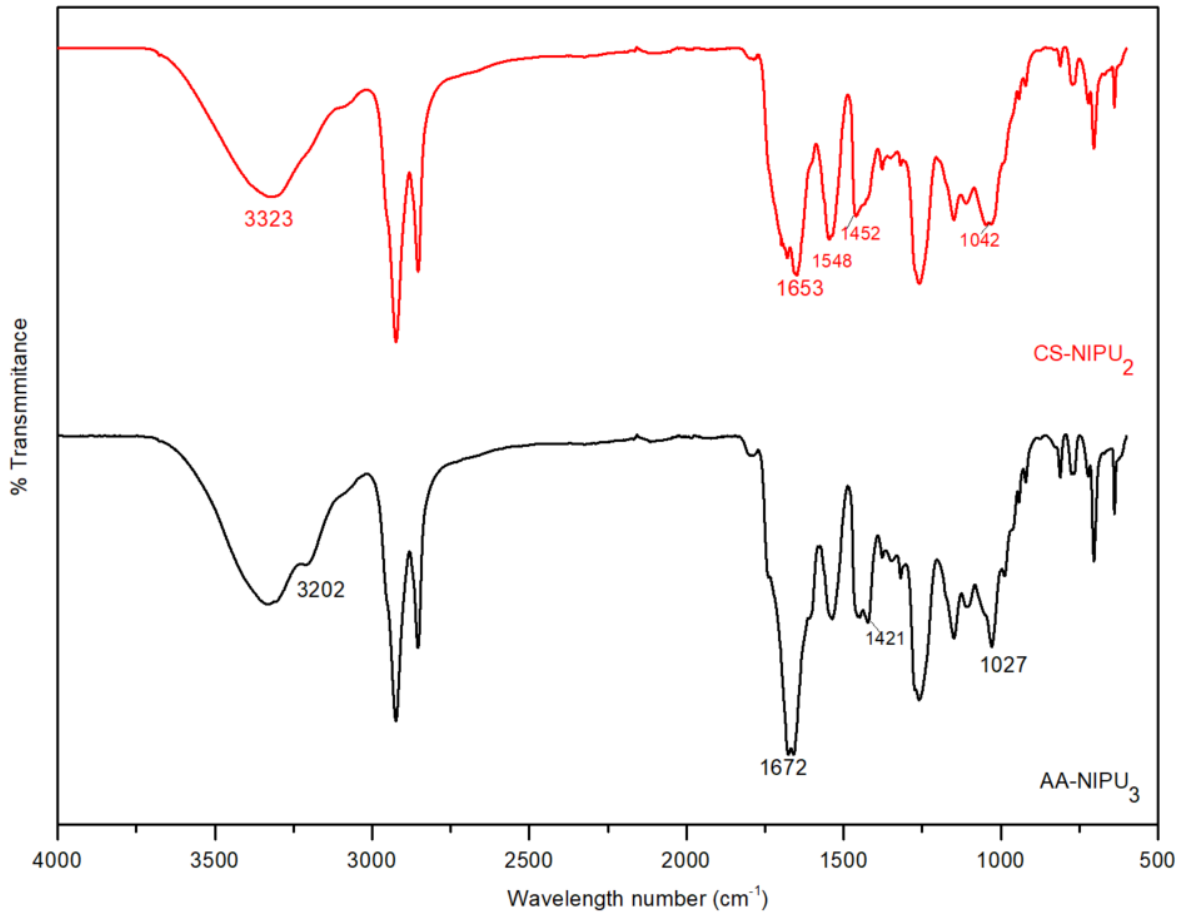

Figure 45: ATR-FTIR spectra of polymeric NIPU films, AM-$NIPU_3$ and CS-$NIPU_2$, before and after the treatment with chitosan of 12 mg/ml.

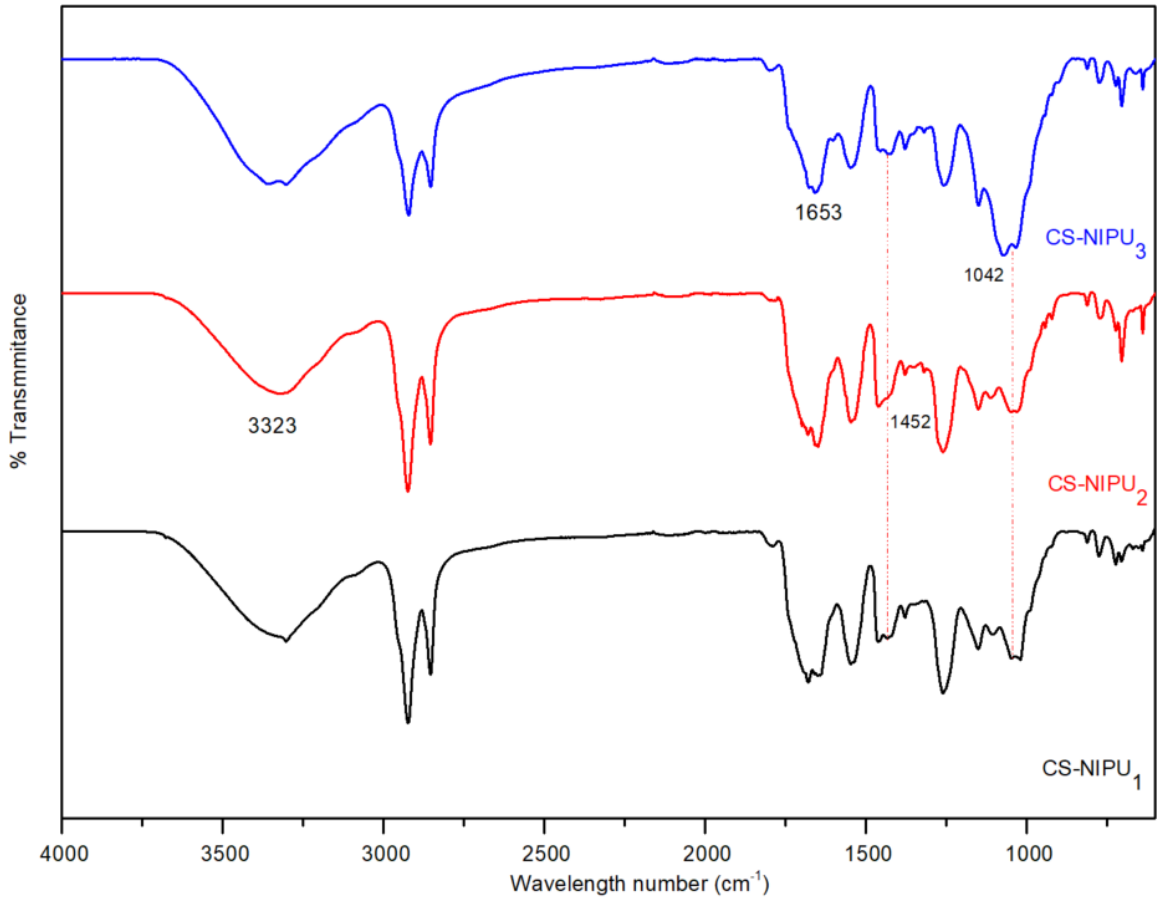

Figure 46: ATR-FTIR spectra of modified NIPU films using different concentrations of CS.

Three different concentrations of CS were used for the grafting reaction. For the sample treated with the smallest concentration, CS-NIPU$_1$, the spectrum remained almost unchanged, specifically related to the C-N stretching and CH_2 deformation of acrylamide groups around 1420 cm^{-1}, in contrast to CS-NIPU$_2$ and CS-NIPU$_3$ treated with higher concentrations of CS, where a decrease in those bands was appreciated and related with chitosan binding groups. Although, the CS-NIPU$_3$, which has the highest CS concentration, shows more changes in the ATR-FTIR respect to the AM-NIPU$_3$. CS-NIPU$_2$ with a concentration of 12 mg/ml was selected to perform the chitosan treatment, because the spectra of different points over the sample surface, did not show any changes, (Figure 48), while different points of the surface spectra for CS-NIPU$_3$ were different, indicating an heterogenous grafting reaction along the surface for this sample (Figure 47). Therefore, a more uniform grafted surface was obtained for CS-NIPU$_2$. To define the best condition to perform the surface modification and to obtain more uniform surfaces, it will be necessary to evaluate the influence of each variable of the process in the resulting product and if the

modification technique as well as the antibacterial agent can be modified differently, so that a minimum damage of the sample will occur.

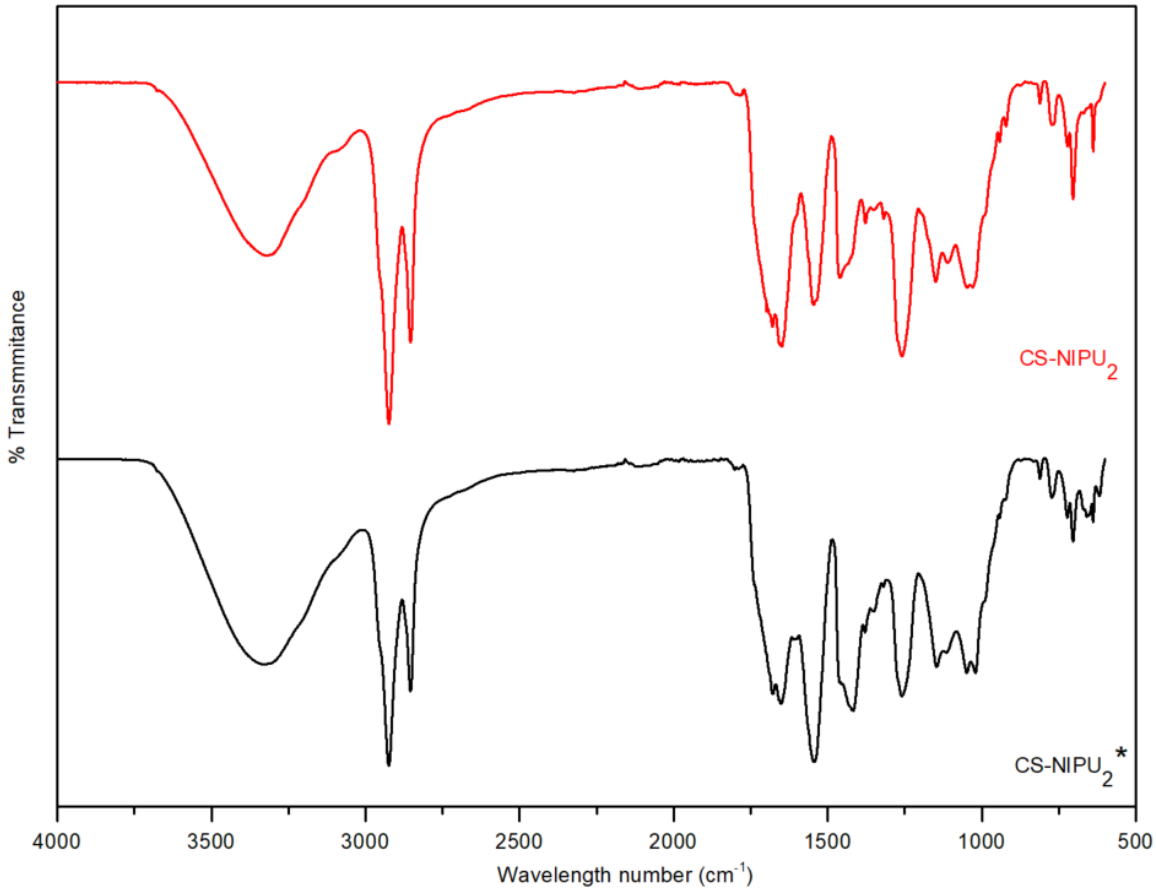

Figure 47: ATR-FTIR spectra of CS-NIPU$_2$ at different points along the surface.

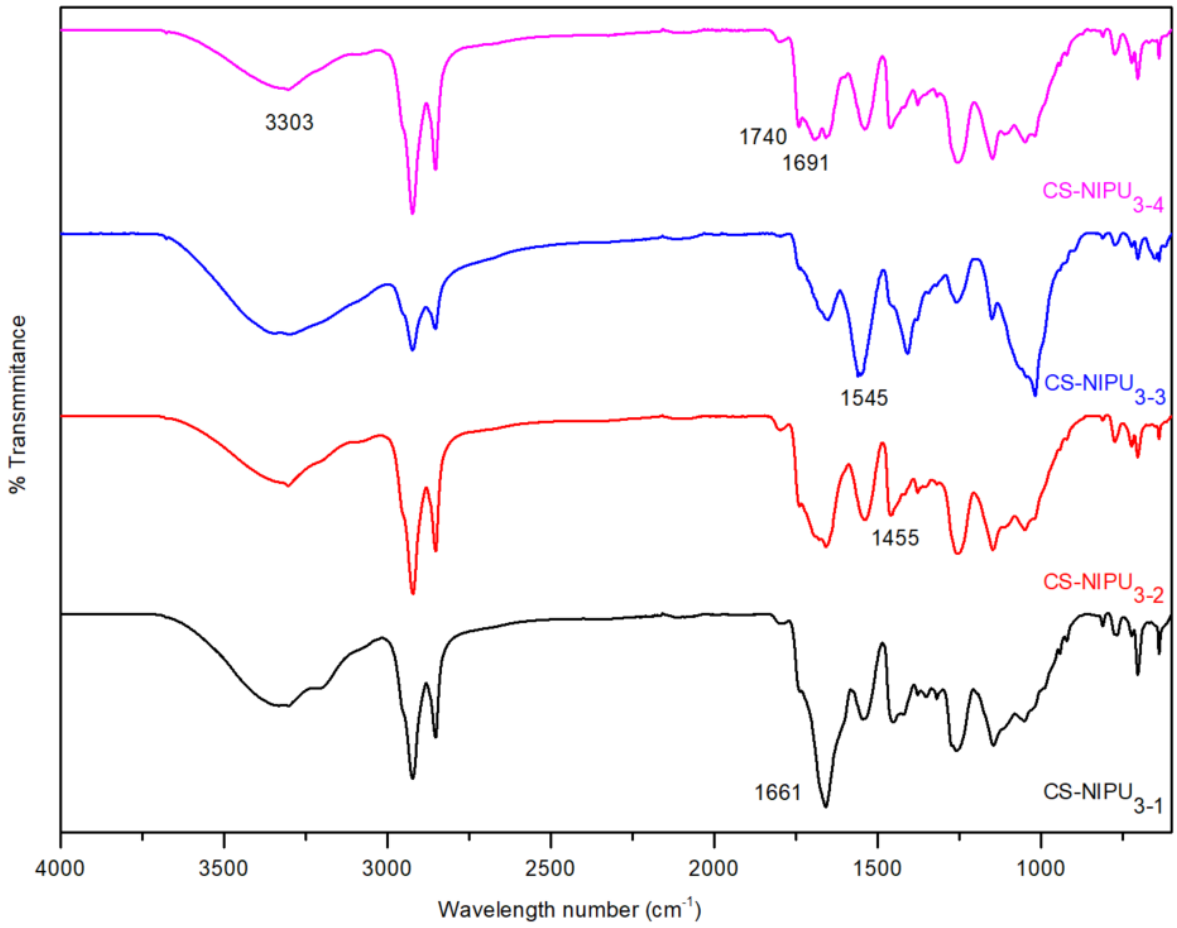

Figure 48: ATR-FTIR spectra of CS-NIPU$_3$ at different points along the surface

To determine the Tg of the NIPU films after the photo grafting of acrylamide and the chitosan treatments, related to the unmodified NIPU films, DSC technique was used. Figure 50 shows the DSC thermograms of the selected system before and after the surface modification and figure 51 shows the thermograms of the modified NIPU films when different CS concentrations were used. A decrease on Tg after each step of surface modification methodology was observed. Photografting of AM procedure, results in a Tg decrease from 7.78 °C, for the unmodified NIPU films to 3.10 °C for the AM-NIPU. Then after the chitosan treatment, a large decrease on Tg until -10.41 °C was determined for CS-NIPU$_2$, while for CS-NIPU$_1$ the Tg showed a smaller decrease until 2.12°C, meaning that there were no appreciable changes between the AM modified NIPU and the resulting CS-NIPU$_1$. For CS-NIPU$_3$, Tg was -11.67 °C, which shows that a higher CS concentration, may lead to a polymer with a relative lower degree of crosslinking. These results demonstrate that after the surface modification treatment, the arrangement of the polymeric network changed, making the polymer more elastic and reversing the crosslinking of the material, as was previously related with the changes on Tg. These features were also appreciated in the physical shape and tact sense of the resulting polymer, and they may improve or deteriorate

the obtained material, depending on the expected properties. Therefore, a more detailed analysis is required.

The chemical modification of the films' surfaces was confirmed through changes in the infrared spectra and Tg. However, to establish the real success of the surface modification technique to impart antibacterial characteristics to the polymer, the following section includes the mechanical, morphological, and biological characterization of the unmodified and modified films.

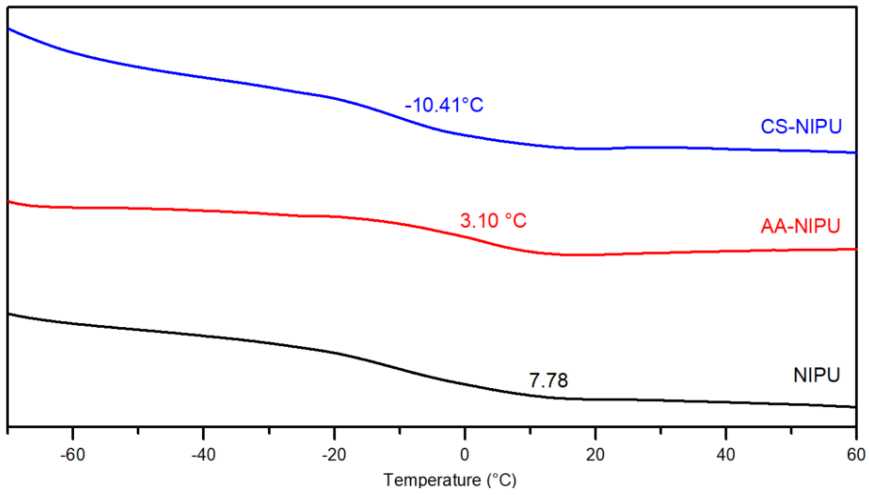

Figure 50: DSC thermograms of the selected NIPU samples before and after of the surface modification process.

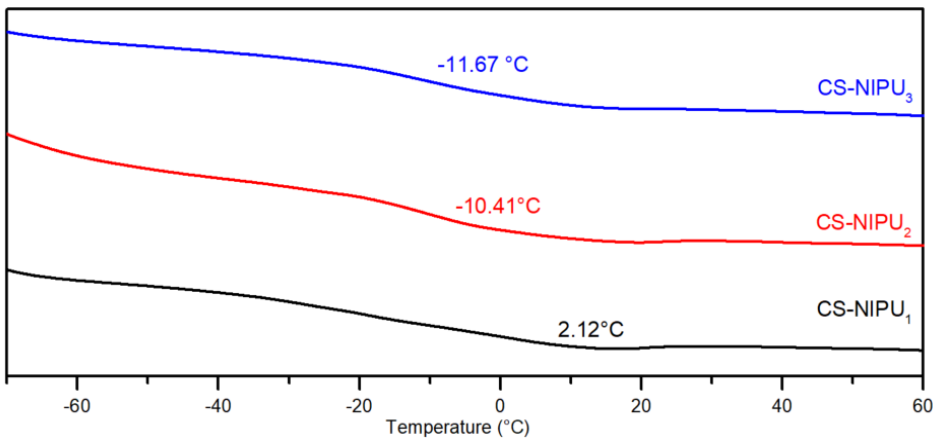

Figure 51: DSC thermograms of chitosan modified NIPU samples using different CS concentrations.

3.8. Characterization of NIPU films modified with chitosan

Once the NIPU polymeric films have been obtained were subsequently modified with chitosan. To establish the potential application of the obtained materials, the final section of this work includes the thermal, mechanical, morphological, and biological characterization of the unmodified and modified NIPU films.

3.8.1. Thermal degradation behavior

The thermal degradation behavior of the prepared $NIPU_3$ precursors, $CSFO_3$ and $PAPO_3$, as well as the unmodified and modified NIPU films was evaluated by thermogravimetric analysis (TGA). TGA thermograms are presented in Figure 52. Table 15 summarizes the temperatures for the tested samples at each one of the given percentages of weight loss and their residual weight above 600°C.

Thermal stability up to 200 °C was noticed for $NIPU_3$ and its precursors, $CSFO_3$ and $PAPO_3$. The thermograms of CSFO present one main degradation peak at 369 °C, which is associated with the thermal decomposition of cyclic carbonated. Considering that temperatures in the range of 288–306° correspond to the thermal decomposition of vegetable oils[114], and particularly for SFO, the thermal decomposition at 304°C has been reported previously[131], a decomposition peak at a higher temperature range (325–335°C) may be related to the carbonated product[114], which is in accordance with the values for carbonated vegetable oils reported in the literature[113]. Therefore, CSFO was more thermally stable than their SFO precursor. A slight degradation step at around 190 °C is observed in the CSFO thermogram, which had been reported as the decomposition of residual TBAB catalyst[132], with a weight loss of 2.5%. CSFO product was used without further purification because no presence of TBAB was appreciated in the spectroscopic analysis. In contrast to CSFO, two main thermal degradation steps were identified in the thermograms of PAPO, corresponding to the copolymer components. The weight loss of the first degradation step at 359 °C can be attributed to the degradation of ester groups, and the weight loss of the second degradation step at 441 °C corresponds to the decomposition of normal polyamide, which confirms the transition of ester into amide during the ammonolysis reaction [8].

For unmodified NIPU, TGA curves indicated that thermal decomposition of NIPU started at 211 °C, after a slight decrease in mass observed between 0 and 150 °C, due to the residual linked water molecules[35]. This thermal degradation may also be referred to the decomposition of low molecular weight compounds. The curve of the first derivative of

weight loss with respect to temperature or the differential thermogravimetric analysis (DTG) for NIPU (Figure 53) shows that NIPU decomposition proceeds in three steps at 220, 342, and 388 °C, corresponding to 6.4%, 44.8%, and 67.1% weight loss, respectively. These values are similar to those reported for other NIPUs from the literature but lower than those of conventional thermosetting PU, as dimer-based PU[133,134]. The first step can be attributed to the degradation of the hydroxyurethanes as a result of CN- bond low breaking energy[135]. Some authors indicated that the urethane bond decomposition in biobased polyurethanes starts at about 150–220 °C due to a primary amine or olefin presence, resulting in the formation of secondary amines and carbon dioxide. The following step was the degradation of the polyol backbone at about 400 °C[136], which confirms the presence of secondary amines from PAPO in the polymeric network. It is noteworthy that, the main weight loss peak at 342°C belongs to the degradation of other parts of the network including aliphatic hydrocarbon structures and to the presence of the hydroxyl functions in β-position of the urethane, which creates intra- and intermolecular hydrogen bonds[43]. The third peak approximately at 390 °C can be ascribed to the diamine degradation[137]. Considering the structure of the starting SFO-based precursors, the thermal stability achieved for the obtained NIPU may be related to the heterogenous structure of the final polymeric network, which was composed by different chemical groups besides urethane, such as amides, ester, and unreacted secondary amines, as was discussed in the ATR-FTIR analysis. However, thanks to the free secondary amines in the PAPO structure, the obtained NIPUs were coated films completely cured, which gives place to a dense structure via intra-molecular hydrogen bonding between urethane and hydroxyl, reflected in a higher thermal stability, as has been previously reported in literature[35].

The residual weight percentage at 600°C for NIPU, performed in oxidative atmosphere, was of 23.11%, which was higher than that of the precursors as is shown in table 15, confirming a higher thermal stability, although the temperature of the first thermal step for NIPU was lower than for PAPO. This behavior can be related to the crosslinking reaction between the precursors, showing that NIPU is composed by a dense structure via intra-molecular hydrogen bonding between urethane and hydroxyl groups, which improves the thermal stability[138].

According to the TGA curves, the variations induced by the presence of secondary amines illustrate that thermal stability was mainly affected by the content of the secondary amine. In other words, after reacting with epoxy groups under the condition of the programmed temperature, the secondary amines still had a good thermal stability and a dominant role.[139]

Table 15: Degradation parameters of unmodified and modified NIPU as well as its precursors: CSFO and PAPO. $T_{5\%}$, $T_{25\%}$, $T_{50\%}$, and $T_{75\%}$ is a temperature of 5, 25, 50 and 75% of weight loss, respectively.

Sample	$T_{5\%}$ (°C)	$T_{25\%}$ (°C)	$T_{50\%}$ (°C)	$T_{75\%}$ (°C)	Residual weight at 600°C (%)
$CSFO_3$	210.74	329.38	359.24	379.42	1.331
$PAPO_3$	260.96	350.54	378.99	429.23	4.262
$NIPU_3$	211.55	306.78	350.36	406.86	23.11
AM-$NIPU_{3\text{-}3}$	134.87	280.96	339.87	390.72	15.32
CS-$NIPU_{3\text{-}3}$	148.59	276.92	327.77	322.51	2.208

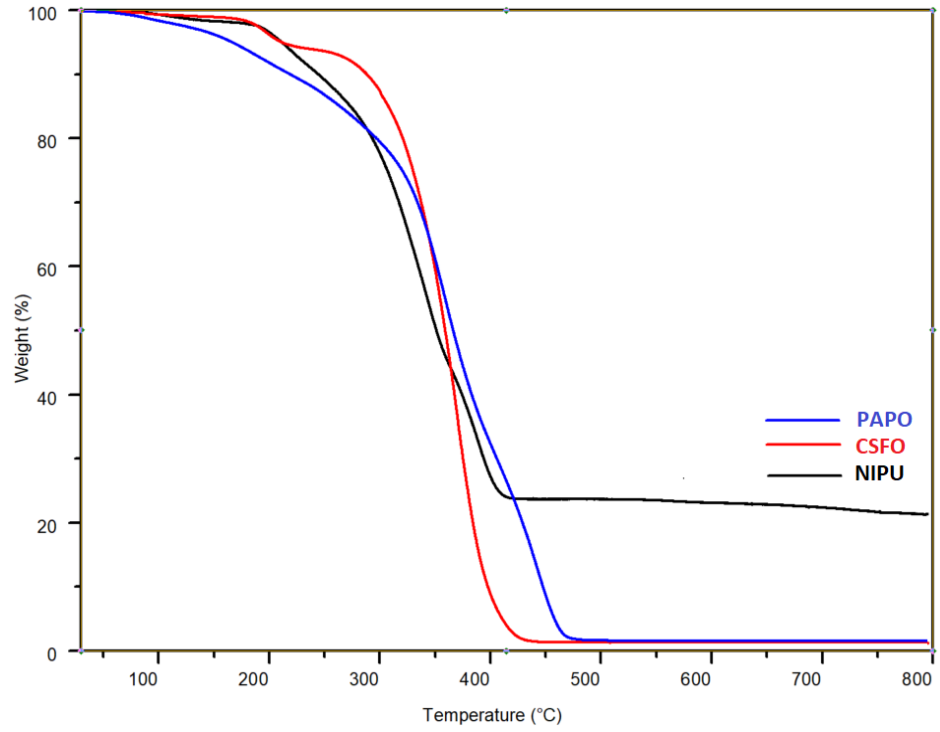

Figure 52: TGA curves of $NIPU_3$ and its precursors: $CSFO_3$ and $PAPO_3$ (10 °C min^{-1}, air).

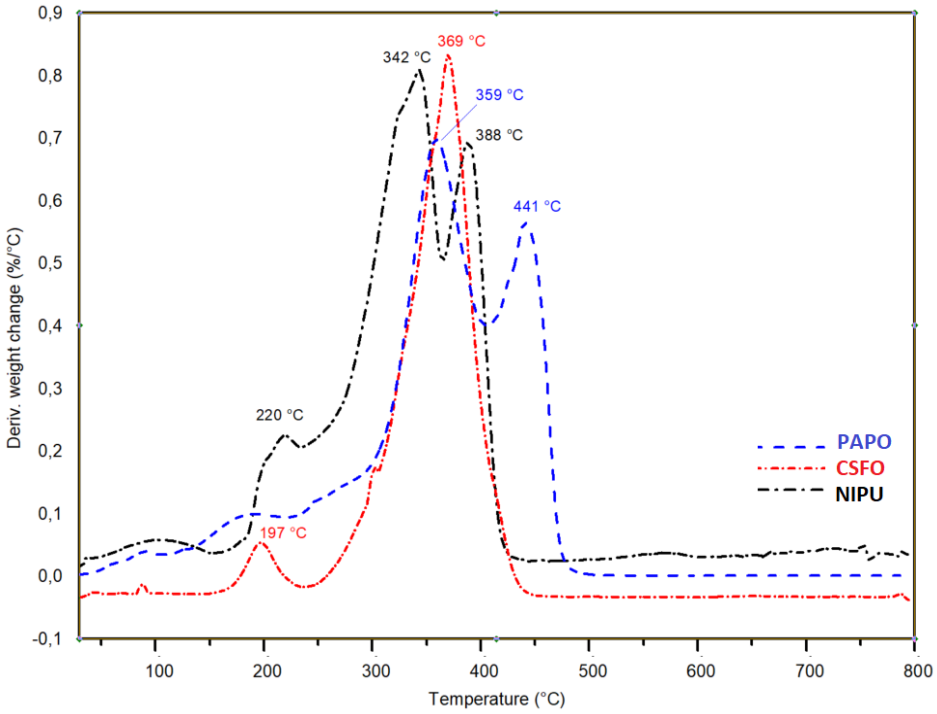

Figure 53: DTG curves of $NIPU_3$ and its precursors: $CSFO_3$ and $PAPO_3$ (10 °C min^{-1}, air).

TGA and DTG curves of the modified NIPUs, AM $NIPU_{3\text{-}3}$ and CS $NIPU_{3\text{-}3}$, are presented in Figures 54 and 55, respectively. Thermal behavior of AM NIPU and CS NIPU show the same trend than the unmodified NIPU. However, distinct decomposition temperatures in the range of 100-250°C were observed in the thermograms of the samples. For AM $NIPU_{3\text{-}3}$ and CS $NIPU_{3\text{-}3}$, the temperature for 5% weight loss (onset temperature) decreased to 134.87 °C and 148.59 °C, respectively. The initial weight loss up to 135°C is due to the removal of moisture and volatile materials [140]. Considering that for pure chitosan of 95% of deacetylation the primary degradation started around 247 °C [141], and that the CS $NIPU_{3\text{-}3}$ samples showed lower onset temperatures in the presence of chitosan, it can be suggest that the degradation steps of chitosan displace to lower temperatures of the first step of NIPUs. These results are comparable with the results described by Zhang et al[142]. Similar behavior was observed in the range of temperatures at 50% weight loss, showing a reduction of the degradation temperatures for similar groups of polyols and CS. The step of mass loss that starts at 300 ◦C and continues up to 400 ◦C is due to the degradation of the–CH_2OH group[140] and the final step of CS degradation involves the carbon ring, which is close to the 600°C[140,143]. The residual weight percentage at 600°C of AM $NIPU_{3\text{-}3}$ and CS $NIPU_{3\text{-}3}$ decreased in 15.3 % and 2.2 %, with respect to NIPU. These changes in the thermal degradation indicate that after the treatment, the thermal stability of the polymers is affected. When AM and CS are grafted into NIPU surface, the reactive chemical groups that were formed carried out a faster thermal decomposition.

The results presented above, demonstrated that after the reaction between $CSFO_3$ and $PAPO_3$ a polymer with enhanced thermal stability was obtained. However, the surface modification treatment resulted in a polymer with distinct thermal behavior, in contrast, the thermal stability of the resulted chitosan modified $NIPU_3$, CS $NIPU_{3\text{-}3}$, decreases, observed by the weight residual at 600 °C.

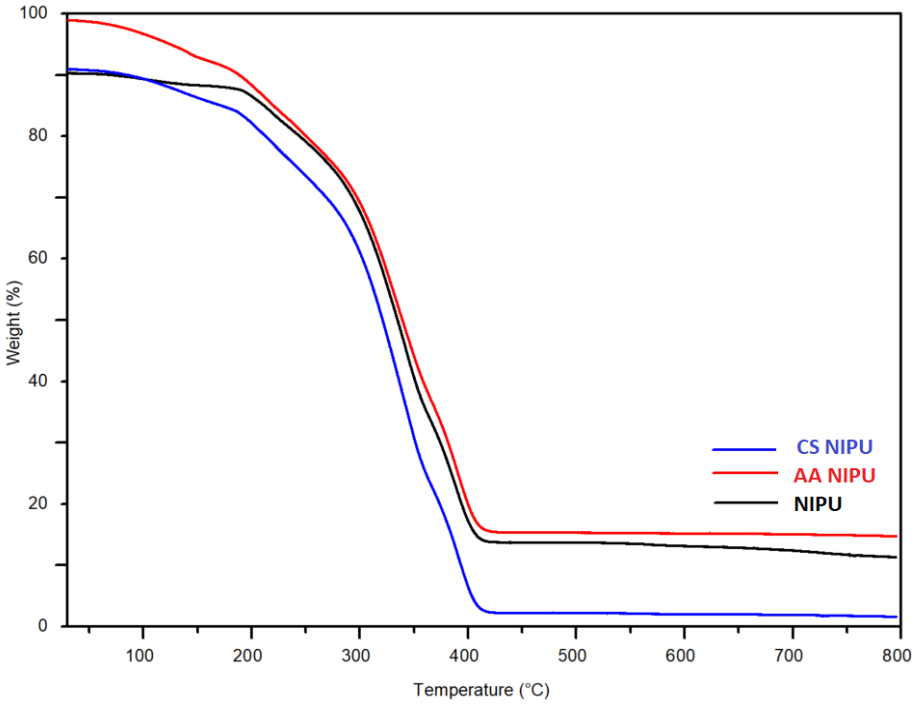

Figure 54: TGA curves of $NIPU_3$, AM $NIPU_{3\text{-}3}$ and CS $NIPU_{3\text{-}3}$ (10 °C min^{-1}, air).

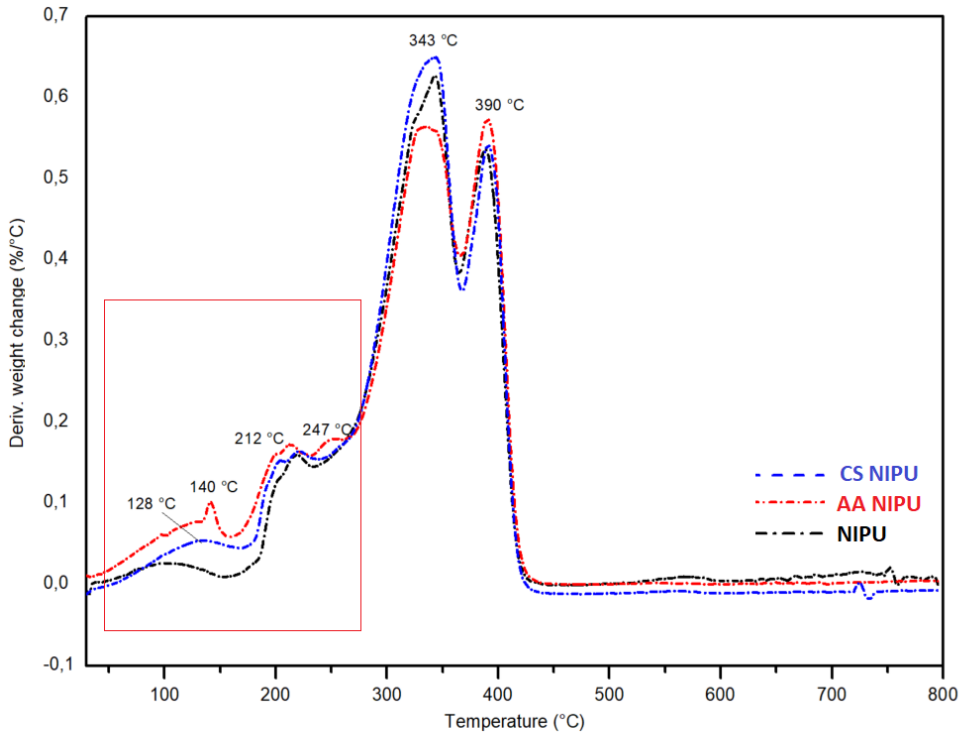

Figure 55: DTG curves of of $NIPU_3$, AM $NIPU_{3\text{-}3}$ and CS $NIPU_{3\text{-}3}$ (10 °C min^{-1}, air).

The effects of the surface modification process, on the hydrophilicity and the morphological characteristics of the prepared NIPU films before and after each step, were studied by using contact angle measurements and scanning electron microscopy (SEM), respectively.

3.8.2. Contact angle measurements

The hydrophilicity of NIPU films was measured by contact angle analysis. Typical methods of contact angle measurement are the sessile drop method (including captive bubble method), the Wilhelmy plate method, and the capillary rise method. Among them, the sessile drop is reported as the most commonly used method[144] and was chosen for determining the contact angles (θ) of the materials. Figure 56 shows a picture of the water drops on the surface of $NIPU_3$, AM $NIPU_{3\text{-}3}$ and CS $NIPU_{3\text{-}3}$ after the contact angle measurement and the results are given in table 16. The results demonstrate that the contact angles decreased after each step of the modification process. Contact angle for unmodified NIPU3 of 114.2° which suggested that the material has a hydrophobic surface, while after to induce the grafting of acrylamide by UV irradiation, the θ value of $NIPU_3$ decreased from 114.2° to 99.0°, related to the introduction of amide groups onto NIPU

surface, and after chitosan treatment, contact angle of CS $NIPU_3$ decreased to 84.2° related to hydrophilic hydroxyl and amino groups introduced by chitosan on the surface. This may be explained because of the presence of polar functional groups such as OH or NH_2, after the modification which increases the hydrogen bounding interactions and therefore decreases water contact angle[63]. Therefore, an increased hydrophilicity was achieved for the final CS $NIPU_3$ material. Similar results were founded in literature for different polyurethanes and for various chitosan coatings [55].

The surface wettability of NIPU was enhanced after the chitosan treatment, deduced from the decrease of contact angle from 114.2° to 84.2°. This result is promising, because the wettability is one the most important factors determining cell adhesion behavior[145], because the surface hydration is the first step in the interaction of a biomaterial with a biological environment that controls protein adsorption and all other subsequent steps in the biological response to materials[56]. However, surfaces with well-defined properties are needed to selectively study the role of wettability on cellular adhesion[145].

Sample	Contact Angle (°)
$NIPU_3$	114.2
AM $NIPU_{3\text{-}3}$	99.0
CS $NIPU_{3\text{-}3}$	84.2

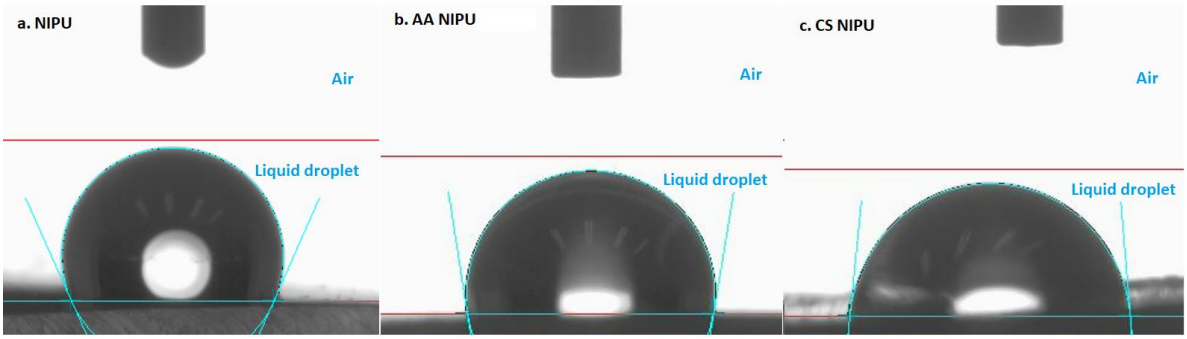

Figure 56: Scheme of contact angle measurement by sessile drop method for NIPU samples after each step of modification process: a) Unmodified $NIPU_3$ b) AM-$NIPU_{3\text{-}3}$ after UV induced grafting of acrylamide and c) CS $NIPU_{3\text{-}3}$ after chitosan treatment.

3.8.3. Scanning electron microscopy (SEM)

SEM was employed to observe the morphological characteristics as well as the effects of the grafting reaction on the surfaces of unmodified and modified NIPU materials. The surface morphologies of $NIPU_3$, AM $NIPU_{3\text{-}3}$ and CS $NIPU_{3\text{-}3}$ samples are shown in figure 57. Morphological changes were identified on the surfaces of the materials after each modification step. However, the surface of the unmodified NIPU films was not completely heterogeneous. Smooth and homogeneous surface was observed in some places of the $NIPU_3$ sample, but the presence of ridges is also found in the polymeric surface. Doley et al [46] , which synthesized a SFO-based NIPU functionalized with multiwalled carbon nanotubes, showed that a SFO-based NIPU surface presents river lines which are relatively smooth associated to polar functional groups like hydroxyl, urethane among the anothers present in polymer networks that facilitate miscibility of the component by strong electrostatic and H-bonding interactions[46].

After the photografting of AM step, the formation of small bumps over the surface of AM-$NIPU_{3\text{-}3}$ was observed, as a morphological effect that had the AM reaction in $NIPU_3$ surface. The posterior chitosan treatment showed a change in the topography of the CS $NIPU_{3\text{-}3}$ polymer, a substantial increase in the surface roughness was observed with the presence of large number of bumps with heterogenous distributions. These features in the roughness of samples had a possible effect in the increase of the polymer hydrophilicity as was also observed with the decrease of the water contact angle measurement of the polymeric samples after the treatment.

There are research reports about the surface modification of conventional PU with chitosan to enhance the antibacterial properties of the polymer[55,146]. Bahrami et al[147], reported surface roughening of isocyanate-based PU films, after a reaction with 70% acrylic acid solution using plasma to perform the grafting. The authors associated the covalent reaction between chitosan amine groups and carboxylic acid groups of the treated PU film, with the strands that they observed penetrate very widely and uniformly from the chitosan-immobilized film surface into the bulk of the film[147]. However, for the case of the isocyanate-free PU surface, such as the one synthesized in the present work, there are still no known reports on the morphological characteristics of NIPU materials modified with biomolecules such as chitosan, which makes this research work only the beginning of a wide range of possibilities for further treatment of this type of materials with biological functionalities such as chitosan, alginate, collagen or heparin[148,149].

Thus, it can be concluded that the unmodified NIPU did not present a homogeneous surface which may influence the incorporation of active groups. The modification process has an effect on the surface topography of the NIPU polymers, associated with the introduction of chemical groups of acrylamide and chitosan.

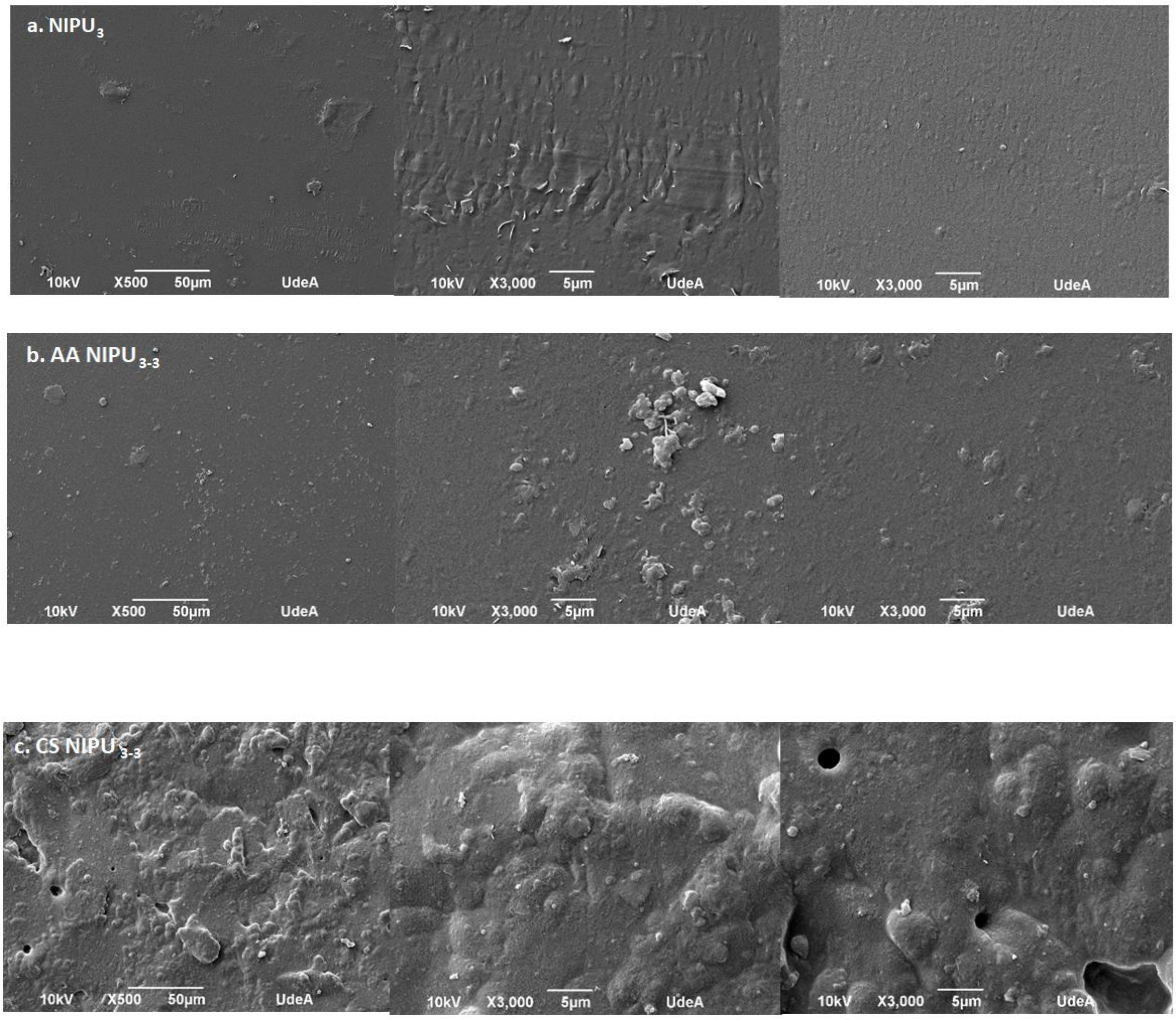

Figure 57: SEM micrographs of (a) $NIPU_3$ (b)AM $NIPU_{3-3}$ and (c) CS_{3-3} NIPU (magnification 500x and 3000x)

3.8.4. Tensile properties

The evaluation of mechanical properties of NIPU samples under tension, was performed at ambient temperature. To investigate the influence of amine functionality of PAPO precursor, mechanical tests were made to $NIPU_2$ and $NIPU_3$ at 24 hours of curing. AM $NIPU_{3-3}$ and CS $NIPU_{3-3}$ samples were very sticky and not suitable for the mechanical test. These samples cannot be extended under tension as was showed in material and methods section. From tensile curves, tensile strength, elongation-at-break, and modulus were calculated for of $NIPU_2$ and $NIPU_3$ at 24 hours of curing and the results are presented in table 17.

Table 17: Crosslink density and tensile property data of $NIPU_2$ and $NIPU_3$*.

Sample	Elongation at break (%)*	Tensile strength (MPa)*	Young's modulus (MPa)*	Crosslink density, υ (mol/m^3)
$NIPU_2$	687.06±10	152.83±6.7	13.72±0.1	1857.32
$NIPU_3$	313.47±5	358.95±0.70	103.90±0.05	14065.28

*The values reported were the average of five measurements ±standard deviation

For the selected $NIPU_3$, which was prepared with the PAPO of highest functionality (478.84 mg KOH/g), tensile strength and Young's modulus increased with respect to $NIPU_2$ prepared with a PAPO with a lower functionality (346.72 mg KOH/g), while elongation at break decreased to 313.47%, demonstrating that a lower number of residual carbonate groups and a higher formation of urethane groups, result in a higher crosslinking density, which is reflected in a higher tensile strength and a lower elongation at break. Comparable mechanical performance has been found by different authors, suggesting potential applications as coating or adhesives for similar NIPU materials[29,35,124,150]. In contrast, the higher elongation at break of $NIPU_2$ (687.06%) may be associated to a higher amount of unreacted secondary amines and residual aliphatic structures of PAPO, producing a network with a lower crosslinking density. As a result, it is obtained a more flexible material with a lower tensile strength.

The crosslinking density was estimated and is reported in Table 16. The huge difference between the crosslinking degree of the two analyzed NIPU samples is directly related with the difference of functionality of PAPO precursors, from which each sample is derived. Therefore, the functionality of $PAPO_2$ and $PAPO_3$ which were given place $NIPU_2$ and $NIPU_3$ respectively, determines the maximum degree of crosslinking that can take place for each NIPU reaction. As it can be seen the crosslinking density increases with the increase of the total amine functionality of the PAPO, showing that $PAPO_3$ is a more reactive precursor, that enhances the mechanical properties of the resulted $NIPU_3$ with the highest crosslinking degree. While for $NIPU_2$, the higher number of unreacted secondary amines is reflected in a lower crosslinking density. These results were in accordance with the results of FTIR, TGA and DSC, as well as to the reports of some authors [22,124,137]. Gholami et al[124], report the synthesis of bio based non-isocyanate polyurethane (NIPU) membranes, obtained from carbonated soybean oil and tetraethylenepentamine. The product with free secondary amines was further treated with epichlorohydrin to produce azetidinium and the obtained modified NIPU had the desired tensile properties suitable for application as wound dressings[124].

Therefore, it was proved that a higher crosslinking density of NIPU leads to an enhanced tensile strength and a lower elongation at break, which is related to the reduction of the

degree of rotational freedom[23], yielding to a less flexible material. These results clearly show that the PAPO of the highest amine functionality generates the improvement of mechanical and thermal properties of the obtained NIPUs. $NIPU_3$ obtained with the PAPO of the highest functionality (478.84 mg KOH/g), result in a polymer with enhanced mechanical properties, showing a strong dependence on the structure of curing agent, cross-linking density and hydrogen bonding between urethane, hydroxyl and ester groups[35]

Although for unmodified NIPU films promising mechanical performance was determined, the surface modification process induced a very appreciable decrease in the mechanical performance and bulk properties of the modified material. Therefore, other treatments as well as antibacterial agents to incorporate biological and antimicrobial characteristics on the surface without affecting the bulk properties must be explored.

Finally, to study the potential application of the modified and unmodified NIPU films as a biomaterial, the i*n vitro* evaluation of the antibacterial activity and *in vitro* evaluation of the cytotoxicity on Detroit ATCC 551 Fibroblasts (ATCC®CCL 110) were performed

3.8.5. Biological Properties

3.8.5.1. In vitro evaluation of the antibacterial activity of materials

The activity of the materials in inhibiting the growth of *S. aureus* and *E. coli* was determined. The ceftazidime sensi-disc, a drug for which the evaluated strains are sensitive, was used as inhibition control and not impregnated sensi-disc as non-inhibition control.

The evaluated materials did not present activity in the inhibition of *S. aureus* and *E. coli*, due to the presence of uniform growth of the bacteria around and on their surface, similar to what was observed in the non-inhibition control. For its part, the positive inhibition control (ceftazidime sensi-disc) showed the formation of bacterial inhibition halos. Table 18 presents the results of the measurement of the inhibition halos around materials and controls. The data represent the inhibition halos in mm after co-cultivation of *S. aureus* and *E. coli* with the samples and controls. The formation of inhibition halos is shown in Figures 58 and 59. The results showed that the NIPU films before and after the treatment with chitosan were almost the same material in the antibacterial activity terms because the Inhibition halos (mm) values were very close and showed that the NIPU surface did not inhibit the growth of *S. aureus* and *E. coli*. These results suggested that different methods and also the use of other antibacterial compound or antibiotics have to be explored to achieve the goal to provide antibacterial functionalities to the NIPU surface. For example, A. Piozzi et al[151] reported that the antibiotics, rifampin and amoxicillin, were adsorbed on polyurethanes exhibiting acidic or basic properties due to the different functional groups

introduced in the polymer side-chain, and the antibiotics (active against gram-positive bacteria) possessed functional groups able to interact with the conventional PU tested[151].

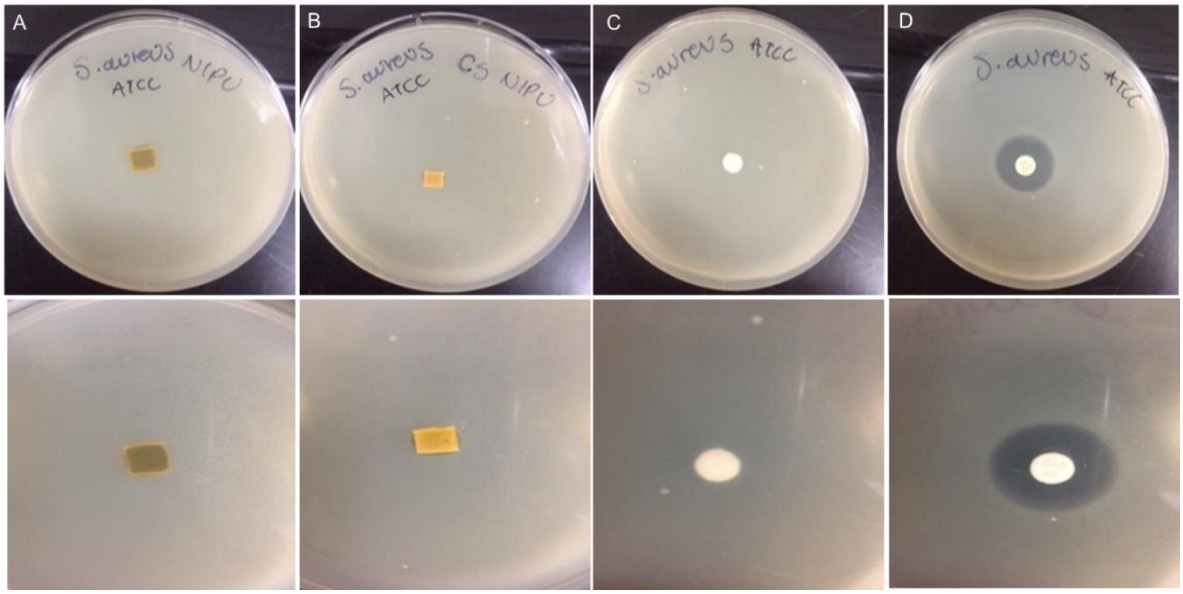

Figure 58: The images correspond to the culture of S. aureus with the materials and controls. Top panel: posterior view; bottom panel: anterior view. A: NIPU Material, B: NIPU CS Material, C: No Inhibition Control D: Ceftazidime Sensi-disc (Positive Inhibition Control).

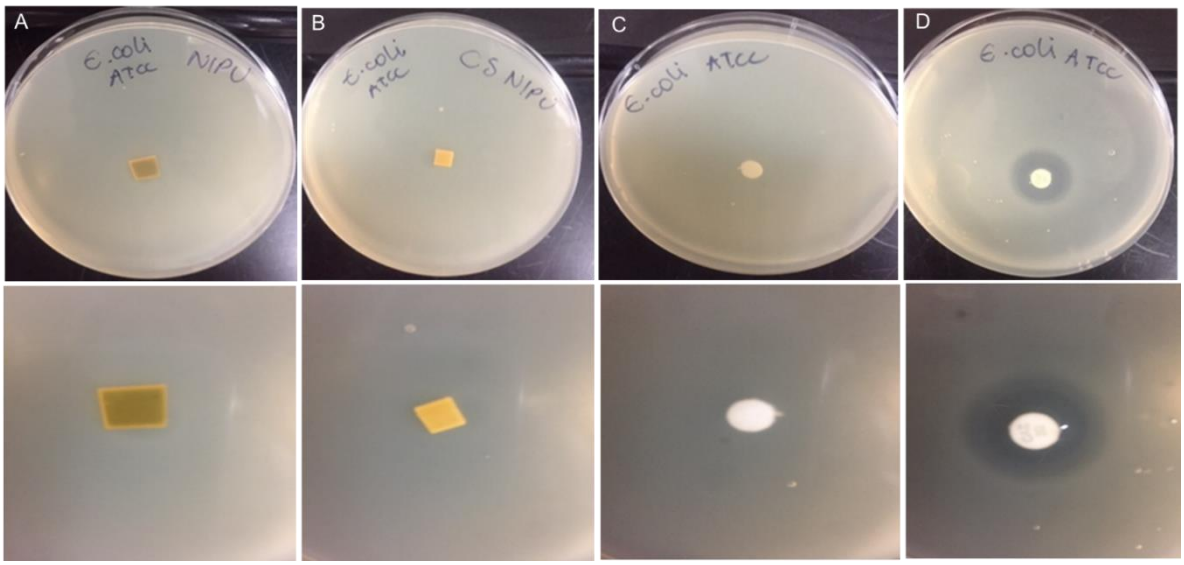

Figure 59: The images correspond to the culture of *E. coli* with the materials and the controls. Top panel: posterior view; bottom panel: anterior view. A: NIPU Material, B:CS NIPU Material, C: No Inhibition Control D: Ceftazidime Sensi-disc (Positive Inhibition Control).

Table 18: Inhibition halos formed around materials and controls.

Sample	Inhibition halos (mm)	
	S. *aureus*	**E. *coli***
NIPU	0	0
CS NIPU	0	0
Ceftazidime sensi-disc (C+)	24	21
Not impregnated sensi-disc (C-)	0	0

3.8.5.2. *In vitro* evaluation of the cytotoxicity of NIPU and CS NIPU on Detroit ATCC 551 Fibroblasts (ATCC®CCL 110).

The cytotoxicity of NIPU materials was evaluated and the results are presented in figure 60 and table 19 and are expressed as the percentage of viability in relation to the untreated control cells. Detroit fibroblasts cultured on $NIPU_3$ an CS $NIPU_{3\text{-}3}$ materials showed a viability of 74.6% and for those cultured on CSNIPU, cell viability was 73.4%. The results are expressed as the mean values of the standard deviation of the viability percentage of the cells cultured on the materials for 48 hours, versus the control cells without treatment, in two independent tests.

No significative difference between the cell viability of the $NIPU_3$ and CS $NIPU_{3\text{-}3}$ samples was observed, which implies that the modification method did not have the desired effect in the $NIPU_3$ material and that it must be changed. However, the cell viability of the unmodified $NIPU_3$ showed a higher value that what it has been reported in previous studies for conventional polyurethane[123], that in fact, it had to be treated to slightly improve the biocompatibility properties. Even the cell viability values for the modified PU samples in the aforementioned study[123] were lower than those obtained in the present study for $NIPU_3$ which was synthesized through a method free of solvents and catalysts. The result is perhaps correlated with the surface composition, which for $NIPU_3$ was shown to be hydrophobic with a water contact angle of 114.2°. It should be noted that biological tests can be altered by many variables, so it is important to test other methods and compounds that can be used to meet the objective of functionalizing NIPU polymers with antibacterial agents.

Figure 61 presents the images obtained for the biological evaluation. It can be seen that the cells cultured with the materials change their normal morphology, being rounded, and agglomerated around the material; in contrast to the untreated control cells that are observed with their usual elongated morphology, in which cells are adhered to the culture well and have a monolayer information. It can be concluded that the obtained NIPU materials before and after the treatment with chitosan were potentially toxic to Detroit cells.

Table 19: Effect of NIPU and CS-$NIPU_{3\text{-}3}$ on the viability of Detroit cells.

Sample	% Viability
$NIPU_3$	74.6 ± 5.9
$CSNIPU_{3\text{-}3}$	73.4 ± 3.7
Not treated control	100.0 ± 2.6

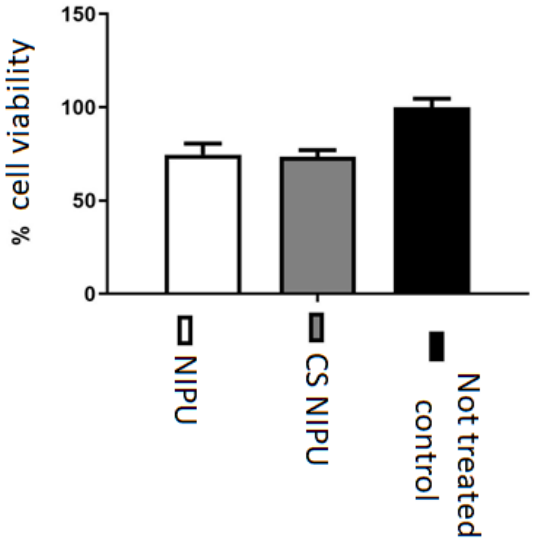

Figure 60: Cytotoxic effect of NIUP and CSNIUP. The bars represent the mean value +/- the standard deviation of the viability percentages of the Detroit cells cultured on NIPU and CSNIPU vs control cells without treatment.

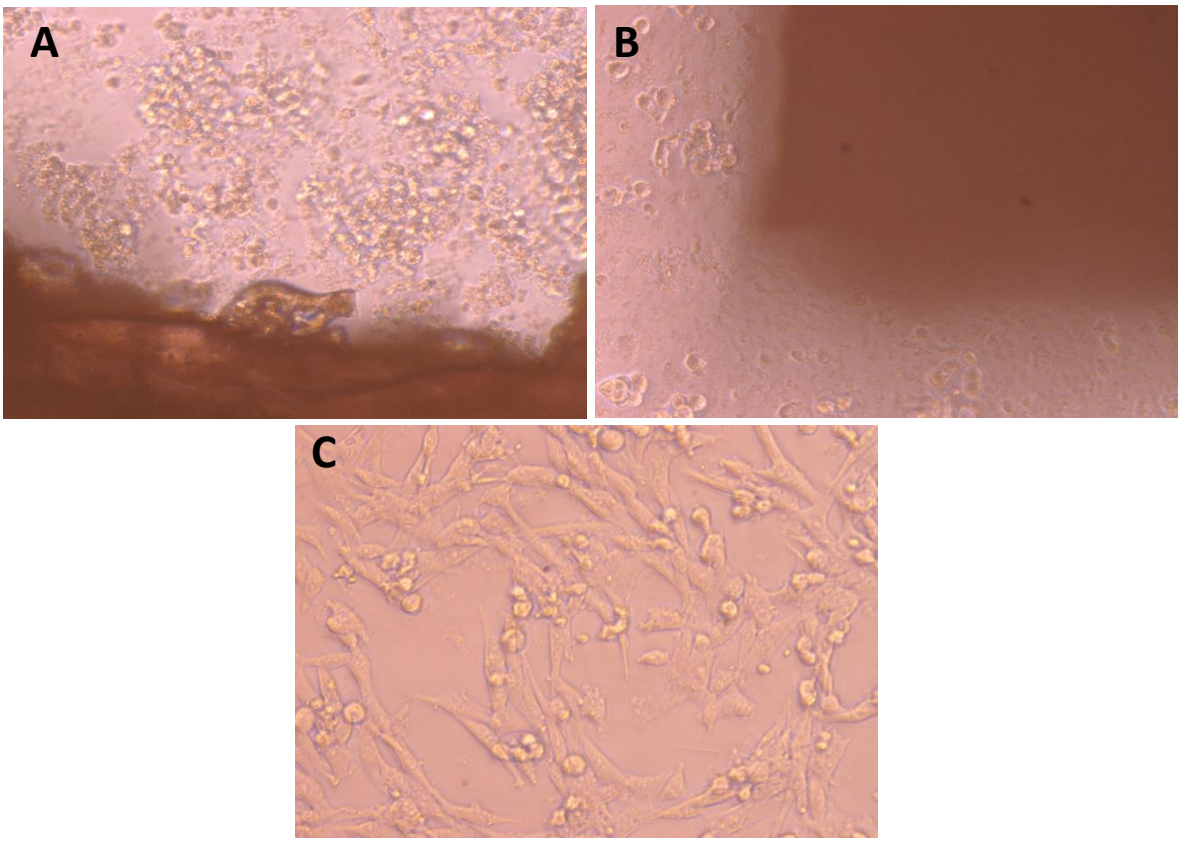

Figure 61. Conventional optical microscopy of Detroit fibroblasts cultured on the materials and control. a) $NIPU_3$ 10X, b)CS $NIPU_{3\text{-}3}$ 10X, c) Untreated control 10X.

NIPU materials have emerged as potential candidates for biomedical applications owing to its sustainability, non-toxicity, biocompatibility and environmentally friendly nature[124,137,152,153]. However, in a first attempt to modify the surface of SFO-based NIPU materials with chitosan, the desired antibacterial characteristics could not be provided, although the rest of the performed chemical, morphological, thermal, and mechanical characterization of NIPU films after each step of the methodology, had shown that NIPU was obtained from sunflower oil and was chemically modified with AM and CS. The failure of the executed method may be explained by the fact that the amount of acrylamide grafted on the surface was excessive, causing all the amino groups present in chitosan to react with all the acrylamide groups of the surface. Therefore, there are not remaining unprotonated amines available to provide the expected antibacterial function of chitosan. On the other hand, it could be of little benefit to use glutaraldehyde in the modification process which could result in cytotoxic effects of the material, interacting or inhibiting the activity of CS in the surface.

Considering the above discussion, it is essential to find the way to relate the surface characteristics with the biological properties, focused on the desired application of the

biomaterial [56], exploring different pathways to modified polymers with biological characteristics[124,137,152,153], and choose what is the most relevant property that affects the desired response to a biological variable, in order to modulate this expected performance. For example, the appropriate concentrations of the modification agents, the surface charge, to estimate the number of protonated amines of chitosan that are available on polymeric surface to provide antibacterial functions and more effectively regulate the desired properties. Also, to study other surface properties of the materials, as composition, thickness, roughness which are considered critical factors that affect protein adsorption and therefore dictate the success of biomaterial interactions[154].

Among the new methods that can be used for surface modification, one of the most promising is the common processes of layer by layer (LbL) self-assembly that occurs through electrostatic forces between particles and molecules. In this case, oppositely charged species are bonded together by a strong ionic bond, resulting in a stable, robust, and uniform structure. Including the use biomolecules such as heparin chondroitin sulfate, gelatin, collagen, alginate, hyaluronic acid, and chitosan, that have showed a significant role in improving the surface biocompatibility properties[1,146,149].

Other example is the soybean-oil-based cationic polyurethane coatings with antibacterial properties that were prepared by Garrison, T. et al [155] with a range of different molar ratios of hydroxyl groups from an amine diol. Recently, Karami, Z. et al[137] published a preliminary study on thermo-mechanical and antibacterial properties of non-isocyanate polyurethane thermoset based on a bio-resourced starshaped epoxy macromonomer in comparison with a cyclo-carbonate fossil based epoxy resin. The bio-resourced NIPU network showed a significant potential of film formation and it could be used in surface coating applications and showed an acceptable antibacterial activity against *E.coli* and *S.aureus*[137].

In a recent study, Gholami et al[124] introduced biobased NIPU membranes that had physicomechanical and biological properties suitable for application as wound dressings by the reaction of soybean oil cyclic carbonate with tetraethylenepentamine. The product with free secondary amines was further treated with epichlorohydrin to produce azetidinium containing crosslinked networks, which provided an excellent antibacterial performance against different bacteria and not cytotoxicity against fibroblasts[124].

It is noteworthy that the SFO based NIPU obtained in this research showed promising physicochemical, thermal and mechanical properties for potential applications as coatings or adhesives[23], as well as other engineering applications such as flame retardants[149,156], due to their good thermal stability and flexibility.

In conclusion, to perform the objective of modify the NIPU surface to provide antibacterial properties it is required to find the best treatment as well as conditions to achieve the expected modification, considering variables such as irradiation time, photoinitiator concentration, graft co-monomer concentration, among many others that can influence the

effectiveness of a modification procedure without modify the bulk structure of the substrate and that employs the most versatile procedures. In this work it was synthesized NIPU polymers using a green method from entirely sunflower oil-based precursors and to change many properties of the NIPU material after subjecting it to acrylamide and chitosan treatment, although the expected biological characteristics were not attained.

4. CONCLUSIONS

4.1. A green alternative pathway for the solvent and catalyst-free synthesis of NIPU based entirely on sunflower oil, which replaces the fossil fuel-derived feedstocks, was presented.

4.2. From epoxidized sunflower oil, both precursors for the synthesis of NIPU were obtained, cyclic carbonate, with a conversion of 90%, and polyamine polyol, with a total amine number of 478 mg KOH. The reaction between CSFO and PAPO gave rise to highly elastic and hydrophobic NIPU films, with a Tg around 10°C.

4.3. The structure of the starting SFO-based materials (SFO-ESFO-CSFO), as well as essential parameters such as iodine value, fatty acid composition, oxirane oxygen number, and relative conversion of the reactions, were investigated by ^{1}H NMR non-destructive technique and the results agreed to the obtained with the laborious and time-requiring analytical techniques.

4.4. A successful surface modification of NIPU films with AM, after a photografting procedure using UV radiation, followed by the covalent attachment with CS, using glutaraldehyde as the crosslinking agent, was performed.

4.5. The surface wettability of NIPU was enhanced after the surface modification, deduced from the decrease of contact angle from 114.2° to 84.2°. By means of SEM analysis, topographic changes were identified on the surfaces of NIPU materials after each modification step associated with the introduction of chemical groups of AM and CS.

4.6. Unmodified NIPU films showed promising mechanical properties with a tensile strength of 358.95 MPa and elongation at break of 313%. Their

potential for film formation makes them suitable for coating application. Instead, the surface modification of the films clearly decreased their mechanical properties.

4.7. The modified and unmodified films did not present differences in the biological evaluation, both in terms of antibacterial properties and cell viability. CS-modified NIPU films did not show antibacterial performance inhibiting the growth of S. aureus and E. coli and the cell viability on Detroit ATCC 551 Fibroblasts of the treated and untreated NIPU films was 75%. Therefore, NIPU and CS NIPU were not suitable as antibacterial biomaterials. Other modification methods as well as bioactive molecules were proposed as promising alternatives pathways that can be explored to enhance the biological response of the NIPU materials.

4.8. The main contributions of this work were: the development of NIPU films, starting from two precursors obtained from ESFO using an environmentally friendly synthetic route, the performance of the surface modification to the NIPU material, introducing different chemical functions as well as changing the morphology and wettability of the NIPU surface, and the complete physicochemical, morphological, thermal, mechanical and biological characterization performed to the materials that allow understanding the hits and misses in the development of this work.

5. PERSPECTIVES

5.1. Perspectives for the synthesis step

For the synthesis step, there are factors that could be considered to enhance both the processing and the final behavior of the NIPU material. One of them is to incorporate other kinds of biobased amines with different chemical structures as well as to study different formulations of amine blends to modulate both the thermal and mechanical properties of the polymers related to the desired application.

Another perspective is to include characterization techniques such as the determination of the pot life and gelation time, during the reaction mixture to prepare NIPU, which could be useful to study the rate of network formation and to understand the crosslinking reaction that gives place to the NIPU polymers, to establish better conditions of processing.

The final factor related to the NIPU synthesis that can be considered is the use of alcohols as solvents to eliminate the intra- and inter-molecular hydrogen bonding between NIPU chains, and possibly increase the chain mobility and lead to higher advancement of polymerization.

5.2. Perspectives for the surface modification step

For the surface modification step, there are many factors that could be explored to improve the biological performance of the NIPUs in terms of the desired antibacterial properties that could make them useful as biomaterials. As the objective was to obtain an antibacterial material, it is important to establish what is the best agent to provide the desired properties to NIPU, as well as the best route to incorporate it on the material surface. If chitosan will still be used as an antibacterial agent, it would be better to incorporate it as an amine precursor in the synthesis of NIPU films, to verify whether this way of preparation provides the expected antibacterial properties to the films. Instead, if it is desired to explore other options, among the different antibacterial agents are founded the silver, chalcone, nitric oxide, antibiotics, or quaternary ammonium salts (QAS). In particular, the application of QAS has gained considerable attention for the preparation of antimicrobial wound dressings, because of their high antimicrobial activity for a wide range of bacteria and low toxicity1.

On the other hand, there are many methods of surface modification that can be explored to incorporate antibacterial agents and enhance the biological response of the material such as the use of liquid-phase chemical oxidants, the self-assembled monolayers, or the application of gas discharge surface treatments. A promising alternative is the low-temperature plasma discharge, which is related to methods that deposit smooth and conformal coatings on biomaterial surfaces and have been widely used to affect biomaterial wettability.

Finally, the most important feature that has to be considered is to understand that depending on the biomedical application, different surface properties are required to obtain a successful biomaterial, because biocompatibility is not a material property but rather a measure of how successfully the biomaterial behaves to different engineering requirements for very different biomedical applications, meaning that there is no single material that is biocompatible in all applications. Thus, it is essential to work on the ability to prepare and characterize the surfaces, depending on the desired application, to find a better method of quantifying a biological response of interest with respect to a surface characteristic[56].

For instance, the overall mechanical properties as high elongation to break and tensile strength values, suggest that the obtained NIPU films could be applied as antibacterial wound dressings, referring to some reported studies[124,153].

On the other hand, purification and extraction processes have to be researched and established to optimize and appropriately characterize the yield of reactions and remove the excess of unreacted monomers as well as to study the effect on biological or surface properties. Therefore, an important challenge to consider as a perspective and useful contribution to future research is to clarify what is the most important surface characteristic that must be determined to modulate the desired biological response.

6. REFERENCES

1. Bahrami, N., Nouri Khorasani, S., Mahdavi, H. & Khalili, S. Layer-by-layer self-assembly of collagen and chitosan biomolecules on polyurethane films. *J. Appl. Polym. Sci.* **137**, 1–13 (2020).
2. Young, R., J. & Lovell, P., A. *Introduction to polymers*. *CRC press* (2011).
3. Włoch, M. & Datta, J. Nonisocyanate Polyurethanes. in *Polyurethane Polymers: Blends and Interpenetrating Polymer Networks* 169–202 (2017). doi:10.1016/B978-0-12-804039-3.00007-5.
4. Cornille, A., Auvergne, R., Figovsky, O., Boutevin, B. & Caillol, S. A perspective approach to sustainable routes for non-isocyanate polyurethanes. *Eur. Polym. J.* **87**, 535–552 (2017).
5. Miao, S., Wang, P., Su, Z. & Zhang, S. Vegetable-oil-based polymers as future polymeric biomaterials. *Acta Biomater.* **10**, 1692–1704 (2014).
6. Karak, N. *Vegetable oil-based polymers: Properties, processing and applications*. *Vegetable Oil-Based Polymers: Properties, Processing and Applications* (2012). doi:10.1533/9780857097149.
7. Blattmann, H. & Mülhaupt, R. Multifunctional β-amino alcohols as bio-based amine curing agents for the isocyanate- and phosgene-free synthesis of 100% bio-based polyhydroxyurethane thermosets. *Green Chem.* **18**, 2406–2415 (2016).
8. Wang, Z. *et al.* Synthesis and characterization of novel soybean-oil-based elastomers with favorable processability and tunable properties. *Macromolecules* **45**, 9010–9019 (2012).
9. Usman, A. *et al.* Chitin and chitosan based polyurethanes: A review of recent

advances and prospective biomedical applications. *Int. J. Biol. Macromol.* **86**, 630–645 (2016).

10. Barison, A. *et al.* A simple methodology for the determination of fatty acid composition in edible oils through 1H NMR spectroscopy. *Magn. Reson. Chem.* **48**, 642–650 (2010).

11. • Polyurethane global market volume 2015-2026 | Statista.

12. Rokicki, G., Parzuchowski, P. G. & Mazurek, M. Non-isocyanate polyurethanes: Synthesis, properties, and applications. *Polym. Adv. Technol.* **26**, 707–761 (2015).

13. Błażek, K. & Datta, J. Renewable natural resources as green alternative substrates to obtain bio-based non-isocyanate polyurethanes-review. *Crit. Rev. Environ. Sci. Technol.* **49**, 173–211 (2019).

14. Bayer, O. Das Di-Isocyanat-Polyadditionsverfahren (Polyurethane). *Angew. Chemie* (1947) doi:10.1002/ange.19470590901.

15. Tryznowski, M., widerska, A., Zołek-Tryznowska, Z., Gołofit, T. & Parzuchowski, P. G. Facile route to multigram synthesis of environmentally friendly non-isocyanate polyurethanes. *Polymer (Guildf).* **80**, 228–236 (2015).

16. Nohra, B. *et al.* From petrochemical polyurethanes to biobased polyhydroxyurethanes. *Macromolecules* **46**, 3771–3792 (2013).

17. Szycher, M. *Handbook of Polyurethanes*. *Choice Reviews Online* vol. 37 (2013).

18. Qi, H. J. & Boyce, M. C. Stress-strain behavior of thermoplastic polyurethanes. *Mech. Mater.* **37**, 817–839 (2005).

19. Alves, P., Ferreira, P., & Gil, M. H. Biomedical Polyurethane-Based Materials. in *Polyurethane: properties, structure and applications* (2012).

20. Kreye, O., Mutlu, H. & Meier, M. A. R. Sustainable routes to polyurethane precursors. *Green Chem.* **15**, 1431–1455 (2013).

21. Pyo, S. H. *et al.* Cyclic carbonates as monomers for phosgeneand isocyanate-free polyurethanes and polycarbonates. *Pure Appl. Chem.* **84**, 637–661 (2012).

22. Farhadian, A. *et al.* Synthesis of fully bio-based and solvent free non-isocyanate poly (ester amide/urethane) networks with improved thermal stability on the basis of vegetable oils. *Polym. Degrad. Stab.* **155**, 111–121 (2018).

23. Kathalewar, M. S., Joshi, P. B., Sabnis, A. S. & Malshe, V. C. Non-isocyanate polyurethanes: From chemistry to applications. *RSC Adv.* **3**, 4110–4129 (2013).

24. Tenorio-Alfonso, A., Sánchez, M. C. & Franco, J. M. A Review of the Sustainable Approaches in the Production of Bio-based Polyurethanes and Their Applications in the Adhesive Field. *J. Polym. Environ.* **28**, 749–774 (2020).

25. Alves, M. *et al.* Organocatalytic synthesis of bio-based cyclic carbonates from CO2 and vegetable oils. *RSC Adv.* **5**, 53629–53636 (2015).

26. Błażek, K. & Datta, J. Renewable natural resources as green alternative substrates to obtain bio-based non-isocyanate polyurethanes-review. *Crit. Rev. Environ. Sci. Technol.* **49**, 173–211 (2019).

27. Gomez-Lopez, A. *et al.* Poly(hydroxyurethane) Adhesives and Coatings: State-of-the-Art and Future Directions. *ACS Sustain. Chem. Eng.* **9**, 9541–9562 (2021).

28. Ghasemlou, M., Daver, F., Ivanova, E. P. & Adhikari, B. Bio-based routes to synthesize cyclic carbonates and polyamines precursors of non-isocyanate polyurethanes: A review. *Eur. Polym. J.* **118**, 668–684 (2019).

29. Kathalewar, M., Sabnis, A. & D'Mello, D. Isocyanate free polyurethanes from new CNSL based bis-cyclic carbonate and its application in coatings. *Eur. Polym. J.* **57**, 99–108 (2014).

30. Garipov, R. M. *et al.* Reactivity of cyclocarbonate groups in modified epoxy-amine compositions. *Dokl. Phys. Chem.* **393**, 289–292 (2003).

31. Monroe, K. *et al. Vegetable Oil-Based Polymeric Materials: Synthesis, Properties, and Applications*. *Encyclopedia of Renewable and Sustainable Materials* (Elsevier Ltd., 2020). doi:10.1016/b978-0-12-803581-8.11521-8.

32. Ghasemlou, M., Daver, F., Ivanova, E. P. & Adhikari, B. Bio-based routes to synthesize cyclic carbonates and polyamines precursors of non-isocyanate polyurethanes: A review. *Eur. Polym. J.* **118**, 668–684 (2019).

33. Poussard, L. *et al.* Non-Isocyanate Polyurethanes from Carbonated Soybean Oil Using Monomeric or Oligomeric Diamines to Achieve Thermosets or Thermoplastics. *Macromolecules* **49**, 2162–2171 (2016).

34. Bähr, M. & Mülhaupt, R. Linseed and soybean oil-based polyurethanes prepared via the non-isocyanate route and catalytic carbon dioxide conversion. *Green Chem.* **14**, 483–489 (2012).

35. Doley, S. & Dolui, S. K. Solvent and catalyst-free synthesis of sunflower oil based polyurethane through non-isocyanate route and its coatings properties. *Eur. Polym. J.* **102**, 161–168 (2018).

36. Badri, K. . Biobased Polyurethane from Palm Kernel Oil-Based Polyol. *Polyurethane* 447–470 (2012) doi:10.5772/32009.

37. Petrovic, Z. S. Polyurethanes from vegetable oils. *Polym. Rev.* **48**, 109–155 (2008).

38. Sawpan, M. A. Polyurethanes from vegetable oils and applications: a review. *J. Polym. Res.* **25**, (2018).

39. Saurabh, T., Patnaik, M., Bhagt, S. L. & Renge, V. C. Epoxidation of vegetable oils: a

review. *Int. J. Adv. Eng. Technol* **2**, 491–501 (2011).

40. Masuchi, M. H. *et al.* Fats from chemically interesterified high-oleic sunflower oil and fully hydrogenated palm oil. *JAOCS, J. Am. Oil Chem. Soc.* **91**, 859–866 (2014).

41. Aerts, H. A. J. & Jacobs, P. A. Epoxide yield determination of oils and fatty acid methyl esters using 1H NMR. *JAOCS, J. Am. Oil Chem. Soc.* **81**, 841–846 (2004).

42. Tamami, B., Sohn, S. & Wilkes, G. L. Incorporation of Carbon Dioxide into Soybean Oil and Subsequent Preparation and Studies of Nonisocyanate Polyurethane Networks. *J. Appl. Polym. Sci.* **92**, 883–891 (2004).

43. Poussard, L. *et al.* Non-Isocyanate Polyurethanes from Carbonated Soybean Oil Using Monomeric or Oligomeric Diamines to Achieve Thermosets or Thermoplastics. *Macromolecules* **49**, 2162–2171 (2016).

44. Doley, S. & Dolui, S. K. Solvent and catalyst-free synthesis of sunflower oil based polyurethane through non-isocyanate route and its coatings properties. *Eur. Polym. J.* **102**, 161–168 (2018).

45. Blattmann, H., Fleischer, M., Bähr, M. & Mülhaupt, R. Isocyanate- and phosgene-free routes to polyfunctional cyclic carbonates and green polyurethanes by fixation of carbon dioxide. *Macromol. Rapid Commun.* **35**, 1238–1254 (2014).

46. Doley, S., Agarwal, V., Bora, A., Borah, D. & Dolui, S. K. Development of sunflower oil-based nonisocyanate polyurethane/multiwalled carbon nanotube composites with improved physico-chemical and microwave absorption properties. *Polym. Compos.* **40**, E1120–E1130 (2019).

47. Tsuji, Y. & Fujihara, T. Carbon dioxide as a carbon source in organic transformation: Carbon–carbon bond forming reactions by transition-metal catalysts. *Chem. Commun.* **48**, 9956–9964 (2012).

48. Ema, T., Miyazaki, Y., Shohei, K., Yono, Y. & Takashi, S. A bifunctional catalyst for carbon dioxide fixation: cooperative double activation of epoxides for the synthesis of cyclic carbonates. *R. Soc. Chem.* **48**, 4489–4491 (2012).

49. Camara, F. *et al.* Reactivity of secondary amines for the synthesis of non-isocyanate polyurethanes. *Eur. Polym. J.* **55**, 17–26 (2014).

50. Farhadian, A., Ahmadi, A., Omrani, I. & Babaei, A. Synthesis of fully bio-based and solvent free non-isocyanate poly (ester amide / urethane) networks with improved thermal stability on the basis of vegetable oils. **155**, (2018).

51. Wendels, S. & Avérous, L. Biobased polyurethanes for biomedical applications. *Bioact. Mater.* **6**, 1083–1106 (2021).

52. Harvey, A. G., Hill, E. W. & Bayat, A. Designing implant surface topography for improved biocompatibility. *Expert Rev. Med. Devices* **10**, 257–267 (2013).

53. Zdrahala, R. J. & Zdrahala, I. J. Biomedical applications of polyurethanes: A Review od Past Promises, Present Realities, and a Vibrant Future. *J. Biomater.* **14**, 67–90 (1999).

54. Xu, L. C. & Siedlecki, C. A. *Antibacterial Polyurethanes*. *Advances in Polyurethane Biomaterials* (2016). doi:10.1016/B978-0-08-100614-6.00009-3.

55. Kara, F., Aksoy, E. A., Yuksekdag, Z., Hasirci, N. & Aksoy, S. Synthesis and surface modification of polyurethanes with chitosan for antibacterial properties. *Carbohydr. Polym.* **112**, 39–47 (2014).

56. Vogler, E. A. *Surface Modification for Biocompatibility*. *Engineered Biomimicry* (Elsevier Inc., 2013). doi:10.1016/B978-0-12-415995-2.00008-8.

57. Agnihotri, S., Dhiman, N. K. & Tripathi, A. *Antimicrobial Surface Modification of Polymeric Biomaterials*. *Handbook of Antimicrobial Coatings* (2017). doi:10.1016/b978-0-12-811982-2.00020-2.

58. Hasirci, N. & Ayse Aksoy, E. Synthesis and modifications of polyurethanes for biomedical purposes. *High Perform. Polym.* **19**, 621–637 (2007).

59. Sangermano, M. & Razza, N. Light induced grafting-from strategies as powerful tool for surface modification. *Express Polym. Lett.* **13**, 135–145 (2019).

60. Hong, K. H., Liu, N. & Sun, G. UV-induced graft polymerization of acrylamide on cellulose by using immobilized benzophenone as a photo-initiator. *Eur. Polym. J.* **45**, 2443–2449 (2009).

61. Zhu, Y., Gao, C., Guan, J. & Shen, J. Promoting the cytocompatibility of polyurethane scaffolds via surface photo-grafting polymerization of acrylamide. *J. Mater. Sci. Mater. Med.* **15**, 283–289 (2004).

62. Feng, Y. *et al.* Grafting of poly(ethylene glycol) monoacrylates on polycarbonateurethane by UV initiated polymerization for improving hemocompatibility. *J. Mater. Sci. Mater. Med.* **24**, 61–70 (2013).

63. Alves, P. *et al.* Surface modification of polyurethane films by plasma and ultraviolet light to improve haemocompatibility for artificial heart valves. *Colloids Surfaces B Biointerfaces* **113**, 25–32 (2014).

64. Yang, J. M., Lin, H. T., Wu, T. H. & Chen, C. C. Wettability and antibacterial assessment of chitosan containing radiation-induced graft nonwoven fabric of polypropylene-g-acrylic acid. *J. Appl. Polym. Sci.* **90**, 1331–1336 (2003).

65. Ferrero, F., Periolatto, M. & Ferrario, S. Sustainable antimicrobial finishing of cotton fabrics by chitosan UV-grafting: From laboratory experiments to semi industrial scale-up. *J. Clean. Prod.* **96**, 244–252 (2015).

66. Bose, S., Robertson, S. F. & Bandyopadhyay, A. Surface modification of biomaterials and biomedical devices using additive manufacturing. *Acta Biomater.* **66**, 6–22

(2018).

67. Benhabiles, M. S. *et al.* Antibacterial activity of chitin, chitosan and its oligomers prepared from shrimp shell waste. *Food Hydrocoll.* **29**, 48–56 (2012).

68. Kong, M., Chen, X. G., Xing, K. & Park, H. J. Antimicrobial properties of chitosan and mode of action: A state of the art review. *Int. J. Food Microbiol.* **144**, 51–63 (2010).

69. Xing, Y. *et al.* Chitosan-based coating with antimicrobial agents: Preparation, property, mechanism, and application effectiveness on fruits and vegetables. *Int. J. Polym. Sci.* **2016**, (2016).

70. Kong, M., Guang, X., Xing, K. & Jin, H. Antimicrobial properties of chitosan and mode of action : A state of the art review. *Int. J. Food Microbiol.* **144**, 51–63 (2010).

71. Ayati Najafabadi, S. A., Keshvari, H., Ganji, Y., Tahriri, M. & Ashuri, M. Chitosan/heparin surface modified polyacrylic acid grafted polyurethane film by two step plasma treatment. *Surf. Eng.* **28**, 710–714 (2012).

72. Yang, S., Lee, Y. J., Lin, F., Yang, J. & Chen, K. Chitosan / Poly (vinyl alcohol) Blending Hydrogel Coating Improves the Surface Characteristics of Segmented Polyurethane Urethral Catheters. 304–313 (2007) doi:10.1002/jbmb.

73. Guillén, M. D. & Ruiz, A. Rapid simultaneous determination by proton NMR of unsaturation and composition of acyl groups in vegetable oils. *Eur. J. Lipid Sci. Technol.* **105**, 688–696 (2003).

74. Barrera-Arellano, D., Badan-Ribeiro, A. P. & Serna-Saldivar, S. O. *Corn oil: Composition, processing, and utilization*. *Corn: Chemistry and Technology, 3rd Edition* (Elsevier Inc., 2018). doi:10.1016/B978-0-12-811971-6.00021-8.

75. Bathini, V., Kalakandan, S. K., Pakkirisamy, M. & Ravichandran, K. Structural elucidation of peanut, sunflower and gingelly oils by using FTIR and 1H NMR spectroscopy. *Pharmacogn. J.* **10**, 753–757 (2018).

76. Guillén, M. D. & Ruiz, A. Edible oils: Discrimination by 1H nuclear magnetic resonance. *J. Sci. Food Agric.* **83**, 338–346 (2003).

77. Knothe, G. & Kenar, J. A. Determination of the fatty acid profile by 1H-NMR spectroscopy. *Eur. J. Lipid Sci. Technol.* **106**, 88–96 (2004).

78. Castejón, D., Mateos-Aparicio, I., Molero, M. D., Cambero, M. I. & Herrera, A. Evaluation and Optimization of the Analysis of Fatty Acid Types in Edible Oils by 1H-NMR. *Food Anal. Methods* **7**, 1285–1297 (2014).

79. Sacchi, R., Addeo, F. & Paolillo, L. 1H and 13C NMR of virgin olive oil. An overview. *Magn. Reson. Chem.* **35**, 133–145 (1997).

80. Vigli, G., Philippidis, A., Spyros, A. & Dais, P. Classification of edible oils by employing 31P and 1H NMR spectroscopy in combination with multivariate

statistical analysis. A proposal for the detection of seed oil adulteration in virgin olive oils. *J. Agric. Food Chem.* **51**, 5715–5722 (2003).

81. ASTM D5554-15. Standard test method for determination of the iodine value of fats and oils. *ASTM Int.* **95**, 16–18 (2015).

82. Shimamoto, G. G., Favaro, M. M. A. & Tubino, M. Simple methods via mid-IR or 1H NMR spectroscopy for the determination of the iodine value of vegetable oils. *J. Braz. Chem. Soc.* **26**, 1431–1437 (2015).

83. Goicoechea, E. & Guillen, M. D. Analysis of hydroperoxides, aldehydes and epoxides by 1H nuclear magnetic resonance in sunflower oil oxidized at 70 and 100 °c. *J. Agric. Food Chem.* **58**, 6234–6245 (2010).

84. Xia, W., Budge, S. M. & Lumsden, M. D. 1H-NMR Characterization of Epoxides Derived from Polyunsaturated Fatty Acids. *JAOCS, J. Am. Oil Chem. Soc.* **93**, 467–478 (2016).

85. Shoolery, J. N. Applications of high resolution nuclear magnetic resonance to study of lipids. in *Dietary fats and health* 220–240 (1983).

86. Johnson, L. F. & Shoolery, J. N. Determination of Unsaturation and Average Molecular Weight of Natural Fats by Nuclear Magnetic Resonance. *Anal. Chem.* **32**, 1136–1139 (1962).

87. Sarpal, A. S. *et al.* Direct Method for the Determination of the Iodine Value of Biodiesel by Quantitative Nuclear Magnetic Resonance (q1H NMR) Spectroscopy. *Energy and Fuels* **29**, 7956–7968 (2015).

88. Domard, A. pH and c.d. measurements on a fully deacetylated chitosan: application to CuII-polymer interactions. *Int. J. Biol. Macromol.* **9**, 98–104 (1987).

89. Jiang, X., Chen, L. & Zhong, W. A new linear potentiometric titration method for the determination of deacetylation degree of chitosan. *Carbohydr. Polym.* **54**, 457–463 (2003).

90. Ingman, F. & Still, E. Graphic method for the determination of titration end-points. *Talanta* **13**, 1431–1442 (1966).

91. Tan, S. C., Khor, E., Tan, T. K. & Wong, S. M. The degree of deacetylation of chitosan: Advocating the first derivative UV-spectrophotometry method of determination. *Talanta* **45**, 713–719 (1998).

92. Rinaudo, M., Milas, M. & Dung, P. Le. Characterization of chitosan. Influence of ionic strength and degree of acetylation on chain expansion. *Int. J. Biol. Macromol.* **15**, 281–285 (1993).

93. Kasaai, M. R. Calculation of Mark-Houwink-Sakurada (MHS) equation viscometric constants for chitosan in any solvent-temperature system using experimental reported viscometric constants data. *Carbohydr. Polym.* **68**, 477–488 (2007).

94. Benaniba, M. T. & Gelbard, G. Epoxidation of sunflower oil with peroxoacetic acid in presence of ion exchange resin by various processes. *Energy Educ. Sci. Technol.* **21**, 71–82 (2008).

95. Babanejad, N., Farhadian, A., Omrani, I. & Nabid, M. R. Design, characterization and in vitro evaluation of novel amphiphilic block sunflower oil-based polyol nanocarrier as a potential delivery system: Raloxifene-hydrochloride as a model. *Mater. Sci. Eng. C* **78**, 59–68 (2017).

96. Yelwa, J. M. & Abdullahi, S. Epoxidation and Hydroxylation of Sunflower Seed Oil. *Int. J. Sci. Res. Chem.* **4**, 1–7 (2019).

97. Omrani, I. *et al.* Synthesis of novel high primary hydroxyl functionality polyol from sunflower oil using thiol-yne reaction and their application in polyurethane coating. *Eur. Polym. J.* **82**, 220–231 (2016).

98. ICONTEC. Norma Técnica Colombiana. NTC 2366 PLASTICS. EPOXIDED VEGETABLE SOJA AND LINSEED OILS. (2000).

99. Samidin, S. & Salimon, J. Synthesis and physicochemical properties of epoxidized tmp trioleate by in situ method. *AIP Conf. Proc.* **1614**, 351–357 (2014).

100. D2074-11, A. Standard Test Methods for Total, Primary, Secondary, and Tertiary Amine Values of Fatty Amines by Alternative Indicator Method. **07**, 2019–2021 (2019).

101. Costamagna, V., Wunderlin, D., Larrañaga, M., Mondragon, I. & Strumia, M. Surface functionalization of polyolefin films via the ultraviolet-induced photografting of acrylic acid: Topographical characterization and ability for binding antifungal agents. *J. Appl. Polym. Sci.* **102**, 2254–2263 (2006).

102. Zuwei, M. *et al.* Surface modification of poly-L-lactide by photografting of hydrophilic polymers towards improving its hydrophilicity. *J. Appl. Polym. Sci.* **85**, 2163–2171 (2002).

103. Tianhong, T. C. Quantifying Polymer Crosslinking Density Using Rheology and DMA. *TA Instruments* 2–4 (2020).

104. McCrum NG, Buckly CP, B. C. *Principles of Polymer Engineering*. (London: Oxford Science Publications, 1997).

105. Khonakdar, H. A., Morshedian, J., Wagenknecht, U. & Jafari, S. H. An investigation of chemical crosslinking effect on properties of high-density polyethylene. *Polymer (Guildf).* **44**, 4301–4309 (2003).

106. Javaid, M. A. *et al.* Evaluation of cytotoxicity, hemocompatibility and spectral studies of chitosan assisted polyurethanes prepared with various diisocyanates. *Int. J. Biol. Macromol.* **129**, 116–126 (2019).

107. Miyake, Y., Yokomizo, K. & Matsuzaki, N. Determination of unsaturated fatty acid

composition by high-resolution nuclear magnetic resonance spectroscopy. *JAOCS, J. Am. Oil Chem. Soc.* **75**, 1091–1094 (1998).

108. Miyake, Y., Yokomizo, K. & Matsuzaki, N. Rapid Determination of Iodine Value by 1H Nuclear Magnetic Resonance Spectroscopy. *J. Am. Oil Chem. Soc.* **75**, 15–19 (1998).

109. Vafakish, B., Barari, M. & Jafari, E. Sunflower seed oil polymerization by ion exchange resins: acidic heterogeneous catalysis. *Bulg. Chem. Commun.* **47**, 558–564 (2015).

110. Hazmi, A. S. A., Aung, M. M., Abdullah, L. C., Salleh, M. Z. & Mahmood, M. H. Producing Jatropha oil-based polyol via epoxidation and ring opening. *Ind. Crops Prod.* **50**, 563–567 (2013).

111. Kumar, S., Samal, S. K., Mohanty, S. & Nayak, S. K. Epoxidized Soybean Oil-Based Epoxy Blend Cured with Anhydride-Based Cross-Linker: Thermal and Mechanical Characterization. *Ind. Eng. Chem. Res.* **56**, 687–698 (2017).

112. Mungroo, R., Pradhan, N. C., Goud, V. V. & Dalai, A. K. Epoxidation of canola oil with hydrogen peroxide catalyzed by acidic ion exchange resin. *JAOCS, J. Am. Oil Chem. Soc.* **85**, 887–896 (2008).

113. Wilkes, G. L., Sohn, S. & Tamami, B. Carbonation of epoxidized vegetable oils and nonisocyanate-polyurethanes derived therefrom. (2004).

114. Doll, K. M. & Erhan, S. Z. The improved synthesis of carbonated soybean oil using supercritical carbon dioxide at a reduced reaction time. 849–854 (2005) doi:10.1039/b511014a.

115. Srivastava, R., Srinivas, D. & Ratnasamy, P. CO2 activation and synthesis of cyclic carbonates and alkyl/aryl carbamates over adenine-modified Ti-SBA-15 solid catalysts. *J. Catal.* **233**, 1–15 (2005).

116. Danish, M., Mumtaz, M. W., Fakhar, M. & Rashid, U. Response surface methodology based optimized purification of the residual glycerol from biodiesel production process. *Chiang Mai J. Sci.* **44**, 1570–1582 (2017).

117. Abbasi, E., Vatankhah, M., Hosseini, Y., Ariana, M. A. & Ayazi, M. Synthesis, structure, and mechanical properties of castor oil-based polyamidoamines toughened epoxy coatings. *J. Appl. Polym. Sci.* **128**, 4023–4030 (2013).

118. Froidevaux, V., Negrell, C., Caillol, S., Pascault, J. P. & Boutevin, B. Biobased Amines: From Synthesis to Polymers; Present and Future. *Chem. Rev.* **116**, 14181–14224 (2016).

119. Camara, F. *et al.* Reactivity of secondary amines for the synthesis of non-isocyanate polyurethanes. *Eur. Polym. J.* **55**, 17–26 (2014).

120. Blattmann, H., Fleischer, M., Bähr, M. & Mülhaupt, R. Isocyanate- and phosgene-free routes to polyfunctional cyclic carbonates and green polyurethanes by fixation

of carbon dioxide. *Macromol. Rapid Commun.* **35**, 1238–1254 (2014).

121. Blattmann, H. & Mülhaupt, R. Multifunctional β-amino alcohols as bio-based amine curing agents for the isocyanate- and phosgene-free synthesis of 100% bio-based polyhydroxyurethane thermosets. *Green Chem.* **18**, 2406–2415 (2016).

122. Babanejad, N., Farhadian, A., Omrani, I. & Nabid, M. R. Design, characterization and in vitro evaluation of novel amphiphilic block sunflower oil-based polyol nanocarrier as a potential delivery system: Raloxifene-hydrochloride as a model. *Mater. Sci. Eng. C* **78**, 59–68 (2017).

123. Miao, S. *et al.* Soybean oil-based polyurethane networks as candidate biomaterials: Synthesis and biocompatibility. *Eur. J. Lipid Sci. Technol.* **114**, 1165–1174 (2012).

124. Gholami, H. & Yeganeh, H. Soybean oil-derived non-isocyanate polyurethanes containing azetidinium groups as antibacterial wound dressing membranes. *Eur. Polym. J.* **142**, 110142 (2021).

125. Javni, I., Hong, D. P. & Petrovič, Z. S. Polyurethanes from soybean oil, aromatic, and cycloaliphatic diamines by nonisocyanate route. *J. Appl. Polym. Sci.* **128**, 566–571 (2013).

126. Feng, L., Yang, H., Dong, X., Lei, H. & Chen, D. pH-sensitive polymeric particles as smart carriers for rebar inhibitors delivery in alkaline condition. *J. Appl. Polym. Sci.* **135**, (2018).

127. Kolek, E., Šimko, P., Šimon, P. & Gatial, A. Confirmation of polymerisation effects of sodium chloride and its additives on acrylamide by infrared spectrometry. *J. Food Nutr. Res.* **46**, 39–44 (2007).

128. Da Silva, R. M. P. *et al.* Poly(N-isopropylacrylamide) surface-grafted chitosan membranes as a new substrate for cell sheet engineering and manipulation. *Biotechnol. Bioeng.* **101**, 1321–1331 (2008).

129. Queiroz, M. F., Melo, K. R. T., Sabry, D. A., Sassaki, G. L. & Rocha, H. A. O. Does the use of chitosan contribute to oxalate kidney stone formation? *Mar. Drugs* **13**, 141–158 (2015).

130. Song, C., Yu, H., Zhang, M., Yang, Y. & Zhang, G. Physicochemical properties and antioxidant activity of chitosan from the blowfly Chrysomya megacephala larvae. *Int. J. Biol. Macromol.* **60**, 347–354 (2013).

131. Dweck, J. & Sampaio, C. M. S. Analysis of the thermal decomposition of commercial vegetable oils in air by simultaneous TG/DTA. *J. Therm. Anal. Calorim.* **75**, 385–391 (2004).

132. Qaroush, A. K., Alsoubani, F. A., Ala'a, M., Nabih, E., Al-Ramahi, E., Khanfar, M. F., ... & Ala'a, F. E. An efficient atom-economical chemoselective CO 2 cycloaddition using lanthanum oxide/tetrabutyl ammonium bromide. *Sustain. Energy Fuels* **2**, 1342–

1349 (2018).

133. Carré, C., Bonnet, L. & Avérous, L. Original biobased nonisocyanate polyurethanes: Solvent- and catalyst-free synthesis, thermal properties and rheological behaviour. *RSC Adv.* **4**, 54018–54025 (2014).

134. Ren, Y., Pan, H., Li, L., Xia, J. & Yang, Y. Synthesis of polyurethane acrylates by hydrogenated castor oil and dimer-based polyester diol and study on pressure-sensitive adhesive. *J. Appl. Polym. Sci.* **98**, 1814–1821 (2005).

135. Błażek, K., Kasprzyk, P. & Datta, J. Diamine derivatives of dimerized fatty acids and bio-based polyether polyol as sustainable platforms for the synthesis of non-isocyanate polyurethanes. *Polymer (Guildf).* **205**, (2020).

136. Cruz-Aldaco, K., Flores-Loyola, E., Aguilar-González, C. N., Burgos, N. & Jiménez, A. Synthesis and thermal characterization of polyurethanes obtained from cottonseed and corn oil-based polyols. *J. Renew. Mater.* **4**, 178–184 (2016).

137. Karami, Z., Kabiri, K. & Zohuriaan-Mehr, M. J. Non-isocyanate polyurethane thermoset based on a bio-resourced star-shaped epoxy macromonomer in comparison with a cyclocarbonate fossil-based epoxy resin: A preliminary study on thermo-mechanical and antibacterial properties. *J. CO2 Util.* **34**, 558–567 (2019).

138. Das, S., Kumar, S., Mohanty, S. & Nayak, S. K. *Synthesis, Characterization and Application of Bio-based Polyurethane Nanocomposites*. *Sustainable Polymer Composites and Nanocomposites* (2019). doi:10.1007/978-3-030-05399-4_39.

139. He, X., Xu, X., Wan, Q., Bo, G. & Yan, Y. Solvent- and catalyst-free synthesis, hybridization and characterization of biobased nonisocyanate polyurethane (NIPU). *Polymers (Basel).* **11**, (2019).

140. Martínez-Camacho, A. P. *et al.* Chitosan composite films: Thermal, structural, mechanical and antifungal properties. *Carbohydr. Polym.* **82**, 305–315 (2010).

141. Kumar, S. & Koh, J. Physiochemical, optical and biological activity of chitosan-chromone derivative for biomedical applications. *Int. J. Mol. Sci.* **13**, 6103–6116 (2012).

142. Zhang, M., Pan, H., Zhang, L., Hu, L. & Zhou, Y. Study of the mechanical, thermal properties and flame retardancy of rigid polyurethane foams prepared from modified castor-oil-based polyols. *Ind. Crops Prod.* **59**, 135–143 (2014).

143. Arévalo-Alquichire, S. *et al.* Polyurethanes from modified castor oil and chitosan: Synthesis, characterization, in vitro degradation, and cytotoxicity. *J. Elastomers Plast.* **50**, 419–434 (2018).

144. Baek, Y., Kang, J., Theato, P. & Yoon, J. Measuring hydrophilicity of RO membranes by contact angles via sessile drop and captive bubble method: A comparative study. *Desalination* **303**, 23–28 (2012).

145. Arima, Y. & Iwata, H. Effect of wettability and surface functional groups on protein adsorption and cell adhesion using well-defined mixed self-assembled monolayers. *Biomaterials* **28**, 3074–3082 (2007).

146. Kara, F., Aksoy, E. A., Yuksekdag, Z., Aksoy, S. & Hasirci, N. Enhancement of antibacterial properties of polyurethanes by chitosan and heparin immobilization. *Appl. Surf. Sci.* **357**, 1692–1702 (2015).

147. Bahrami, N., Nouri Khorasani, S., Mahdavi, H., Ghiaci, M. & Mokhtari, R. Low-pressure plasma surface modification of polyurethane films with chitosan and collagen biomolecules. *J. Appl. Polym. Sci.* **136**, 1–10 (2019).

148. Drozd, N. N. *et al.* Chitosan / heparin layer-by-layer coatings for improving thromboresistance of polyurethane. *Surfaces and Interfaces* **28**, 101674 (2022).

149. Wang, X., Pan, Y. T., Wan, J. T. & Wang, D. Y. An eco-friendly way to fire retardant flexible polyurethane foam: Layer-by-layer assembly of fully bio-based substances. *RSC Adv.* **4**, 46164–46169 (2014).

150. Guan, J. *et al.* Progress in Study of Non-Isocyanate Polyurethane Progress in Study of Non-Isocyanate Polyurethane. *Ind. Eng. Chem.* **50**, 6517–6527 (2017).

151. Piozzi, A., Francolini, I., Occhiaperti, L., Venditti, M. & Marconi, W. Antimicrobial activity of polyurethanes coated with antibiotics: A new approach to the realization of medical devices exempt from microbial colonization. *Int. J. Pharm.* **280**, 173–183 (2004).

152. Khatoon, H., Iqbal, S., Irfan, M., Darda, A. & Rawat, N. K. A review on the production, properties and applications of non-isocyanate polyurethane: A greener perspective. *Prog. Org. Coatings* **154**, (2021).

153. Gholami, H., Yeganeh, H., Burujeny, S. B., Sorayya, M. & Shams, E. Vegetable Oil Based Polyurethane Containing 1,2,3-Triazolium Functional Groups as Antimicrobial Wound Dressing. *J. Polym. Environ.* **26**, 462–473 (2018).

154. Agnihotri, S., Dhiman, N. K. & Tripathi, A. *Antimicrobial surface modification of polymeric biomaterials*. *Handbook of Antimicrobial Coatings* (2017). doi:10.1016/B978-0-12-811982-2.00020-2.

155. Garrison, T. F. *et al.* Thermo-mechanical and antibacterial properties of soybean Oil-Based cationic polyurethane coatings: Effects of amine ratio and degree of crosslinking. *Macromol. Mater. Eng.* **299**, 1042–1051 (2014).

156. Figovsky, O. L., Shapovalov, L. & Axenov, O. Advanced coatings based upon non-isocyanate polyurethanes for industrial applications. *Surf. Coatings Int. Part B Coatings Trans.* **87**, 83–90 (2004).